UNIVERSITY OF BIRMINGHAM

Temperature Controlled Single Column Continuous Hydrophobic Interaction Chromatography of Proteins

by

Alexander James Brean

a thesis submitted
to the University of Birmingham
for the degree of
Doctor of Philosophy

Biochemical Engineering
School of Chemical Engineering
College of Engineering and Physical Sciences
January 2024

Acknowledgements

I am deeply grateful to Professor Owen Thomas for his unwavering support and reassurance during the most challenging moments. I also thank Lauren Garbett and Gabby Bruque for their kind words and valuable advice. My sincere appreciation goes to my secondary supervisor, Professor Matthias Franzreb, whose enthusiasm made my trips to Germany the most enjoyable part of this PhD. I am indebted to Professor Daniel Bracewell and Dr. Tim Overton for their guidance and encouragement.

I was privileged to supervise several exceptional MSc students: Daniel Zanarotti, Diana Pieruccini, Sarah McKay, Emily Rae, and Yang Jiao, who were instrumental in completing this thesis, especially during the COVID-19 shutdown and while I was dealing with personal injuries (two broken hands, two separate accidents, two weeks apart). I also thank Jarrod Thomas for reading the thesis and providing valuable feedback.

Finally, I thank my family: my brother, James Brean, whose groundbreaking work in atmospheric chemistry inspires me; my mother, who has always believed in me; and my father and his partner for their steadfast love and support.

This work was supported by the UK Engineering and Physical Sciences Research Council (EPSRC) Centre for Doctoral Training in Emergent Macromolecular Therapies, and I am grateful to Lonza for generously providing Rituximab samples.

Contents

List of Figures

List of Tables

List of Abbreviations

Abbreviation	Definition
Δ	Change In / Difference Between
ADCC	Antibody-Dependent Cell-Mediated Cytotoxicity
ADCP	Antibody-Dependent Cellular Phagocytosis
AEX	Anion Exchange
AFC	Annular Flow Chromatography
AS	Ammonium Sulphate
As	Asymmetry
BSA	Bovine Serum Albumin
C	Constant Region
CAGR	Compound Annual Growth Rate
CD	Cluster of Differentiation
CDC	Complement-Dependent Cytotoxicity
CDR	Complementarity-Determining Regions
CEX	Cation Exchange
CHO	Chinese Hamster Ovary Cells
DNA	Deoxyribonucleic Acid
FF	Fast Flow
Fab	Fragment Antigen Binding
Fc	Fragment Crystallisation / Fragment Constant
FcR	Fc Receptor
FDA	Food and Drug Administration
FPLC	Fast Protein Liquid Chromatography
G	Gibbs Free Energy
H	Heavy Chain
HSA	Human Serum Albumin
HCP	Host Cell Proteins
HIC	Hydrophobic Interaction Chromatography
HIV-1	Human Immunodeficiency Virus Type 1
HMW	High Molecular Weight
IEP	Isoelectric Point
IEX	Ion Exchange Chromatography
Ig	Immunoglobulin
J	Joining Chain
Kd	Dissociation Constant
kDa	Kilodaltons
L	Light Chain
mAb	Monoclonal Antibody
PCC	Periodic Counter-Current Chromatography
pH	Potential of Hydrogen
q_{max}	Maximum Binding
$q\Phi$	Change in Binding Between Temperatures
R	Universal Gas Constant
RFC	Radial Flow Chromatography

S	Entropy
SDS-PAGE	Sodium Dodecyl Sulphate Polyacrylamide Gel Electrophoresis
SEC	Size Exclusion Chromatography
siRNA	Small Interfering RNAs
SMBC	Simulated Moving Bed Chromatography
SPA	Staphylococcal Protein A
Φ	Temperature
TCZR	Travelling Cooling Zone Reactor
T_{end}	Transition End Temperature (DSC)
THZR	Travelling Heating Zone Reactor
T_{M1}	Melting Curve 1 Temperature (DSC)
T_{M2}	Melting Curve 2 Temperature (DSC)
TNFα	Tumour Necrosis Factor Alpha
T_{onset}	Onset Temperature (DSC)
US$	United States Dollar
UV	Ultraviolet
V	Volume
v	Velocity
V	Variable Domain
CV	Column Volume
V_e	Elution Volume
v_{linear}	Linear Velocity
V_o	Void Volume
$v_{volumetric}$	Volumetric Flow Rate
W	Width
κ	Kappa Light Chain
κ'	Retention Factor
λ	Packing Factor/Lambda Light Chain
φ	Phase Ratio

Chapter 1

Introduction

1.1. The Global Biopharmaceutical Industry

The global pharmaceutical market is presently valued at approximately US$1.65 trillion (Biospace, 2024), with biopharmaceuticals emerging as a growing subdivision. The biopharmaceutical sector, defined by its focus on biologically derived therapies, commands a market share estimated at US$419 billion, which accounts for 25.3% of the overall pharmaceutical sector (Biospace, 2022). In recent decades, the biopharmaceutical industry has experienced a compound annual growth rate (CAGR) of 13.8% (Shaikh and Jaiswal, 2018; Stratis, 2023). Projections suggest that the market will expand to US$856 billion by 2030 (Biospace, 2022), a trajectory that underscores the growing importance of biopharmaceutical in the global healthcare system.

This growing sector encompasses an array of therapeutic modalities, including but not limited to monoclonal antibodies (mAbs), recombinant proteins, gene and cell therapies, and nucleic acids such as siRNAs. Such diversity is required to treat a myriad of pathologies across medicine. Key to this growth has been the rise of antibody-based therapeutics, with monoclonal antibodies (mAbs) are at the forefront. Indeed, mAbs alone are anticipated to reach a market value of US$391 billion by 2030 (Stratis, 2023).

The success of mAbs can be attributed to their high degree of versatility and target specificity in treating a variety of conditions. These agents have become indispensable in addressing oncological, autoimmune, and infectious diseases, as well as conditions such as cardiovascular and neurological disorders. Their ability to precisely target disease-related antigens while minimising off-target effects makes them particularly effective.

Yet, while the growth of the mAb market remains strong, the development and production remain resource intensive. High manufacturing costs, and a complex regulatory environment are frequently cited as obstacles. To comprehend the full scope of these challenges and the requisite technological solutions, a deeper understanding of antibody structure and function is required.

1.2. Antibody Structure & Function

Antibodies, also known as immunoglobulins, are Y-shaped glycoproteins, optimised for antigen recognition and binding (**Figure 1 a**). As essential components of the immune system, they are produced by B-lymphocytes to neutralise pathogens, orchestrate immune responses, and dictate immune tolerance.

Structurally, antibodies are composed of four polypeptides: two light chains and two heavy chains. The heavy (H) and light (L) chains have variable (V) domains, and constant (C) domains, named: (V_H, V_L, C_L, C_{H1}, C_{H2}, C_{H3}). When assembled, the V_H, V_L, C_L, CH_1 domains form the antigen binding fragment (Fab), responsible for antigen recognition. The CH_2, CH_3 domains constitute the crystallisable fragment (Fc) region, which mediates immune effector functions such as complement activation and antibody-dependent cell mediated cytotoxicity (ADCC) (Mian et al., 1991; Janeway Jr et al., 2001).

Light chains are further subclassified into kappa (κ) or lambda (λ) types, with both subtypes functioning equivalently despite minor differences in flexibility and serum half-life (Bräuninger et al., 2001; Montaño and Morrison, 2002). The antigen-binding specificity of each antibody is dictated by the unique amino acid sequence within its variable region, enabling precise and high-affinity interactions with distinct antigens.

Antibody stability is maintained by disulfide bonds. Interchain disulfide linkages anchor the two H chains together and secure the association between the heavy and light chains. The hinge region, located between the Fab and Fc fragments, grants flexibility to the Fab arms, facilitating their independent motion (**Figure 1 a**). The structural versatility of antibodies allows them to perform a wide range of immune functions. This versatility is further exemplified by the existence of distinct antibody isotypes, each specialised to different immunological roles and responses. Each possess alterations in their H chain that differentiate them structurally and functionally.

1.2.1. Types of Antibodies

Antibodies are divided into five major isotypes: IgG, IgD, IgE, IgA and IgM (**Figure 1 b**). These isotypes differ in the constant region of the H chain, which bind to Fc class specific receptors, such as FcγR, FcεR, FcαR, and FcRα/μ (Fc receptor, specific for IgG, IgE, IgA, and IgM respectively). Through these interactions, antibodies exert many of their host-effector functions, playing a critical role in immune defence mechanisms (Burton and Woof, 1992; Lu et al., 2018).

IgG is the most abundant class in human serum and is produced by activated B-lymphocytes in response to specific antigens. IgG has a monomeric structure and is highly specific. When a pathogen is re-encountered, IgG is critical for long-term immunity because of its rapid secretion by activated memory-B cells. IgG is further divided into four subclasses: IgG1, IgG2, IgG3, and IgG4, each with its own properties (Schroeder and Cavacini, 2010; Napodano et al., 2021). Each subclass of IgG exhibits variations in the hinge region between the Fab and Fc regions (Vidarsson et al., 2014). These

modifications involve alterations in the length and flexibility of hinge region, as well as the number and location of disulfide bonds (**Figure 2**).

IgD functions predominantly as a membrane-bound receptor on mature B-cells. It plays a key role in the initiation and regulation of the immune response and inflammation. It is involved with CD79a and CD79b signalling on the surface of B-cells, and co-signalling with IgM; however, its function remains unclear (Geisberger et al., 2006). It is likely that, as research progresses, more functions will be discovered.

IgE is one of the lowest concentration immunoglobulins in the serum. However, it is highly potent and triggers hypersensitivity, parasitic, and allergen responses. IgE mediates the immune response by binding to Fcε receptors on mast cells, basophils, and eosinophils. Upon binding, IgE triggers degranulation and the release of pro-inflammatory cytokines such as histamine, TNFα, IL-4 and IL-9 (Galli and Tsai, 2012). This process is the driver of hypersensitivity and the allergic response.

IgA is the second most abundant serum immunoglobulin. It is particularly concentrated in the colostrum, the first milk produced by human mothers. Generally found as a monomer in serum, IgA typically exists as a dimer on mucosal surfaces, known as secretory IgA. This dimerisation occurs via a joining (J) chain linking two monomers. IgA is crucial for protecting surfaces through direct neutralisation of toxins, viruses, and bacteria. IgA is also divided into two sub-classes; IgA1 and IgA2, which have slightly different hinge region structure (Schroeder and Cavacini, 2010).

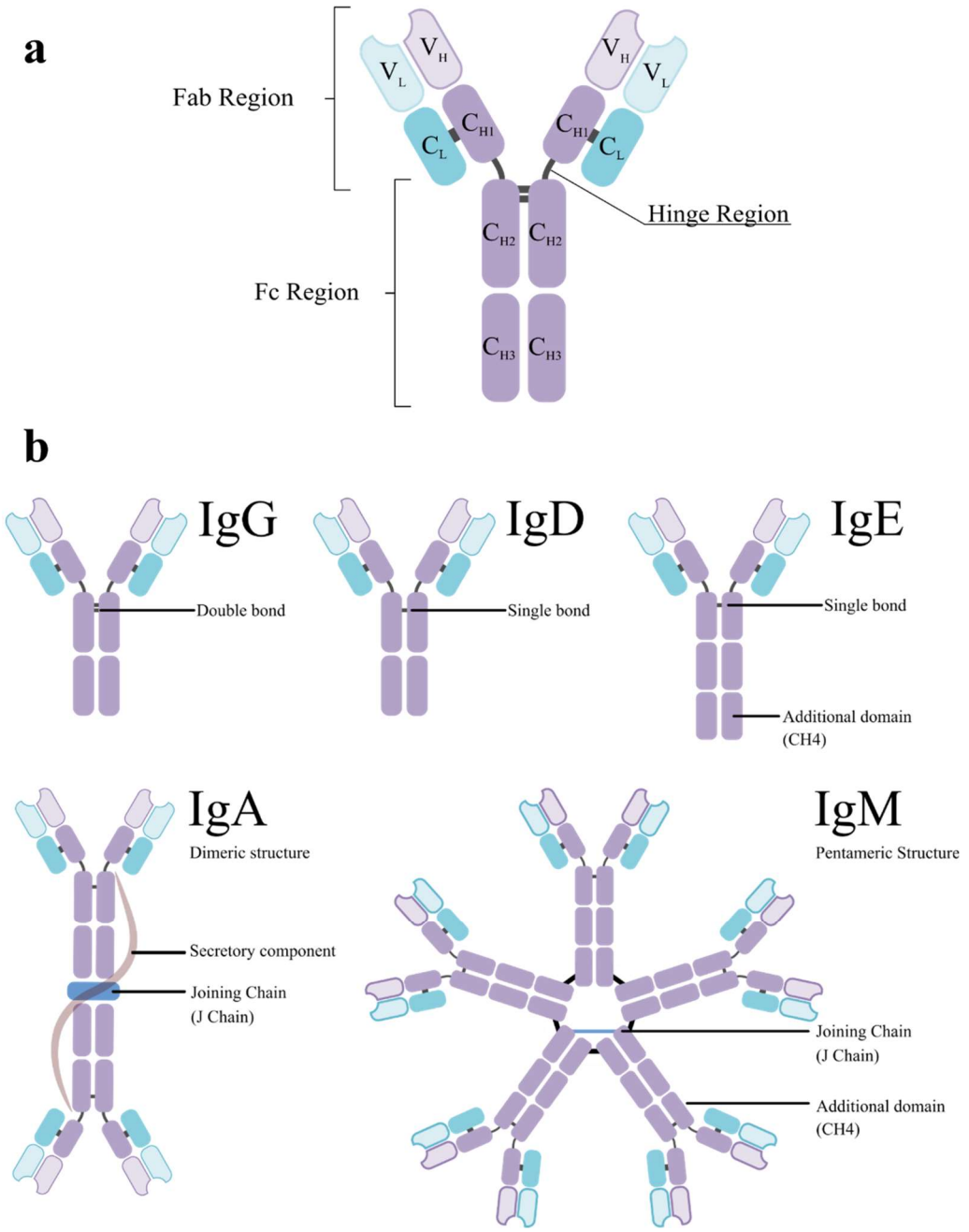

Figure 1: The structures of antibodies. (a) The structure of IgG1. Each antibody comprises constant (C) and variable (V) domains, as well as heavy (H) and light (L) chains. The antibody is divided into two functional regions: the antibody fragment antigen binding (Fab) region, responsible for antigen recognition, and the fragment crystallisation (Fc) region, responsible for effector functions. The flexible hinge region connects the Fab to the Fc regions. (b) the structures of IgG, IgD, IgE, IgA, and IgM. IgG has two disulfide bonds which link the H chains together. In IgD and IgE, the H chains are linked by a single disulfide bond. IgE has an extended Fc region featuring an additional CH4 domain. IgA is found as a dimer, connected by a joining (J) chain, and IgM has a pentameric structure, with repeating J chains and an additional CH4 domain. Original image produced using Inkscape 1.2.2.

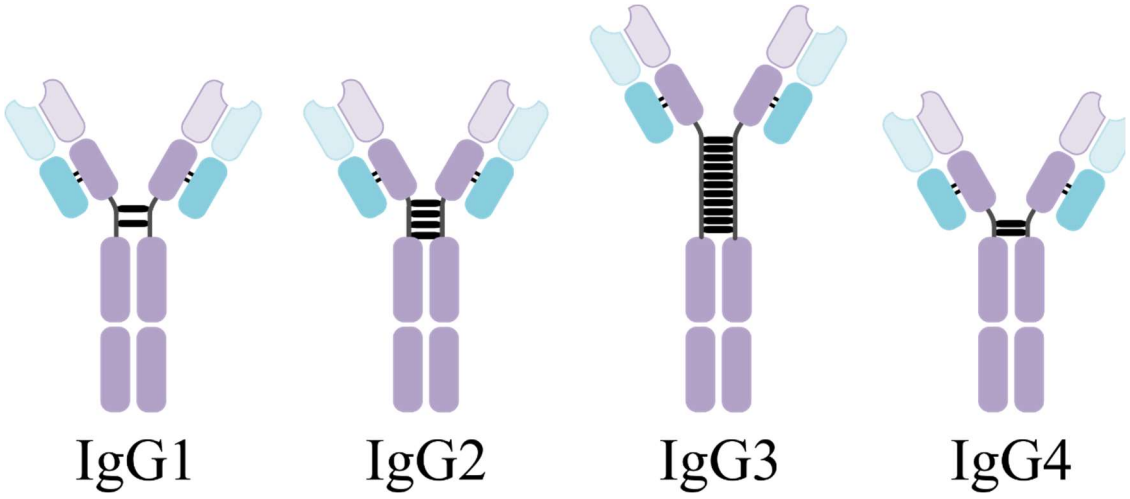

Figure 2: The Structure of the IgG Subclasses. IgG has four subclasses, namely IgG1, IgG2, IgG3, and IgG4. The length and flexibility of the hinge region differ substantially among these subclasses. For example, IgG1 features a 15-amino-acid hinge that is highly flexible. IgG2 has a 12-amino-acid hinge, equipped with a rigid poly-proline helix and four inter-H chain disulfide bonds. Conversely, IgG3 boasts a long, flexible hinge region comprising 62 amino acids, with up to 11 disulfide bonds: this unusually long structure results from a duplication of the hinge exon (Roux et al., 1997; Vidarsson et al., 2014). Original image produced using Inkscape 1.2.2.

IgM is the first antibody expressed during B cell development, and the first antibody to be produced during infection. It is unique for having a pentameric structure, facilitated by an additional C_{H4} domain in the Fc portion of the H chain. These C_{H4} domains enable the formation of additional disulfide bonds which support the pentameric structure. This multivalent structure confers high avidity for the target antigen, making it particularly effective in the primary immune response and in mediating agglutination and opsonisation (Boes, 2000).

While each antibody isotype is specialised for distinct immunological functions, their shared capacity to recognise and bind antigens with remarkable specificity remains a unifying feature. This specificity, determined by the unique structure of the variable region, is key to the antibody's ability to target a vast array of pathogens, and is further refined during the immune response.

1.2.2. Antigen Binding & Specificity

Although the range of possible antibody epitopes is vast, the antibody-antigen interaction is highly specific. This specificity is determined by the variable region, which includes the complementarity-determining regions (CDRs) that are responsible for antigen binding. The amino-acid sequence of these regions dictates the specificity. The immense diversity in these regions arises through a process called V(D)J recombination, in which the variable (V), diversity (D), and joining (J) gene segments are randomly recombined during B-cell development. Genetic recombination of the CDR generates a vast repertoire of antibodies, capable of recognising antigens that the immune system has not previously encountered. This process is further diversified by the addition or deletion of nucleotides at the junctions of the recombined segments, a phenomenon known as junctional diversity, which significantly expands the antibody repertoire. For example, position 96 in the light chain is a common source of diversity due to imprecise gene splicing (Tonegawa, 1983; Jeske et al., 1984). Structural analysis reveals these regions are rich in Tyrosine, Tryptophan, Serine, Asparagine, Aspartic Acid, Threonine, Arginine, and Histidine (Mian et al., 1991; Nguyen et al., 2017). B lymphocytes with autoreactive antibodies are typically removed through mechanisms such as receptor editing, anergy, or apoptosis, to maintain immune tolerance (Gay et al., 1993; Cambier et al., 2007; Wright et al., 2021).

The antibody-antigen interaction is driven by non-covalent interactions, including hydrophobic interactions, electrostatic interactions, hydrogen bonds and van der Waals forces (van Oss et al., 1986; Reverberi and Reverberi, 2007; Sela-Culang et al., 2013;

Akiba and Tsumoto, 2015; Bayer, 2019). This diverse range of interactions contributes to the wide range of antigens that antibodies can recognise.

Antibody specificity and affinity are adaptable and are refined through the immune response. Antibodies expressed on the surface of naïve B-cells have a wider specificity than their mature counterparts, allowing them to recognise a range of antigens and epitopes. Following recognition, the B-cell receptor undergoes internalisation and affinity maturation is driven by somatic hypermutation of the CDR region, such that the target specificity remains but the affinity is greatly enhanced. B-cells that produce antibodies with weak affinities are targeted for programmed cell death, while B-cells with high affinity antibodies proliferate (Jain and Salunke, 2019). While somatic hypermutation is changing the antibody's affinity, the effector functions can also be changed. In a process known as isotype switching, the constant domains of the Fc region are changed, so the antibody specificity is maintained but the effector functions are altered. This may alter antibody class from that which was initially expressed on the surface of the B-cell, such as IgM, or IgD, to an antibody class more suitable for a mature immune response, such as IgG, IgA or IgE (Stavnezer et al., 2008; Jain and Salunke, 2019; Wang et al., 2020). The result is mature B-cells with highly specific antibodies that bind with greater affinity. These B-cells then develop into memory B cells, which maintain long-term immunity, and plasma cells, which rapidly secrete mature antibodies during the immune response.

While the specificity and high-affinity binding of antibodies are critical for recognising a wide range of antigens, the functional significance of this interaction extends beyond mere recognition. Once bound to their target, antibodies can exert effects that neutralise pathogens and enhance their clearance from the body. Two key mechanisms by which

antibodies achieve this are neutralisation and opsonisation, which play vital roles in immune defence.

1.2.3. Neutralisation & Opsonisation

The binding of antibodies to antigens can directly neutralise the pathogen through several mechanisms. For example, antibodies can neutralise pathogens by binding to their external surface. This can render the infectious agent non-infectious, as observed with antibodies raised against E1 glycoprotein of Sindbis virus, inducing conformational changes that inhibit the infection of the host cell (Hernandez et al., 2008). Similarly, in Aphthovirus, antibody binding to the virion capsid causes structural disruption, exposing the viral RNA genome (McCullough et al., 1987). Antibodies against HIV-1 gp120 block gp120-CD4 interaction, preventing the HIV-1 virion capsid from fusing with the cell membrane, and the virion particle from gaining intracellular access to T-cells (Klasse et al., 2012).

Antibodies can also inhibit pathogen motility. Antibodies specific to Vibrio cholerae have been demonstrated to prevent bacterial motility without directly destroying the pathogen (Bishop et al., 2010). This has also been demonstrated in Pseudomonas aeruginosa, where antibodies generated against the flagella inhibit bacterial movement (Campodónico et al., 2010).

Once bound, the antibody-antigen structure is known as the immune complex. Immune complex formation leads to opsonisation by phagocytes, such as macrophages and neutrophils. In this process, the immune complex is engulphed by the phagocyte, internalised, and destroyed. Fcγ receptors, expressed on the surface of the macrophage,

interact with the Fc region of antibodies bound to target antigens, triggering endocytosis and degradation of the target antigen. IgG and IgM are both potent activators of phagocytosis via FcγR and Fcμ receptors (Fujisawa, 2008; Forthal, 2014).

While neutralisation and opsonisation are key mechanisms by which antibodies neutralise pathogens, their ability to interact with host immune cells and proteins through the Fc region further amplifies their role in immune defence. These interactions trigger a variety of host effector functions, engaging multiple components of the immune system to enhance pathogen elimination.

1.2.4. Host Effector Functions

Besides antigen binding, antibodies can interact with host proteins via the Fc region to employ various host effector functions. These effector functions coordinate parts of the immune system, including macrophages, monocytes, neutrophils, complement, and natural killer cells (Burton and Woof, 1992; Lu et al., 2018).

One example of this is antibody-dependent cellular phagocytosis (ADCP). This occurs when IgG binds to extracellular pathogens. The Fc region identifies the target for opsonisation via Fcγ receptors expressed on phagocytes. This initiates ADCP, where the target is engulfed by the phagocyte and destroyed. This tagging assists in the removal of immune complexes from infected tissues (Van Erp et al., 2019).

Another critical host effector function is ADCC. In ADCC, bound IgG activates Fcγ receptors on natural killer cells, neutrophils, monocytes, and eosinophils. This proximity triggers the cells to secrete proteins that destroy the cell membrane, such as perforin and

granzyme, as well as proinflammatory cytokines such as tumour necrosis factor α, which further recruits the immune system (Vidarsson et al., 2014; Lu et al., 2018).

Complement-dependent cytotoxicity (CDC) is an additional host effector function antibodies can leverage. The complement system can promote inflammation and directly destroy pathogen cell membranes via the membrane attack complex. The formation of the MAC involves a cascade of over thirty plasma proteins that can be activated via the classical, lectin, or alternative pathway. For CDC, complement is activated in the classical pathway when C1q binds to the Fc region of IgG1 and IgM molecules. C1q initiates a complex cascade of protein interactions that result in C3 and C5 convertase activation, MAC formation, proinflammatory cytokine secretion, and lysis of the target cell (Dunkelberger and Song, 2010; Noris and Remuzzi, 2013).

By leveraging ADCC, ADCP, and CDC, antibodies enhance their pathogen killing potential, and potentiate other parts of the immune system. While antibodies play crucial roles in natural immune processes such as neutralisation, opsonisation, and the activation of host effector functions, their therapeutic potential extends far beyond these physiological roles. The clinical application of antibodies has revolutionised modern medicine, offering powerful tools for diagnosis and treatment.

1.2.5. Clinical Relevance of Antibodies

Antibodies derived from blood plasma are polyclonal, originating from multiple B-cell lineages, resulting in structural heterogenicity and broad antigen specificity. The first polyclonal antibody therapy was pioneered by Emil von Behring in 1890. He pioneered serum therapy for the treatment of diphtheria. His method involved inoculating rats,

guinea pigs and rabbits with attenuated diphtheria bacterium. After allowing the animals immune system to respond and confirming the animals were immune via re-exposure, the serum was administered to animals that had developed diphtheria, effectively treating the disease (Winau and Winau, 2002; Kaufmann, 2017). These findings were published later the same year (Behring, 1890). By 1894, vials of serum were being sold for the treatment of human patients (Winau and Winau, 2002). For his work, he was awarded the first Nobel Prize in medicine and physiology in 1901 (Kaufmann, 2017). Today, polyclonal antibodies are widely used in a range of applications, including for diagnosis, treatment of infectious diseases, immune modulation, and the treatment of autoimmune disorders.

For diagnostic purposes, polyclonal antibodies can provide broad specificity to a range of epitopes which is particularly useful in enzyme-linked immunosorbent assays (ELISA), nephelometric assays, and lateral flow based immunodiagnostic applications (Brown, 2008). This broad specificity allows the assay to be sensitive to a broad range of antigen variations and helps to prevent false negatives that may arise from a more limited pool of antibodies.

Polyclonal antibodies are used for the treatment of immune deficiencies and in the treatment of autoimmune disorders. For example, Privigen is an intravenous immunoglobulin preparation, manufactured from a pool of healthy human donors. It provides a multitude of polyclonal antibodies, providing broad protection against a range of pathogens and is used to treat humoral immunodeficiency (Jolles et al., 2005; Stein et al., 2009). Polyclonal preparations also have immunomodulatory effects and can treat conditions such as chronic inflammatory demyelinating polyneuropathy, where the immune system targets the neuron myelin sheath (Léger et al., 2013; Schwab and

Nimmerjahn, 2013). Destruction of the myelin sheath reduces neuronal transmission speed, and this mechanism is observed in diseases such as multiple sclerosis, Leber's hereditary optic neuropathy and adrenomyeloneuropathy (Popescu and Lucchinetti, 2012).

Another polyclonal antibody preparation used for immunomodulation is anti-thymocyte globulin (ATG). ATG is derived from horse and rabbits immunised with human T-cells. ATG preparations are rich in cytotoxic anti T-cell antibodies. Several proteins, such as CD2, CD3, CD4, CD8, CD11a, CD18, CD25, CD44, and CD45 are expressed on the surface of T-cells (Johnson, 2016). ATG preparations contain antibodies specific to these T-cell markers. ATG administration causes rapid, but temporary T-cell depletion, likely via two pathways: antibody mediated cytotoxicity or Fas-dependent apoptosis of T-cells (Mohty, 2007). There is also evidence that ATG enhances the generation of immunoregulatory T-regulator cells, particularly CD4+, CD25 and Foxp3+ cells (Lopez et al., 2006). ATG is used for treating acute transplant rejection (Afable et al., 2011; Siddiqui et al., 2019), and may be used in other disorders where T-cell depletion is required. In these scenarios, antibodies that bind a range of epitopes are desirable, however some situations call for a more specific antibody response, where mAbs are better suited.

1.3. Monoclonal Antibodies (mAbs)

In contrast to polyclonal antibodies, monoclonal antibodies (mAbs), derived from a single B-cell lineage, are identical with specificity for a singular epitope (Bayer, 2019). These are synthesised from genetically modified cell lines, the first of which was developed by

Köhler and Milstein in 1975. This involved the fusion of an immortalised myeloma cell with a B-lymphocyte, combining the replication capabilities of the former with the antibody synthesis capabilities of the latter (Kohler and Milstein, 1975). Selection of successful hybridomas was achieved using hypoxanthine-aminopterin-thymidine (HAT) media, a system that inhibits de novo nucleotide synthesis via aminopterin, a dihydrofolate reductase (DHFR) inhibitor. As a result, cells are forced to rely on the salvage pathway for nucleotide biosynthesis. Myeloma cells, which are HGPRT-deficient due to targeted genetic manipulation, cannot survive in HAT media. Hybridomas, which inherit a functional Hprt gene from plasma cells, can utilise the salvage pathway, enabling sustained growth and mAb secretion.

The first FDA-approved therapeutic mAb, Orthoclone OKT3, marked a significant milestone in medicine. Orthoclone targets the CD3 complex, a protein expressed on the surface of T-cells. Orthoclone was used to treat organ transplant rejection, by supressing T-cell mediated cytotoxic responses to foreign major histocompatibility complexes (MHC) molecules on transplanted tissues (Goldstein, 1987; Todd and Brogden, 1989; Smith, 1996). Since then, mAbs have revolutionised clinical practice, with numerous therapies approved for a range of diseases. Examples include Tezepelumab, an anti-IL-5 mAb for severe asthma; Herceptin (trastuzumab), targeting HER2-positive breast cancer; Regkirona (regdanvimab), for moderate-to-severe SARS-CoV2 infections; Ibalizumab (ibalizumab-uiyk), used in multidrug-resistant HIV; and Romosozumab, a sclerostin inhibitor for postmenopausal osteoporosis. The capacity of mAbs to selectively bind specific molecular targets underpins their broad therapeutic applicability, making them indispensable tools in modern medicine.

The initial mAb therapies such as Orthoclone were using murine-derived antibodies, which resulted in an anti-mouse antibody response from the patient. Murine antibodies are also incapable of leveraging human host effector functions as mouse CH_2 and CH_3 domains differ structurally from human Fc regions. This prevented ADCC and CDC responses to be leveraged by the early mAb therapies. To circumvent these limitations, chimeric antibodies were developed, which incorporated human constant regions into the murine Fab region. This improved compatibility with the human immune system but did not allow for the use of host-effector functions. Further refinement led to humanised antibodies, where only the CDRs were murine, and the rest being derived from human genetic material. Further advancements led to fully human antibodies, produced using transgenic murine platforms such as the HuMab mouse. Antibodies using this platform are fully capable of leveraging the human immune system (Tsurushita et al., 2005; Harding et al., 2010; Sushant and Onkar, 2021).

Monoclonal antibodies offer distinct therapeutic benefits over small-drug counterparts, such as high selectivity and specificity, minimising off-target effects and reducing the effective dosage. They can also leverage native immune system functions via the Fc region. Moreover, their relatively large molecular weight (> 150 kDa) prevents glomerular filtration by the kidneys, thus enhancing their serum half-life and extending their therapeutic effect. This extends their therapeutic effect and lowers the dosage. These advantages have resulted in mAbs becoming fundamental to modern medicine.

1.3.1. Rituximab

The first mAb to be approved in the field of oncology was Rituximab, a chimeric IgG1κ mAb first approved for the treatment of follicular lymphoma in 1997, now also used for the treatment of non-Hodgkin lymphoma, chronic lymphocytic leukaemia, and autoimmune diseases such as rheumatoid arthritis, and granulomatosis with polyangiitis (Stübgen, 2008; Pierpont et al., 2018; Leandro and Isenberg, 2021). Rituximab's target is CD20, a 33–37 kDa transmembrane protein that is highly expressed on the surface of immature and mature B-lymphocytes, but not on inactive plasma cells, or pro-B cells. The exact function of CD20 is not fully understood, although it is hypothesised to act as a calcium channel subunit (Pavlasova and Mraz, 2020).

Rituximab depletes immature and mature B-cells by binding CD20 and triggering CDC and ADCC against the B-lymphocytes (Clynes et al., 2000). Rituximab inactivates the transcription factor signal transducer and activator of transcription 3, and triggers intercellular apoptotic pathways by upregulating the apoptosis signalling molecule Bax, and downregulating c-myc (Alas and Bonavida, 2001). This results in nuclear condensation and degradation of cellular proteins (Maloney et al., 1994; Reff et al., 1994). The B cell depletion occurs rapidly following administration, with effects lasting 2-3 months in a dose-dependent manner, and reportedly up to 6-12 months in some patients (Bergantini et al., 2020). As demand for mAbs, such as Rituximab, has surged due to their broad therapeutic potential, the manufacturing processes for these biologics have undergone substantial refinement. Today, the production of mAbs follows a highly standardised and scalable process, ensuring both efficiency and consistency across different antibody products. Rituximab's well-characterised structure, extensive clinical

use, and robust production methods make it an ideal model antibody for the development and optimisation of chromatography techniques.

1.4. Manufacture of Monoclonal Antibodies

Most mAbs used in therapeutic applications are of the IgG1 subclass, though other subclasses such as IgG2 and IgG4 are also utilised in certain cases. The manufacture of these therapeutics often follows a unified platform process, which is widely applied to the majority of mAbs though some modification may be required depending on the specific product. This platform process is divided into upstream and downstream processing stages.

This framework is adjusted based on the physicochemical characteristics of the product, such as isoelectric focusing point (pI), hydrophobicity, glycosylation, structural modifications such as chimeric additions or drug payloads, and propensity for aggregation. For example, some mAbs are prone to aggregation under low pH environments (typically pH 3-5), therefore the amount of time spent at low pH and the neutralisation strategy are critical considerations to prevent aggregation and maximise product yield. This may require screening a range of neutralisation buffers at different concentrations to minimise product loss. Although this part of the process is modified to accommodate for the properties of the target molecule, other unit operations such as centrifugation, filtration, and chromatography will typically remain unchanged.

The broad applicability of this platform approach simplifies and accelerates regulatory approval due to the use of well-established processes validated in previous therapies. Newer molecules can reference similar purification strategies from already approved

molecules, citing them as precedent. This is often done through comparability or bio similarity, reducing the need to fully validate every process as if it were a new or experimental process. While this conservatism in the bioprocess industry ensures safety and consistency, it can also make the introduction of innovative techniques, such as continuous bioprocessing or single-use technologies, challenging (Farid, 2007).

The production of mAbs is inherently a multi-stage process, with each phase contributing to the overall quality, yield, and safety of the final therapeutic product. To ensure consistent manufacturing, the platform process is typically divided into two key stages: upstream and downstream processing. Upstream processing focuses on optimising production of the desired antibody through careful cell line selection, such as Chinese hamster ovary (CHO) cells, and bioreactor optimisation, while downstream processing ensures the final product's purity, potency, and suitability for clinical use by removing impurities and contaminants through multiple filtration and chromatography steps. Each of these stages plays a critical role in achieving high product quality and maintaining regulatory compliance, and thus warrants a detailed examination.

1.4.1. Upstream processing

Monoclonal antibodies are usually expressed in mammalian cell lines, such as CHO cells, NS0 myeloma cells, or PER.C6 cells (Li et al., 2010; Gronemeyer et al., 2014). These cell lines have several advantages; (i) they are capable of all the post translational and glycosylation events required which enhances product stability, (ii), they are reliably capable of producing product titres of 5 $g \cdot L^{-1}$ in a typical 14 day batch (Shukla et al., 2017), (iii), they are well established with a wealth of research and documentation, and

(iv), are less likely to generate an immunogenic product because of their mammalian physiology. Other cell types have been experimented with, such as insect (Palmberger et al., 2011), yeast (Barnard et al., 2010; Berdichevsky et al., 2011), plants (Hiatt et al., 2014; Sheshukova et al., 2016), and bacteria (Levy et al., 2001). These alternative lines have distinct advantages, as they are easier and cheaper to grow at scale. For example, plant cell lines do not need to be maintained at 37 °C for optimal growth, and bacteria do not need expensive media additives, such as foetal calf serum. Additionally plant, insect, and bacterial cell lines are unlikely to harbour infectious viruses that are harmful to patients (Levy et al., 2001; Pogue et al., 2010). However, despite these studies and advantages, mammalian cell lines remain dominant due to their similar physiology, capacity to perform post-translational modifications and well-established use. Most mammalian cell lines now utilise chemically defined, serum-free media in industrial production processes to avoid the variability and contamination risks associated with serum additives.

Upstream manufacturing involves expression of the product and growth of recombinant cell lines expressing in a bioreactor. Cell lines are cultured in large bioreactors (>10,000 L) and are typically stirred batch fed reactors (Kelley, 2009; Chen et al., 2018). In these systems, nutrients such as glucose and amino acids are added incrementally to avoid nutrient depletion and minimise toxic by-product accumulation, allowing for higher cell densities and protein production. For mammalian cell culture, parameters such as dissolved oxygen (30-50%), carbon dioxide (5%), temperature (37 °C), pH (7.0 – 7.4), optical density, and waste products are continuously monitored and adjusted as needed (Lindskog, 2018). These parameters are carefully controlled to ensure optimal cell growth

and productivity, as oxygen is crucial for aerobic respiration, pH influences cellular metabolism and protein folding, and waste products such as lactate and ammonia can inhibit cell growth if not properly managed. Once a sufficient titre (>5 $g \cdot L^{-1}$ of product) is achieved, usually 10-14 days after seeding, the reactor contents are drained for downstream processing (Kelley, 2009).

1.4.2. Downstream processing

Downstream processing (DSP) begins immediately following the harvest of the bioreactor and is designed to purify and stabilise the mAb. This multi-stage process is divided into clarification, primary capture, polishing, and formulation, with each stage serving a critical role in removing contaminants and refining the product for clinical use.

1.4.2.1. Clarification & Feedstock additives

Feedstock collected from the bioreactor contains cells, cellular debris, organelles, DNA fragments from lysed cells, and host cell proteins (HCP); these large molecular weight contaminants give the feedstock a turbid appearance, typically quantified by optical density. Clarification aims to remove these contaminants to prepare the feedstock for downstream processing, improving process efficiency and extending the lifespan of chromatography media by preventing fouling.

Feedstock additives are employed to aggregate contaminants, facilitating their removal during size-based clarification processes. These additives enhance clarification efficiency, process yield, and clearance of impurities during mAb recovery (Kang et al., 2013). The range of chemicals that can aid clarification steps are diverse, including sugars

(Riske et al., 2007), caprylic acid (Brodsky et al., 2012; Zheng et al., 2015; Trapp et al., 2018), salts (Ko and Ahn, 2007), and polymers (Kang et al., 2013; McNerney et al., 2015). For example, chitosan is a polysaccharide, chemically modified by deacetylation. This results in a semi-soluble positively charged polymer at acidic and neutral pHs, which readily interacts with cellular debris that is often negatively charged at the same pH, such as DNA and cellular debris. This interaction results in the separation of the feedstock and the cellular debris (Riske et al., 2007). These additions will increase the mean particle size in the feedstock, assisting later size-based separation strategies, particularly centrifugation.

Centrifugation serves as the primary technique for separating large molecular weight materials from the feedstock. Centrifugal force is not a true force but rather the effect of inertia in a rotating system, which causes particles to separate based on their density. This method effectively isolates significant contaminants such as cells and cell fragments. In large-scale operations, disk stack centrifuges are preferred due to their efficiency in processing large volumes (Kempken et al., 1995; Bender and Wolk, 1998; Kelley, 2007). These devices feature a series of static disks within a rotating bowl, which maximises the sedimentation area and minimises the path required for settling, allowing for rapid and continuous operation (Shukla and Kandula, 2008; Ott et al., 2022). Commercial centrifuges such as the Alfa Laval PureFerm 750 are capable of processing up to 25,000 $L \cdot h^{-1}$. As the centrifuge separates components purely with mechanical force, there is no chemical alteration of the feedstock that requires further processing, however, product quality should be monitored, as centrifugation can impose shear stress on the product, causing unwanted product aggregation (Hutchinson et al., 2006; Rayat et al., 2016). Shear

stress, resulting from high-speed rotation during centrifugation, can lead to protein denaturation or aggregation, negatively impacting product quality and yield. However, shear stress can often be mitigated by optimising centrifuge design, speed, and feed flow rate.

Another method employed is depth filtration, which uses a multi-layered structure to trap a spectrum of particle sizes. Unlike traditional membrane filters with fixed pore sizes, depth filters are usually composed of three parts; (i) a fibre matrix (typically cellulose or polypropylene fibres) bound with a binder to provide structural rigidity and a porous base matrix (Ostreicher et al., 2019); (ii) a filter aid (diatomaceous earth or perlite) which enhances the filtration capacity by increasing the porosity and surface area of the filter (Khanal et al., 2018), usually applied as a pre-coat layer; and (iii) a positively charged binding agent that binds negatively charged biomolecules such as DNA fragments and HCP that are negatively charged at physiological pH, unlike antibodies which are typically neutral or protonated (pI 7-8). The electrostatic interactions between the negatively charged cellular debris and the positively charged binding agent retains smaller molecules that would otherwise pass through the porous matrix (Nejatishahidein and Zydney, 2021). This configuration allows for effective mechanical and electrostatic filtration, trapping larger particles near the surface and smaller ones deeper within the matrix.

Centrifugation and depth filtration complement each other effectively. While centrifugation quickly removes larger, denser particles, depth filtration addresses smaller particles embedded within the feedstock. Together, these methods significantly enhance the removal of cellular debris, paving the way for subsequent purification stages.

1.4.2.2. Primary Capture & Polishing

Primary capture and polishing are critical phases in the mAb manufacture process, employing chromatographic techniques to isolate and purify the target product. During Primary Capture and Polishing, several steps are conducted sequentially: (i) separation of the target product from the remaining components in the bioreactor such as cell culture media, and small proteins that were not removed during clarification; (ii) rapid concentration; and (iii) enhancing purity to meet the required specification. This is achieved using chromatography, a technique that separates mixtures based on their differential retention to the stationary phase. In these steps, the product is either retained while unwanted byproducts pass through, or vice versa. Details of the exact chromatography mechanisms will be expanded upon in **Section 1.5.**

Primary Capture is the initial separation of mAbs from the bulk fluid, cell culture media, nutrients, and smaller proteins and lipids that were not previously removed during clarification. Because the feedstock is highly concentrated with product, as high as 5-10 $g \cdot L^{-1}$ (Shukla et al., 2017), primary capture prioritises processing speed and total capacity. This is typically achieved using affinity chromatography resins, which bind specific parts of the antibody. Before polishing, a low-pH hold is common for viral inactivation. As the elution of many affinity chromatography steps requires exposure to a low-pH buffer, this step is prolonged to ensure maximum viral inactivation before proceeding to polishing for dedicated aggregate removal.

Polishing is implemented after primary capture to further enhance purity, using additional chromatography steps that utilise different binding mechanisms than those used in

primary capture, such as cation and anion exchange chromatography (CEX, and AEX). The purpose of polishing is to further remove small contaminants, DNA fragments, HCP, high-molecular weight aggregates, and leached ligands from the previous affinity chromatography step. A deeper exploration of affinity chromatography and ion exchange chromatography for bioprocessing will be presented in the next **Section, 1.5.**

1.4.2.3. Final Formulation

The final step in the traditional mAb platform process is ultrafiltration and diafiltration, to concentrate the product, perform buffer exchange, and as a final viral removal step. Here, high salt buffers from ion exchange elution are removed and exchanged for storage buffers. These usually employ cellulose, polyvinylidene difluoride or polyether sulfone based filters with pore sizes as low as 10 – 400 angstroms, resulting in a molecular weight cut-off as low as 3 kDa. Aqueous buffer is passed into the permeate while the product is concentrated in the retentate. As the volume of the retentate decreases, the product is concentrated. This can concentrate the target product as high as necessary to achieve the appropriate therapeutic dosage (Shire et al., 2004; van Reis and Zydney, 2007; Zydney, 2016). The concentrated buffer can subsequently be displaced by the final buffer of interest, using the same system, completing the product formulation.

1.5. Chromatography methods in Bioprocessing

Chromatography plays a central role in the bioprocessing industry, particularly in the purification and characterisation of mAbs, and other proteins. As a cornerstone of downstream processing, chromatography is fundamental to both the high-throughput purification of biotherapeutics and their rigorous quality control**,** ensuring that products

consistently meet the stringent regulatory standards required for clinical use (Jagschies et al., 2007; Carta and Jungbauer, 2020).

Several chromatography techniques are routinely employed across the various stages of bioprocessing, including capture, intermediate purification, and polishing**.** These methods, such as ion exchange chromatography (IEX)**,** affinity chromatography**,** size exclusion chromatography (SEC)**,** and hydrophobic interaction chromatography (HIC), exploit specific physicochemical properties of proteins and biomolecules, allowing for highly selective separation. By leveraging differences in charge, size, hydrophobicity, and binding affinity, these techniques are essential for achieving high-purity biotherapeutic products. A detailed examination of each technique follows.

1.5.1. Ion Exchange Chromatography

Ion exchange chromatography (IEX) exploits differences in net charge between solutes for separation. All amino acids contain an amino group, and a carboxylic acid group, and a variable side chain (R group), which differentiates the amino acid. Each of these groups can carry a charge. For example, the amino groups carry a positive charge when protonated ($-NH_3^+$), while carboxylic acid groups carry a negative charge when deprotonated (COO^-). Because amino acids can possess positively and negatively charged groups simultaneously, they are known as zwitterions. The degree of protonation versus de-protonation is dictated by the pH environment. The pH at which the protein has no net charge (equal positive and negative charge) is known as the isoelectric point (IEP) (Fekete et al., 2015; Cummins et al., 2017).

IEX exploits differences in the net charge of solutes for separation. The pH of the aqueous environment is adjusted to modulate the net charge of the target protein relative to the stationary phase. This stationary phase, which may carry either a positive charge (anion exchanger) or a negative charge (cation exchanger), enables selective interaction with oppositely charged solutes. Many mammalian secretome proteins have isoelectric points (pI) in the range of 4.3–7, while mAbs typically range from 6.1 to 9.4 (Goyon et al., 2017; Kornecki et al., 2017). This provides a strong basis for separating otherwise closely related proteins through careful adjustment of pH and ionic strength during the chromatographic process.

Binding of the solute occurs in a low-salt environment; here, solutes bearing a charge opposite to that of the stationary phase will bind (Fekete et al., 2015; Cummins et al., 2017). To elute, a high salt buffer (such as 1 M sodium chloride or sodium sulphate) is used that contains strongly charged ions. The dissolved ions, typically having higher ionic strength, effectively compete with the bound solutes for binding sites, thus displacing them. This process employs a step gradient. For a more nuanced separation, a salt gradient can be used to further differentiate closely related proteins. With a gradient, proteins with similar net-charges can be separated into discrete elution peaks, however, this is mainly useful for analytical purposes, rather than manufacturing purposes.

AEX and CEX resins are divided into strong and weak ion exchangers. Strong exchangers remain charged across the full pH range, whilst weak exchangers are only charged in a fixed pH range. The name weak and strong exchanger describes the tightness of the interaction and the pH range to which the resin remains charged. A strong exchanger typically has stronger binding than a weak exchanger, and remains charged across the full

pH range (Cummins et al., 2017). Examples of strong and weak CEX and AEX ligands are sulfonic acid or carboxylic acid groups (CEX strong and weak, respectively), and quaternary ammonium or amine groups (AEX strong and weak, respectively).

CEX and AEX resins have very high maximum binding capacities (100-200 mg protein·mL resin-1) compared to other techniques and are excellent at separating closely related proteins, which are otherwise very challenging to separate via other methods, making ion exchange indispensable for achieving high purities (Fekete et al., 2016; Madadkar et al., 2017). A CEX resin employed in bind and elute mode is highly effective at removing HCPs, leached Protein A, and high molecular weight (HMW) aggregates. Alternatively, an AEX resin can be employed in flowthrough mode. In this mode, the pH of the mobile phase is adjusted so IgG possesses no net charge (near neutral, depending on the mAb). Negatively charged contaminants will bind as IgG passes in the flowthrough. In these polishing applications, CEX and AEX resins excel. Often a bind and elute CEX, and a flowthrough AEX step is paired together for complete polishing.

It is also simple to predict the isoelectric focusing point of the target protein, which can be predicted from its amino acid sequence. This prediction informs the selection of a suitable mobile phase pH and ion exchange resin. However, this can be complicated by post-translational modifications such as glycosylation, which may alter the charge. Therefore, small-scale trials are essential before proceeding to large-scale production.

Because a high salt buffer is required for elution, a buffer exchange is usually required immediately afterwards, adding further complexity and cost to the process, unless a

complementary step can be used instead. HIC requires high salt to initiate binding, thus it can be neatly paired with ion exchange, without the need for further processing.

1.5.2. Affinity Chromatography

Affinity chromatography exploits chemical or biological interactions between ligand and solute. These interactions are highly specific, and thus affinity resins cannot be applied broadly to a range of molecule types, unlike other resins. These resins are routinely employed in the primary capture step. For mAbs, Protein A chromatography is by far the most widely used; however, alternatives such as Protein G, and Protein L are also available.

Protein A is found on the surface of *Staphylococcus aureus, (Staphylococcus Protein A, or SPA)* which readily binds IgG_1, IgG_2, and IgG_4 between CH_2 and CH_3 in the Fc region. This protein has evolved as a key virulence factor for the pathogen that hinders the host immune response. SpA protects the bacterium by binding to the Fc region of IgG antibodies, preventing opsonisation, and host effector functions (Jendeberg et al., 1995; Jendeberg et al., 1997; Kanje et al., 2020). Protein A also binds antibody variable H chains when encoded by the VH_3 gene family. Binding to this sub-population of IgGs has been shown to trigger B-cell apoptosis, weakening the host immune system (Hillson et al., 1993; Goodyear and Silverman, 2003). Approximately 50% of serum antibodies are encoded by this gene (Schroeder and Cavacini, 2010).

Protein A has been exploited for the purposes of affinity chromatography. These resins use Protein A as the ligand, exploiting the natural affinity of Protein A for IgG Fc region. In Protein A affinity chromatography, optimal binding occurs at pH 6.0-9.0. Mobile phase

conductivity for optimal binding varies if the ligand has been genetically modified, but native Protein A ligands bind under physiological conditions (Bio-Rad, 2016; Cytiva, 2021). Elution is caused by using a low-pH buffer such as 0.1 M sodium citrate pH 3.0 – 6.0. A low pH hold is often employed as a convenient viral inactivation step, (Shukla et al., 2007a; Mazzer et al., 2015; Imura et al., 2021). However, exposing the product to a low pH environment frequently results in the generation of antibody aggregates, which later must be removed during polishing.

Protein A resins offer high binding capacities and high specificity for IgG. However, they suffer from several disadvantages, including high costs of $8,000 – $15,000/L, ligand leaching, fouling from non-specific interactions, and caustic instability. To address these concerns, modern Protein A resins feature a recombinant Protein A ligand, modified with greater binding capacities, and greater tolerance of extreme pHs for elution and cleaning purposes (outside pHs 4-10). These changes enhance the resins lifespan and allow for thorough cleaning regimens to be employed (Müller and Vajda, 2016; Pabst et al., 2018; Ramos-de-la-Peña et al., 2019). When protein A chromatography is removed from a process, cost of manufacture is reduced by 20% (Gupta et al., 2021; Bansode et al., 2022). Despite these savings, Protein A resins remain the dominant method of performing primary capture.

Given the significant financial burden imposed by Protein A chromatography, researchers have explored alternative proteins, such as Protein G and Protein L. However, they have not experienced widespread adoption. Protein G requires lower pH environments for elution (pH < 2.5), which exposes the product to harsher conditions, potentially compromising stability, and is less specific than Protein A (Bio-Rad, 2016). Protein L

selectively binds antibodies with kappa light chains and is therefore less versatile. Despite ongoing research and development efforts, the industrial preference still leans towards Protein A due to its robust performance and well-established protocols. Nevertheless, the economic pressures associated with Protein A continue to drive the search for more cost-effective and versatile alternatives.

1.5.3. Size Exclusion Chromatography

Size exclusion chromatography (SEC) separates solutes based on their size. Unlike other adsorptive techniques, SEC utilises a purely size-based exclusion mechanism, with neither binding nor elution involved. The stationary phase is devoid of ligands, and instead, features a chromatography resin with a spectrum of pore sizes. For example, a Superdex® 200 increase 10/300 SEC column manufactured by Cytiva has a fractionation range of 10 – 600 kDa, achieved by a range of pore sizes that retain proteins of different molecular weights. This results in solutes of varying sizes being retained differently by the stationary phase. In this example, IgM (900 kDa) would elute very early, being excluded from all pores. Conalbumin (76 kDa), being smaller, enters more of the available pores and thus would elute later as it is retained to a greater extent. (Barth et al., 1994; Ricker and Sandoval, 1996). Ferritin (450 kDa) being an intermediate size would be mildly retained by the stationary phase, entering only the larger pores.

Ideally, only the steric effects of the pores would impact the separation. However, unexpected hydrophobic and electrostatic interactions between the solute and the stationary phase may occur. This interaction increases the retention of solutes undergoing these interactions, potentially interfering with accurate size estimations. Electrostatic

interactions can be nullified by increasing the salt in the mobile phase, and Hydrophobic interactions can be avoided by modifying the mobile phase (Cytiva, 2024).

SEC is highly useful for analytical chromatography. By separating components into different fractions, SEC results in a lower concentration of each individual component in its respective fraction. Nevertheless, SEC is extremely useful for analysing samples, particularly aggregate analysis and estimating purification. For example, in large-scale antibody production, analysing a small sample by SEC can determine the efficacy of HCP removal and assess the aggregation state of the product (Brusotti et al., 2018). SEC is also very effective at buffer exchange and desalting because smaller buffer components, such as salts, elute later after penetrating the porous matrix, while larger proteins elute earlier, bypassing these pores**.**

1.5.4. Hydrophobic Interaction Chromatography

Hydrophobic interaction chromatography (HIC) is a versatile adsorptive technique, which uses hydrophobic ligands to interact with non-polar regions on the solute surface. As such, HIC is favoured as a "gentle" technique ideal for delicate biomolecules, as it does not rely on harsh buffers for binding or elution **(Figure 3)**. The selectivity of HIC is orthogonal to ion exchange (IEX), and thus the two techniques are often employed together. This is especially useful as IEX requires elution in high salt buffers, and HIC requires binding with salt. HIC is often used to separate closely related proteins and oligomeric states (Shukla et al., 2006; McCue, 2009; Liu et al., 2010; Ewonde et al., 2022).

HIC was first described by Tiselius as salting out chromatography (Tiselius, 1948). HIC then rapidly developed into its modern iteration in the 1970s - 1980s by several pioneering

groups, (Er-el et al., 1972; Hjertén, 1973; Hofstee, 1973; Porath et al., 1973; Shaltiel and Er-El, 1973; Hjertén et al., 1974; Hofstee, 1976; White et al., 1981; Hjertén et al., 1986). Since then, HIC has seen extensive use in bioprocessing, mostly in analytical or polishing tasks because of low binding capacities compared to ion exchange (IEX) and affinity chromatography (AC).

1.5.4.1. HIC Theory

The strength of the solute-ligand hydrophobic interaction is modulated by various salts in the mobile phase (Shukla et al., 2006; Zhang and Cremer, 2006; Ewonde et al., 2022). The Hofmeister series (**Figure 3**, and **Figure 4)** classifies cations and anions as kosmotropic or chaotropic based on their ability to regulate hydrophobic interactions. Chaotropes disrupt water-water and like-like interactions, promoting heterogeneous protein-water interactions (Zhang and Cremer, 2006). This increases protein solubility, as water molecules will readily interact with proteins while chaotropic salts are present. Conversely, kosmotropes promote like-for-like or homogeneous interactions; they strengthen water-water and non-polar-non-polar interactions. As such, they promote binding between non-polar regions on the solute surface and hydrophobic ligands. The like-like nature of these bonds causes protein precipitation at high concentrations, as water molecules preferentially interact with each other rather than the protein surface. This phenomenon is known as salting out and is well documented with kosmotropic salts (Green and Hughes, 1955; Dixon and Webb, 1961; Scopes, 1993; Duong-Ly and Gabelli, 2014). In HIC, kosmotropic salts in the mobile phase promote binding. The most common salt employed in HIC is ammonium sulphate (hereby referred to as AS). In HIC, binding

occurs at high salt (typically >1000 mM) and elution is induced by lowering the salt concentration.

To separate by hydrophobicity, a high-to-low salt gradient is used. Solutes elute in order of least-to-most hydrophobic. This can be used to separate closely related oligomeric states, such as aggregates from monomers. HIC can also be used in flow-through operation, selectively retaining aggregates; this can be used as a powerful polishing step in bioprocess separations.

HIC suffers from several limitations compared to other chromatographic techniques: (i) lower maximum binding capacities, typically in the range of 10–30 mg/mL resin, versus the 50–100 mg/mL achievable with ion exchange or affinity resins; (ii) its utility is constrained by ligand density, as high densities can denature proteins or cause irreversible binding due to excessive hydrophobic interactions; and (iii) its reliance on high concentrations of kosmotropic salts, such as AS, introduces additional challenges. These salts, while essential for stabilising hydrophobic interactions, require subsequent buffer exchange prior to final formulation. Furthermore, their ecological risks, including toxicity to aquatic ecosystems, necessitate specialist disposal methods, increasing operational costs. Innovative approaches such as low-salt or temperature-modulated HIC have been proposed to mitigate some of these drawbacks.

Despite widespread use, the exact nature of the solute-ligand interaction remains unclear. A couple of competing theories have emerged to explain these; one of the earliest is the Solvophobic theory that cites surface tension as the major driver of binding/elution

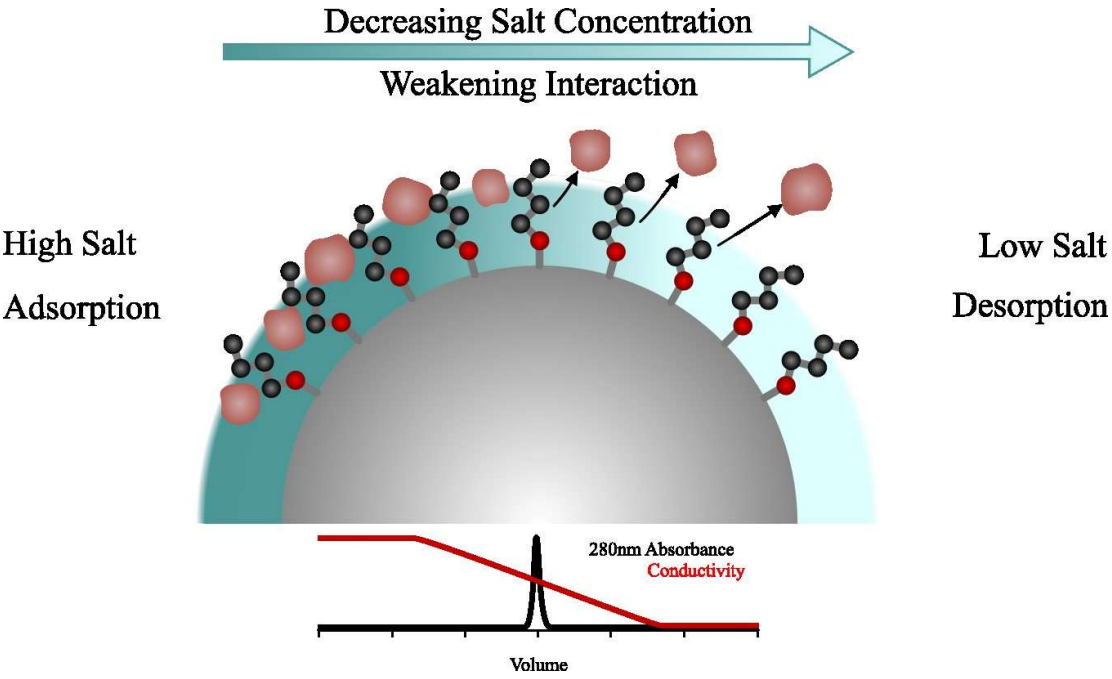

Figure 3: Representation of Hydrophobic Interaction Chromatography. HIC resins use non-polar ligands to attract hydrophobic solutes. Absorption of hydrophobic solutes to the stationary phase is promoted in the presence of kosmotropic salts, as described by the Hofmeister series. The strength of the hydrophobic interaction is increased with the concentration of kosmotropic salts in the mobile phase. An example chromatography trace depicts a typical HIC gradient, running from high to low salt. When the hydrophobic interaction is sufficiently weakened to cause elution, a peak is observed at 280 nm. Original image produced using Inkscape 1.2.2.

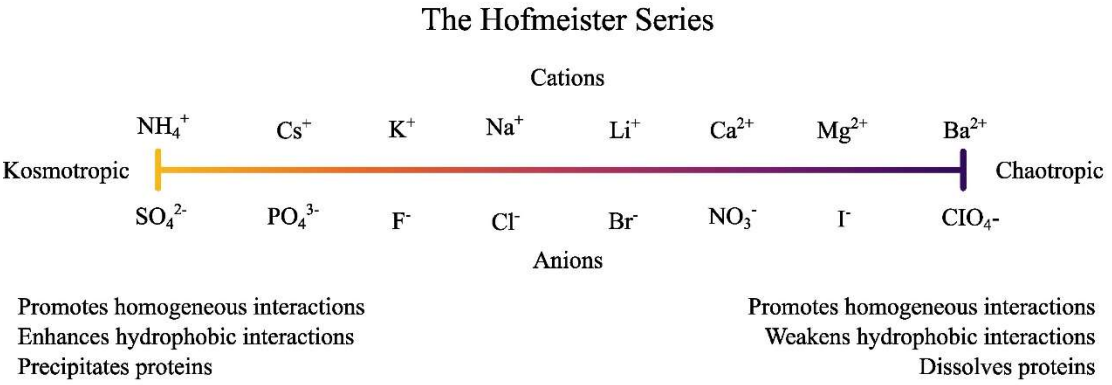

Figure 4: Hofmeister Series of Salts, showing the categorisation of cations and anions as kosmotropic or chaotropic based on their effect on proteins in aqueous solutions. Kosmotropes enhance hydrophobic interactions by strengthening hydrogen bonds between water molecules, which indirectly enhances hydrophobic interactions. Kosmotropes promote homogeneous, or "like-for-like," interactions such as water-water and protein-protein interactions. Conversely, chaotropes promote heterogeneous interactions, such as polar-nonpolar interactions. By promoting heterogeneous interactions, they reduce the probability of homogeneous interactions occurring, thereby reducing the adsorption of nonpolar residues to hydrophobic ligands. Original image produced using Inkscape 1.2.2.

(Horvath et al., 1976). According to Horvath, an increase in the surface tension of the mobile phase enhances the thermodynamic favourability of hydrophobic interactions. This increase in surface tension leads to a stronger tendency for water molecules to form hydrogen bonds among themselves rather than with hydrophobic groups. Consequently, proteins with hydrophobic patches are driven towards the like-for-like non-polar interactions with the hydrophobic ligands of the HIC stationary phase (Horvath et al., 1976). Reducing the salt concentration allows water-protein hydrogen bonds, thus the protein dissolves back into the mobile phase (Horvath et al., 1976; Melander and Horváth, 1977; Shukla et al., 2006).

Another theory emphasises the interaction of two phenomena: Van der Waals forces and electrostatic interactions (Srinivasan and Ruckenstein, 1980). The authors propose that electrostatic interactions dominate in low-salt environments, whilst Lyotropic salt effects dominate at higher salt concentrations. Kosmotropic salts such as AS enhance van der Waals forces between solute and ligand, and chaotropic salts and organic solvents reduce these forces. Srinivasan points to the role of an electrical double layer on the surface of the stationary phase as a contributing factor.

HIC is commonly employed in bioprocessing in two main operating modes: (i) bind and elute, and (ii) flowthrough. In the bind-and-elute mode, a fixed quantity of feedstock is applied to the chromatography column, followed by washing with an equilibration buffer to remove non-bound or loosely bound proteins. A lower-conductivity buffer is then applied to elute the bound proteins. In contrast, flowthrough operation involves applying a feedstock enriched with a specific salt concentration, enabling selective binding of a subpopulation of proteins while the remainder is collected in the flowthrough.

This sensitivity to subtle variations in hydrophobicity makes HIC particularly advantageous for polishing applications, especially in the context of antibody manufacture. Aggregated or misfolded antibodies, which exhibit higher hydrophobicity compared to their correctly folded monomeric counterparts, can be selectively removed through optimisation of salt conditions and stationary phase selection. This approach has been routinely applied in the bioprocessing of mAbs prone to aggregation, improving product quality and stability.

1.5.4.2. Temperature Effects in HIC

Temperature significantly influences binding and elution performance in HIC, an effect well-established in literature (Grinberg et al., 1989; Geng and Chang, 1990; Haidacher et al., 1996; Vailaya et al., 1996) and recognised by commercial resin manufacturers (TOSOH, 2018; Cytiva, 2020). Understanding this relationship is essential for optimising HIC processes, especially when aiming for temperature-controlled elution.

The retention coefficient (κ') in HIC, which quantifies the strength of solute retention by the stationary phase, is influenced by temperature (Er-el et al., 1972; Queiroz et al., 2001; Lienqueo et al., 2007). The relationship is described by **equation 1** below:

$$\ln \kappa' = \ln \varphi - \left(\frac{\Delta G}{R\Phi}\right) \qquad \textbf{(1)}$$

Where κ' quantifies the degree to which the solute is retained by the stationary phase, the greater κ', the stronger the hydrophobic interactions are between the solute and stationary phase. φ represents the phase ratio, which is defined as a volume ratio of stationary phase to the inter-particle volume (void volume). It represents the quantity of chromatography

support available for binding. ΔG represents the change in Gibbs free energy, indicating the thermodynamic favourability of the binding interaction. A negative ΔG indicates that the solute's binding to the stationary phase is thermodynamically favourable, reflecting stronger hydrophobic interactions under given conditions. R is the Universal Gas Constant. Φ represents the temperature in kelvin.

As **Equation 1** illustrates, temperature plays a significant role in modulating hydrophobic reactions in HIC. Generally, increasing the temperature raises the retention coefficient (κ') by strengthening the hydrophobic interactions between the solute and the stationary phase. In practical terms, this effect can enhance solute binding under higher temperatures, which can be especially advantageous in reducing the reliance on high salt concentrations.

The Langmuir model (**Equation 2**) is also commonly applied to describe binding behaviours at equilibrium in HIC systems:

$$q* = \frac{q_{max} c^*}{K_D + c^*} \quad \textbf{(2)}$$

Where q^* is the amount of protein bound to the stationary phase at equilibrium, qmax is the theoretical maximum binding capacity, c^* represents the concentration of free protein in solution, and K_D is the dissociation constant, indicating the binding affinity, with smaller values reflecting stronger binding.

Several studies have investigated the effects of temperature on HIC, though it has yet to be fully exploited for elution purposes (Haidacher et al., 1996; Muca et al., 2009a; Müller et al., 2013; Bobaly et al., 2016). The most comprehensive investigation into temperature

as a practical mechanism of elution is by Müller & Franzreb (2012), who systematically examined the influence of temperature on HIC resins, including Phenyl Sepharose 6 Fast Flow (Fast Flow is hence forth abbreviated to FF), Butyl Sepharose 4FF, and Octyl Sepharose 4FF. Using varied temperatures (Φ = 40, 25, and 10 °C) and AS concentrations (0.1, 0.3, and 0.5 M), they found that Butyl Sepharose 4FF showed the most pronounced temperature-dependent changes in binding with bovine serum albumin (BSA). The weak hydrophobicity of the butyl ligand made it particularly responsive to temperature changes, as indicated by the significant difference in the difference in bound protein across temperatures ($\Delta q\Phi$).

Furthermore, in experiments with a binary feedstock containing BSA and lysozyme, Müller and Franzreb demonstrated selective binding by applying the feed at 40 °C. Under these conditions, lysozyme passed through the column without binding, while BSA was retained. Subsequently, lowering the column temperature to 10 °C facilitated BSA elution. This study highlighted temperature's role as a potential independent elution mechanism, although not all bound BSA could be removed solely by temperature manipulation.

These findings underscore the potential of temperature-controlled HIC for continuous chromatography applications, where temperature rather than mobile phase composition could regulate binding and elution. This method could also reduce the need for kosmotropic salts, lowering process costs and environmental impact while simplifying buffer requirements. Müller and Franzreb (2012) used BSA as the model protein in their chromatography research. To further explore temperature-assisted HIC it is important to

describe the model protein that will be used to further expand this work. BSA has been widely employed due to its well-characterised structure and accessibility.

1.6. Albumin as a model protein in Chromatography Research

Albumin, one of the most abundant proteins found in blood plasma, plays a pivotal role as a transport protein and an osmotic regulator. Human serum albumin (HSA), synthesised in the liver, constitutes approximately 50% of all plasma proteins, with a typical concentration range of 34 – 54 mg·mL^{-1} (Fanali et al., 2012; Moman et al., 2017). Structurally, albumin is a 583-residue heart shaped protein, with three α-helix-rich domains, each containing two sub-domains connected by flexible loops (Sugio et al., 1999; Bhattacharya et al., 2000; Kragh-Hansen et al., 2002; Topală et al., 2014).

This intricate quaternary organisation is stabilised by 17 disulfide bonds and a single cysteine residue, which, when covalently linked, reduces the rate of aggregation (Kragh-Hansen, 1990; Militello et al., 2003; Holm et al., 2007).

Albumin can bind a wide range of molecules, including bilirubin, ions, fatty acids, amino acids, and metals (Peters Jr, 1995; Kragh-Hansen et al., 2002; Fanali et al., 2012; Sargent, 2018). As albumin is a highly soluble protein, this binding enhances the solubility and reduces the toxicity of these molecules (Kragh-Hansen et al., 2002). For instance, the binding of albumin to fatty acids enhances their solubility the which have a low aqueous solubility (<1 μM) allows for their efficient transport in the serum (Bhattacharya et al., 2000). Binding of albumin to fatty acids occurs at nonpolar regions in the crevices between its subunits. Additionally, serum albumins bind to various lipophilic drugs, including methadone, propranolol, thiopental, furosemide, warfarin, methotrexate,

alfentanil. Sudlow et al describes two drug interaction sites that binds carboxylic acids, heterocyclic molecules, and aromatic carboxylic acids; however, these do not account for all the molecules albumin interacts with (Sudlow et al., 1975; Kragh-Hansen et al., 2002; Moman et al., 2017).

Serum albumins also regulate osmotic pressures within the blood plasma, as seen in albumin deficiency (Moman et al., 2017). Albumins impact on osmotic pressure is disproportionate to its high concentration. Under physiological conditions, the net negative charge of albumin attracts cations, increasing electrolyte concentration in the serum and thereby enhancing osmotic potential (Pappano et al., 2013).

Albumin is easily separated from plasma via heat shock fractionation, cold ethanol precipitation, or chromatography. In heat shock fractionation, the serum is heated to 60 °C with 40 mM caprylic acid. Most serum proteins are not stable under these conditions and form an insoluble coagulum. The soluble albumin can be concentrated via ultrafiltration or precipitation. This process can achieve purities > 98% (Denizli, 2011; Sargent, 2018). Alternatively cold ethanol precipitation developed by Cohn et al. (Cohn et al., 1946), uses the addition of ethanol in five stages to fractionate various plasma proteins (Cohn et al., 1946; Burnouf, 2007; Denizli, 2011; Sargent, 2018). Albumin is one of the last proteins to precipitate in fraction V, and precipitates at 40% ethyl alcohol, pH 4.8. Albumin can also be separated by ion exchange, or affinity chromatography via the Cibacron Blue F3GA ligand (Besselink et al., 2015; Balkani et al., 2016; Raoufinia et al., 2016; Rios et al., 2023).

As albumins are separated from blood plasma, BSA is readily available as a biproduct of cattle farming. As the plasma is so accessible, it has quickly become a model protein in research. In solutions, BSA forms dimers and other HMW structures, with the ratio of these forms influenced by the aqueous environment and the presence of inorganic salts (Bloomfield, 1966; Holm et al., 2007; Madeira et al., 2022). This property is likely a result of the multiple non-polar regions exposed on the surface of the protein, usually present for fatty acid binding. BSA dimer formation is likely a result of hydrophobic interactions achieved by molecules that overcome electrostatic repulsion of similarly charged protein molecules (Babcock and Brancaleon, 2013). The degree of aggregation is dependent on the protein concentration, and presence of inorganic salts. Specifically, more high-molecular weight oligomers form at less than 0.4 $g \cdot L^{-1}$, and maximum formation is achieved at NaCl concentrations of 0.125 M. The type of inorganic salt added also significantly alters high-molecular-weight oligomer formation (Madeira et al., 2022).

Due to their concentration in plasma, functional importance, and ease of separation, serum albumins are inexpensive and have been widely used in research, (Peters Jr, 1995; Raoufinia et al., 2016). BSA is particularly common, due to its low cost and ease of access.

The propensity of BSA to form monomers, dimers/trimers and higher order structures makes it ideal as a candidate molecule for studying purification, as it naturally forms a range of oligomers with a variety of physicochemical properties. Larger oligomers of BSA will be more hydrophobic, hence presenting an interesting opportunity for temperature-based HIC. These molecules may be preferentially retained, provided that the correct salt and temperature is employed.

1.7. New DSP Technologies - Continuous Manufacture

The bioprocessing industry has traditionally relied on batch manufacturing, where products are produced in discrete quantities, or lots. This approach affords a high degree of control over product quality but is limited in scalability and efficiency. In contrast, continuous manufacturing involves an uninterrupted, steady-state production process, for example, an assembly line in the automobile industry. By operating machinery continuously, the equipment downtime and operational footprint can be minimised. For the bioprocessing industry, this method presents several advantages, including smaller equipment footprints, reduced labour costs, improved resin utilisation, lower buffer consumption and enhanced product consistency (Walther et al., 2015; Xenopoulos, 2015; Pollock et al., 2017; Hummel et al., 2019).

With escalating production costs, the bioprocessing industry is increasingly viewing continuous manufacturing as a promising solution to these pressures (Walther et al., 2015; Xenopoulos, 2015; Pollock et al., 2017; Hummel et al., 2019). However, despite the potential, the adoption of continuous downstream processing has been met with significant challenges (Jungbauer, 2013; Zydney, 2016). Although there have been notable successes in upstream manufacturing, such as perfusion bioreactors (Gronemeyer et al., 2014; Rathore et al., 2015), downstream processing remains a bottleneck. The industry still predominantly relies on batch processing in downstream stages, with limited compelling continuous solutions available.

The hesitance in adopting continuous manufacturing within the bioprocessing industry can be attributed to several factors (Kumar et al., 2020; Balfour, 2021; Laermann-Nguyen

and Backfisch, 2021; National Academies of Sciences and Medicine, 2021). Firstly, there is a high capital investment required for continuous solutions, although these are usually recouped in the long term by improvements in efficiency. Additionally, there is a systemic cultural resistance due to the familiarity of batch processing. Continuous manufacture requires large changes in facility operations, which is a significant barrier. Pharmaceutical companies are generally risk-averse, due to the high cost incurred during drug production. A shift from well-understood batch processes without extensive study can be perceived as risky. There is also an absence of clear regulatory framework surrounding continuous processes, and effective scale-down models are essential, but are challenging to develop. Finally there is added complexity in the implementation of continuous processes, often requiring more process analytical technology integration, and more digital infrastructure (Kumar et al., 2020).

Other industries are not subject to the same challenges. Biopharmaceutical products are also subject to rigorous quality controls, requiring any change in manufacturing technique, particularly those that alter product composition, to require revalidation or resubmission to regulatory authorities such as the Food and Drug Administration (FDA). This regulatory burden fosters a conservative approach within the industry, making it wary of adopting new paradigms such as continuous manufacturing.

Despite these advantages, current continuous manufacturing methods, such as periodic counter-current chromatography (PCC), annular flow chromatography (AFC), and simulated moving bed systems (SMBC), require complex and intricate setups (PCC and SMBC), or suffer from poor resin utilisation (AC). These complexities pose challenges in scalability and ease of use, often deterring their adoption.

1.7.1. Periodic Counter-Current Chromatography

Periodic Counter-Current Chromatography (PCC) employs multiple columns interconnected to achieve quasi-continuous operation in chromatographic separations. In PCC, two or more columns are interconnected (see **Figure 5**), each operated independently. This allows for simultaneous operation, where some columns are loaded, while others are undergoing washing or elution phases (Angelo et al., 2018; Shi et al., 2021).

In PCC, each column is loaded and eluted sequentially. This careful coordination of loading and elution ensures that feedstock can be applied continuously. When one column is saturated, the breakthrough is applied to a fresh column while the loaded column is eluted (Zydney, 2016; Shi et al., 2021). This setup ensures a near-constant processing capability, enhancing both throughput and efficiency. PCC has significant benefits, such as: (i) improved productivity; (ii) efficient resin utilisation; (iii) minimising buffer usage and; (iv) simplified scalability by adding more columns. In a study by Angelo and colleagues, adoption of PCC resulted in a resin productivity increase by a factor of 2.5, and a 37% improvement in capacity use while buffer consumption was halved (Angelo et al., 2018). Similarly, Shi and colleagues reported a 97.6% resin utilisation when employing a three-column PCC process for continuous mAb manufacture (Shi et al., 2021). However, the complexity of PCC lies in its requirement for multiple columns connected in series. Full resin utilisation is challenging to achieve, as the differing durations of loading, washing, and elution phases often result in at least one column remaining idle. Furthermore, PCC systems demand intricate valve setups and sophisticated software integration for effective operation. With multiple active columns,

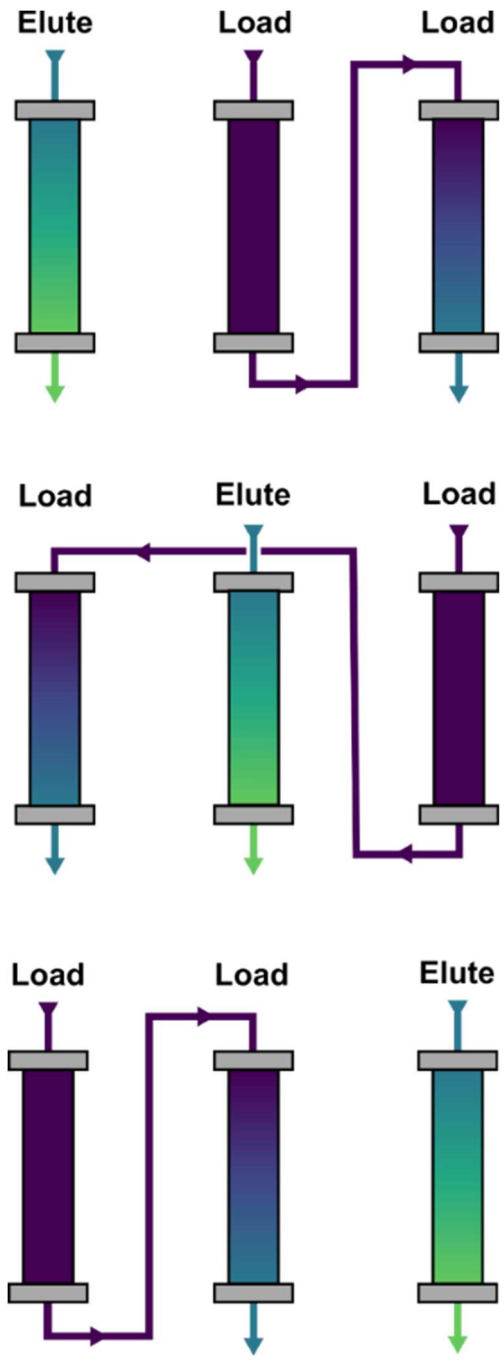

Figure 5: Illustration of PCC, showing the configuration of PCC with two or more columns interconnected through a complex network of valves. The arrangement allows for simultaneous operations where one subset of columns is in the loading phase (indicated by purple arrows for feed) while another subset is in the elution phase (indicated by green arrows for extract), demonstrating the quasi-continuous nature of the process. This setup leverages an array of standard columns to enhance separation efficiency and productivity. Original image produced using Inkscape 1.2.2.

extensive monitoring is necessary, involving UV sensors, conductivity meters, and pH meters for every column for routine operation. The output of all columns also needs to be monitored simultaneously. While PCC is effective, it requires intensive method development and optimisation, making it a resource and capital intensive technique.

1.7.2. Annular Flow Chromatography

Annular flow chromatography (AFC) provides a truly continuous solution. In AFC, the resin is packed within the outer wall of a large rotating column (**Figure 6**). The feedstock and elution buffers are introduced at fixed points at the top of the column. As the column rotates, solutes are eluted at different positions, depending on their retention (Hilbrig and Freitag, 2003; Zydney, 2016). The continuous rotation allows for continuous load and elution.

Radial flow chromatography (RFC) is a similar technology that introduces the feedstock, wash, and elution buffers from the outer edge of a cylindrical chromatography column. The mobile phase passes towards the inside of the column to a collected outlet in the centre. RFC has been operated continuously in some studies by alternating segments of the column between load, wash, elute and regeneration steps (Lay et al., 2006).

However, both AFC and RFC designs suffer from poor resin utilisation, most of the resin is not actively engaged in loading or elution as the drum rotates. This inefficiency limits their effectiveness in large-scale applications. Radial flow has specifically been utilised for removing aggregates via SEC (Buchacher et al., 2001).

Although these technologies have been studied, there are no recent advancements, and currently no commercial continuous AFC or RFC devices available. This lack of development is likely due to the technologies inefficient resin utilisation and poor productivity, posing significant challenges for practical implementation.

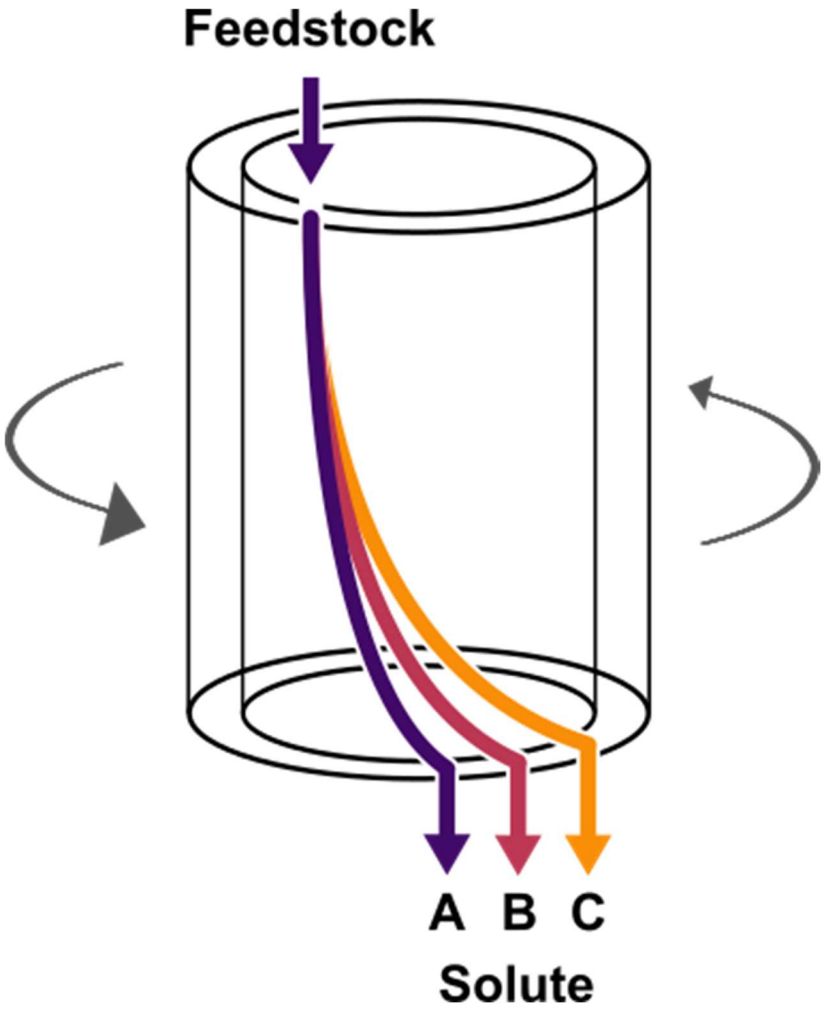

Figure 6: Schematic Representation of Annular Flow Chromatography (AFC), showing a circular drum packed with chromatography media where feedstock is introduced from a fixed location as the drum rotates. The rotation facilitates the separation of solutes based on their retention times; solutes with different retentions elute at distinct locations around the drum, marked as A, B, and C. This method allows for continuous operation and efficient separation of multiple components simultaneously. Original image produced using Inkscape 1.2.2.

1.7.3. Simulated Moving Bed Chromatography

Simulated moving bed chromatography (SMBC) is an advanced chromatography technique that achieves continuous operation by using multiple columns connected in a loop (**Figure 7**). The feedstock is applied to the loop, and the solutes separate based on their different affinities to the stationary phase. As the feedstock separates, a region of low-affinity solute will appear a region of low-affinity solute appears ahead of, and a region of strongly retained solute behind, the bulk feedstock (Jungbauer, 2013; Girard et al., 2015; Zydney, 2016).

The innovation in SMB is a complex series of valves, periodically adjusted to elute these solute regions in a controlled manner as they progress through the loop. This periodic valve adjustment simulates a moving stationary phase, a unique feature that sets SMB apart from traditional batch chromatography. The simulation of a moving bed, achieved by dynamically altering the feed introduction and solute extraction points along with solvent flow, maintains continuous separation maintains continuous separation (Seidel-Morgenstern et al., 2008; Jungbauer, 2013; Aniceto and Silva, 2014). This approach offers significant advantages in efficiency, solvent usage, and scalability compared to traditional batch methods, making SMB Chromatography a valuable technique for large-scale and continuous separation processes. For example, in a study by Girard and colleagues, SMBC outperformed batch chromatography in mAb purification using two Protein A chromatography resins. Productivity was enhanced from 0.15 and 0.39, to 0.63 and 1.77 kg product L $resin^{-1}$ day^{-1} for resin 1 and 2, respectively. Buffer consumption was also reduced, from 1.65 and 1.00 to 1.14 and 0.94 for resin 1 and 2, respectively. IgG

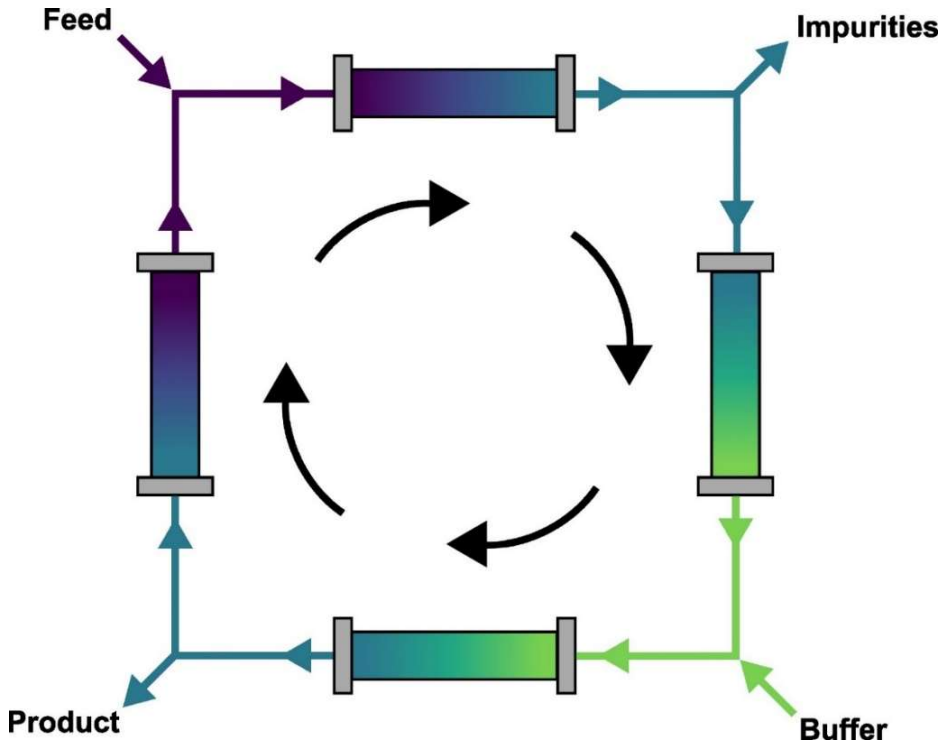

Figure 7: Schematic Illustration of SMBC, showing the continuous flow system with multiple columns connected in a loop. The feedstock in binding buffer is introduced through the purple arrow, while the separation process unfolds as the mobile phase circulates (indicated by black arrows), simulating the movement of the stationary phase. The blue arrows indicate the extraction points for the product and impurities. Carefully timed valve switching, and the continuous circulation of the mobile phase enable ongoing product separation and collection. Original image produced using Inkscape 1.2.2.

purity as analysed by HPLC-SEC, was unaffected by the change to SMBC (Girard et al., 2015).

These productivity and efficiency improvements not only lower the cost of goods but also reduce waste. The study also examines SMBC for ion-exchange polishing. For this application, SMBC enhanced ion exchange productivity from 1.0 to 6.1 kg product·L

resin·day^{-1}, and halved buffer consumption without compromising purity (Girard et al., 2015). However, these benefits are accompanied by several drawbacks. SMBC systems are highly complex, requiring substantial capital investment, which makes them viable primarily for larger-scale operations. The technique demands multiple columns, precise valve timing, sophisticated software integration, and highly skilled operators.

1.7.4. Travelling Cooling/Heating Zone Reactor Chromatography

Precise temperature control is essential for studying the effects of temperature on HIC. The Travelling Cooling Zone Reactor (TCZR) provides a bespoke solution by utilising a localised temperature difference to facilitate protein desorption from a heated stationary phase.

The TCZR comprises a heated cabinet, a travelling cooling zone (TCZ), and a thin-walled (1 mm) stainless steel column. The thin wall of the column ensures efficient thermal transfer between the cooling zone and the packed bed's centre. The TCZ does not cover the entire length of the bed; instead, the TCZ is 2.5 cm high, and can be moved vertically along the length of the column using a linear actuator (**Figure 8**). This design allows for a localised temperature difference to be applied at any point along the packed bed.

During operation, the cabinet is heated to the binding temperature (Φ = 40 °C) while the TCZ is cooled to the elution temperature using a Peltier element. The protein solution is applied to the column while the bed is maintained at the binding temperature. The TCZ then moves down the column at 0.1 mm·s^{-1}, applying a temperature deference that facilitates protein desorption. The maximum achievable temperature deference in certain

setups was $\Delta\Phi$ = 30 °C. When combined with a thermoresponsive chromatography resin this setup enables temperature-controlled adsorption and desorption.

As the TCZ travels along the length of the column, the concentration of protein within the cooled resin builds, resulting in a sharp elution peak once the TCZ clears the bottom of the bed. The cooling zone is flanked by two heatsinks, set at 8 °C above the binding temperature, creating a sharper and more controlled temperature deference for thermoresponsive chromatography. This sharpens elution peaks as the cooling zone is bordered by regions of enhanced binding, creating a more defined transition. Once a single travel is complete, the TCZ rapidly moves to the top of the column (v = 20 mm·s-1) to begin a new cycle. As the TCZ travels along the length of the column, protein concentration within the cooled resin accumulates, resulting in a sharp elution peak once the TCZ clears the base of the bed. The cooling zone is flanked by two heatsinks, which operate at a higher temperature than the binding temperature. In thermoresponsive chromatography this arrangement intensifies elution peaks, as the cooling zone is surrounded by regions of increased binding potential (8 °C above binding temperature), creating a clear temperature shift. Once each cycle is complete, the TCZ resets rapidly (v = 20 mm·s-1) to the column's top to initiate a new cycle. This innovative system is effective at producing distinctive sharp elution peaks. Müller et al. first introduced the TCZR in 2013. They used thermoresponsive cation exchange media (ThermoCEX), with anionic copolymer chains immobilised onto a Sepharose base matrix. This resin exhibited temperature-dependent binding of lactoferrin, with significantly greater affinity at higher temperatures (Müller et al., 2013).

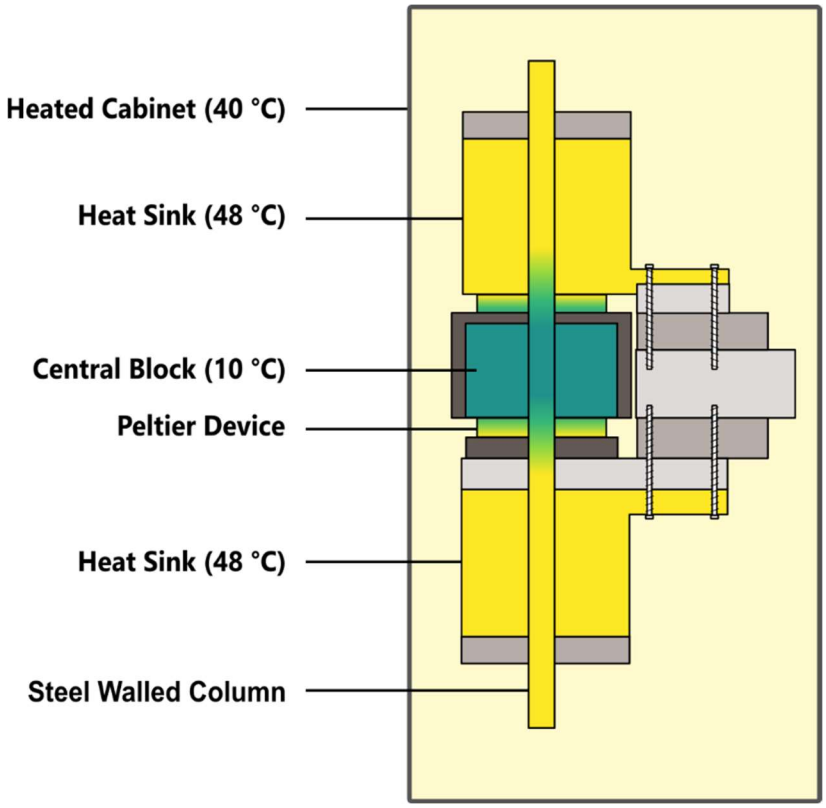

Figure 8: Schematic of the Travelling Cooling Zone Reactor (TCZR) system, featuring a thin-walled stainless steel column (1 mm thickness) enclosed in a heated cabinet (40 °C). A central cooling block (10 °C) moves vertically along the column to apply a precisely controlled, localised temperature deference along the packed bed. Heatsinks on either side of the cooling zone, set to 48 °C, enhance protein binding outside the cooled area, creating sharp elution peaks. The TCZ and the heated cabinet are not drawn to scale. Original image produced using Inkscape 1.2.2.

Initially, jacketed columns were used to establish proof of concept before proceeding to TCZR chromatography. In these experiments, temperature-mediated desorption was achieved under isocratic conditions, i.e., without using salts for protein desorption. In the first experiment, a single large elution peak was generated by switching the jacketed column inlet from Φ = 42 °C water to Φ = 22 °C water. In a second experiment, four elution peaks were generated by pulsing 22 °C water through the jacket, with the column temperature returning to 42 °C between cycles. These studies provided the proof of concept for the TCZR.

The ThermoCEX media was then utilised with the TCZR for temperature-controlled chromatography under isocratic conditions. Lactoferrin was eluted in eight sharp, concentrated peaks, each decreasing in magnitude as the loaded protein was progressively depleted.

Although not explicitly stated in the original publication, the well-defined peaks likely result from the increased temperature not just returning to the binding temperature, but elevating by approximately +8 °C. This elevation occurs due to the Peltier elements' thermal shuttling effect, which dissipates heat into the adjacent heatsinks, ensuring that as soon as the cooling zone passes the column's base, the temperature is rapidly increased. This results in the distinctively sharp peaks observed in TCZR chromatography.

The peaks contained 65% of bound lactoferrin; this yield could potentially be improved by lowering the elution temperature to increase the magnitude of the temperature difference.

Cao et al. (2015) further developed the TCZR, expanding on the ThermoCEX media from Müller et al. (2013) work by synthesising nine thermoresponsive cation exchangers. This was achieved by grafting copolymers with varying proportions of thermoresponsive (N-isopropylacrylamide), hydrophobic (N-tert-butylacrylamide), and negatively charged (acrylic acid) units onto three different cross-linked agarose media, each with distinct particle sizes and pore dimensions (Cao, 2015). Batch adsorption and TCZR chromatography studies were conducted to identify the most effective resin for thermoresponsive chromatography. This was quantified by the ratio of Qmax at the binding and elution temperatures, as well as the ratio of thermoresponsive peak heights

observed in the TCZR. The B2 resin was selected for further testing, and the TCZR was tested for continuous chromatography for the first time. Eight cycles of TCZR were conducted under isocratic conditions, effectively separating a binary feedstock of lactoferrin and bovine serum albumin (BSA), as evidenced by SDS-PAGE gel analysis of the feedstock, flowthrough fractions, and peak fractions. The study revealed that complete BSA desorption was not achievable, as evidenced by BSA removal during sodium hydroxide cleaning, highlighting a limitation in the process.

The concept of the Travelling Cooling Zone was further expanded into the Travelling Heating Zone Reactor (THZR) by Ketterer et al. in (2019). Unlike the TCZR, which uses a cooling mechanism, the THZR controls adsorption and desorption via a heating zone within a temperature-controlled cabinet. Using a thermoresponsive recombinant protein A resin to bind mAbs at 15 °C, the THZR avoids low-pH buffers for elution. Instead, desorption is induced by heating to 42 °C, a feature that prevents aggregation issues common with Protein A chromatography. The THZR effectively separated mAbs from BSA in three applications: (i) continuous mAb concentration (4.5-fold), (ii) quasi-continuous mAb-BSA separation (98.7% purity), and (iii) quasi-continuous buffer exchange. The THZR **o**utperformed conventional tangential flow filtration and ultrafiltration, removing 99.9% of the starting buffer.

Despite its efficacy, the THZR resin has limitations, such as low dynamic binding capacity (<20 mg·mL-1), high salt sensitivity (limiting high-salt wash options), large particle sizes, and restricted flow rates due to poor pore diffusion (Ketterer et al., 2019). The progression from TCZR to the THZR represents significant advancements in temperature-controlled chromatography, especially for continuous processes. The TCZR

and THZR systems offer an elegant solution to continuous downstream processing, with several advantages over SMBC and PCC. Notably, they do not require complex and expensive FPLC systems; instead, they can operate with basic systems such as the ÄKTA Pure or ÄKTA Avant. TCZR and THZR do not require complex interconnected valves or software, nor do they necessitate the use and monitoring of multiple columns, unlike PCC and SMBC. Additionally, they surpass AFC in resin utilisation efficiency. Further research is essential to leverage the full potential of these systems, especially as the need for innovation in continuous downstream processing grows.

1.8. Thesis Overview

The increasing clinical relevance of mAbs has necessitated a substantial scale-up in biopharmaceutical production. To address this rising demand, numerous biopharmaceutical companies have invested in large-scale manufacturing facilities employing standardised platform processes (Shulka and Gottschalk, 2013; Shukla et al., 2017).

Despite the operational advantages of continuous downstream processing methods, their adoption within the industry has been limited. The primary impediments include the excessive generation of equilibration, wash, elution, and regeneration buffers, contributing to inefficiency and waste. Additionally, the mechanical and software complexities of existing continuous chromatography systems render them costly and challenging to implement. Thus, there is a clear demand for innovative technologies that can facilitate continuous processing while offering sustainable advantages, such as reduced buffer and salt consumption.

This thesis seeks to advance a continuous chromatography solution, specifically through the development and application of the TCZR system. Unlike conventional continuous chromatography approaches that typically rely on multiple columns and intricate control mechanisms, the TCZR offers a streamlined alternative, employing a single-column system with temperature modulation. Prior applications of this technology have focused on thermo-responsive cation exchange chromatography (Müller et al., 2013; Cao, 2015), and a thermally responsive protein A mutant (Ketterer et al., 2019). In this work, we extend the utility of the TCZR to hydrophobic interaction chromatography (TCZR-HIC), broadening its application in bioprocessing.

Chapter 2 documents the materials, methods, and instrumentation used in the below results chapters. As the TCZR, chromatography methods, and analysis are closely related between these chapters, these have been documented in a stand-alone chapter to avoid redundancy.

Chapter 3 presents a new application of the TCZR using HIC. In this work, TCZR-HIC is employed to purify bovine serum albumin isocraticly, meaning that the salt concentration remains constant during both binding and elution, which contributes to the process's sustainability. A local temperature decreases of $\Delta\Phi$ = 30 °C was used to facilitate protein desorption, effectively decoupling the elution process from the mobile phase composition. This setup enables continuous TCZR-HIC with a single column, offering a more sustainable and simplified alternative to traditional multi-column systems.

Chapter 4 builds upon the principles established in **Chapter 3**, exploring the application of TCZR-HIC to a thermally stable and commercially significant mAb, Rituximab. The feasibility of utilizing TCZR-HIC in a bioprocessing context is evaluated with Rituximab as a model system. While the technique demonstrates potential, optimal results necessitate a greater temperature deference than the current TCZR instrumentation can achieve.

Chapter 5 summarises the findings from the preceding studies and outlines possible directions for this research. Recommendations for enhancing the TCZR system are discussed, with a focus on overcoming the limitations identified in the current setup.

To conclude, this thesis aims to elucidate the capabilities of TCZR-HIC through the purification of two model proteins, BSA and Rituximab. The research expands upon the foundational work by Müller and Franzreb, demonstrating continuous single-column purification and exploring the applicability of TCZR-HIC in an industrial bioprocessing context. The findings offer promising insights into the future of sustainable continuous chromatography technologies for biopharmaceutical production.

Chapter 2

Materials and Methods

2.1. Materials

Butyl Sepharose™ 4FF media, Superdex 200 Increase, 300/10 GL size exclusion column, Gel Filtration Cal Kit High Molecular Weight, Blue Dextran 2000, and single-use PD-10 desalting columns packed with Sephadex G-25 were obtained from Cytiva UK Ltd (Little Chalfont, Bucks, UK). Butyl-650M, Butyl-650S, Phenyl-650M and Phenyl-650S resins were provided by TOSOH Biosciences (Grove City, OH, USA). Lot numbers of the hydrophobic resins can be found in **Table 1**. Two preparations of Rituximab were kindly supplied by Lonza Biologics (Slough, Berks, UK): a highly polished lot purified by IEX (Lot: 6783623/B53, 25 mM sodium citrate, 0.154 M sodium chloride, 99.5% monomer by SEC) and a neutralized Protein A eluate (96.8% monomer by SEC). SEC comparison is shown in **Figure 22**. Bovine serum albumin (BSA, Cat. no. A7906, lyophilized powder, ≥98% by agarose gel electrophoresis) was acquired from Merck KGaA (Darmstadt, Germany) and used without further purification. Preparations were stored at -80 °C, and buffer exchanged prior to use Other chemicals supplied by Merck included the following: ammonium sulphate (Cat. No. A4418, ≥99%), disodium hydrogen phosphate (Cat No. S0876, ≥99%), sodium bicarbonate (Cat. No. S8875, ≥99.5%), sodium chloride (Cat. No. S/3120/63, >99.5%), Oxoid™ Phosphate Buffered Saline (PBS) tablets (Cat. No. BR0014G, >99%), sodium hydroxide (Cat. No. S0845, anhydrous ≥98%), hydrochloric acid (Cat. No 320331, ACS reagent, 37%), absolute ethanol (Cat. No. E/0650DF/17, >99.8%), and acetone (Cat. No. 270725, HPLC grade, ≥99.9%). Glycine (Cat. No. 357002, ≥99%), tri-sodium citrate dihydrate (Cat. No. 106448, ≥99%), citric acid (Cat. No. 100241, ≥99.5%), Invitrogen™ Alexa Fluor™ 647 NHS Ester (Succinimidyl Ester) (Cat. No. A20006) and Invitrogen™ anhydrous DMSO (Cat. No D12345) for fluorophore

tagging of BSA were purchased from Thermo Fisher Scientific (Waltham, MA, USA). All buffers and solutions were freshly made with purified 18.2 MΩ·cm water from a Sartorius arium® advance EDI Pure Water System (Sartorius AG, Göttingen, Germany), adjusted to the desired pH using 1 M NaOH or 1 M HCl and Fisherbrand accumet XL200 pH and conductivity meter (Fischer Scientific UK, Loughborough, Leics, UK), filtered through 0.22-µm pore MF-Millipore™ membrane filters (Fischer Scientific) and degassed for chromatography experiments.

Table 1: Tabulated hydrophobic resins with their lot number, particle number, pore exclusion limit (kDa) and ligand density (if available from CoA)

Resin Name	Lot Number	Median Particle Size (µm)	Pore Exclusion Limit (kDa)	Ligand Density (µmol·mL^{-1})
A - Butyl Sepharose 4FF	10,281,131	90	30,000	44
B - Butyl Sepharose 4FF	10,309,247	90	30,000	47
C - Butyl Sepharose 4FF	10,317,570	90	30,000	50
Butyl 650M	65BUMB03B	65	5,000	-
Butyl 650S	65BUSD11C	35	5,000	-
Phenyl 650M	65PHMD002EA	65	5,000	-
Phenyl 650S	65PHSD006FA	35	5,000	-

2.2. Rituximab solubility in ammonium sulphate

To assess solubility, Rituximab was exposed to a gradient of AS concentrations. A series of 150 µL solutions containing AS (0.65–1.2 M) were combined with 50 µL of phosphate-buffered Rituximab (350 µg protein; 10 mM phosphate, pH 7.5, prepared fresh). The mixtures were incubated at room temperature (21 ± 2 °C) for 30 min in a 96-well UV-STAR® microplate from Greiner (Stonehouse, UK) (Cat no. 655801) to ensure equilibration. Absorbance values were measured at 400, 500, 600, and 700 nm using a TECAN Spark Multimode microplate reader (Wilmington, DE, USA). Percentage transmittance was calculated with the following formula:

$$T\% = antilog(2 - A) \quad (3)$$

Where, T is percentage transmittance (%), and A is absorbance. To assess temperature effects on solubility, plates were equilibrated to test temperatures for 30 min. Above 20 °C, microplate temperature control was employed; for sub-ambient conditions, plates were incubated in a refrigerator. Absorbance readings were taken immediately post-equilibration.

2.3. Batch adsorption experiments

In batch binding tests, 125 µL portions of 40% (*v/v*) slurries of Butyl 4 Sepharose FF, Butyl-650M, Butyl-650S, Phenyl-650M and Phenyl-650S matrices, previously equilibrated with 50 mM sodium phosphate buffer, pH 7.5 variously supplemented with AS (hereafter abbreviated to AS), were mixed with 125 µL aliquots of varying initial BSA or Rituximab concentration (made up in the same buffer) and incubated at 10, 21, or 40 °C with shaking at 1100 rpm in an Eppendorf Thermomixer comfort shaker (Eppendorf SE, Hamburg, Germany) for 1 h. After an additional 0.5 h at the selected temperature without shaking, adsorbent particles were sedimented by pulse centrifugation (2000 g, 30 s) in a VWR ministar centrifuge (Radnor, PA, USA), and the supernatants were carefully removed and analysed for residual protein content (section 2.7). The equilibrium of BSA or Rituximab loadings on supports (q^*) were computed from the differences in initial (c_0) and equilibrium (c^*) bulk phase protein concentrations, and where appropriate the resulting q^* vs. c^* data were fitted to the simple Langmuir model (**Section 1.5.4.2, Equation 2**). Data were fitted to the model using the $\chi 2$ minimisation

procedure of OriginPro® 2022 software (OriginLab Corporation, Northampton, MA, USA).

2.4. Preparation of dye conjugated BSA

BSA was fluorescently labelled with Alexa Fluor 647, an amine-reactive dye selected for its resistance to quenching at high degrees of labelling and to photobleaching, (Berlier et al., 2003) using the manufacturers' recommended protocol. Dye-labelled BSA conjugates were separated from unreacted dye by SEC using PD-10 columns. Fractions containing both dye and protein were pooled, analysed (**section 2.9**) and employed in CLSM studies (**section 3.3.2**).

2.5. Confocal Laser Scanning Microscopy (CSLM)

CSLM was used to observe combined influences of AS concentration and temperature on distribution of BSA in Butyl Sepharose 4FF beads. Portions (125 µL) of a 40% (*v/v* slurry) of Butyl Sepharose™ 4FF (Batch B) pre-equilibrated for 1 h in 50 mM sodium phosphate buffer pH 7.5 supplemented with 0.3 – 1.5 M AS were incubated with a 125 µL aliquots of 8 mg·mL^{-1} protein solutions (comprising a 1:100 mix of dye-conjugated BSA to native unlabelled BSA) in the same buffers in screw-capped vials protected from light at Φ = 10, 21 and 40 °C. After 1.5 h of mixing in a Thermomixer (Eppendorf SE, Hamburg, Germany), the supports were recovered from solution by low-speed pulse centrifugation (2000 g, 10 s) in a Mini Star Silverline microfuge (VWR International, Lutterworth, Leics, UK), washed (3 × 200 µL) and re-suspended in 0.5 mL of the same binding buffer at the binding temperature. Aliquots (20 µL) of the support slurries were pipetted onto microscope slides, covered with a coverslip, and analysed with a Zeiss LSM 780 microscope

using an LD LCI Plan-NEOFLUAR 25×/0.8 oil-immersion objective (Carl-Zeiss Microscopy GmbH, Jena, Germany). The samples were excited with the system's helium'neon 633 nm laser line (gain = 500, 2% laser power) and images were captured with ZEN 2.1 software (Carl-Zeiss Microscopy GmbH, Jena, Germany), and then processed (**section 2.9**).

2.6. Pulse-response HIC experiments

The effect of temperature on elution under binding conditions at various salt concentrations was evaluated by a pulse-response chromatography screening study using Tricorn™ 5/50 columns (Cytiva, Marlborough, MA, USA) containing 1 mL beds of Butyl 4 Sepharose FF Batch B, or Butyl-650M, connected to an AKTAprime plus system (GE Healthcare, Uppsala, Sweden). BSA pulses (2 mg in 0.50 mL) or Rituximab pulses (1.6 mg in 0.50 mL) were applied to equilibrated columns submerged in a Techne TE-10A circulating water bath (Thermo Fisher Scientific, Waltham, MA, USA) held at the binding temperature Φ = 40, 50, or 60 °C. Binding was followed by a wash with binding buffer at the same temperature as the stationary phase. For experiments conducted with Butyl Sepharose 4FF, this was done until the UV baseline had returned to zero. For experiments performed with Butyl-650M, washing was performed for ~12CVs. Following washing, columns were stripped with 20% (*v/v*) ethanol at binding temperature or transferred to an iced-water cooling bath (maintained at Φ = 10 °C) to trigger elution before stripping with 20% (*v/v*) ethanol at Φ = 10 °C. Flow leaving the columns was continuously monitored for conductivity and UV absorbance at 280 nm. Although Rituximab absorbs strongly at 215 nm, 280 nm is used throughout this thesis in most cases, as strong signals at 215 nm can cause detector saturation. Absorbance at 215 nm is used when signals at 280 nm are

low. The temperatures of the water and iced-water baths were continuously logged (Elitech RC-5+, Elitech Technology Inc., San Jose, CA, USA) during experiments and remained constant.

2.7. Basic set-up and description of procedures

A brief description of the TCZR set-up is given below. For more detail the reader is referred to our previous studies (Müller et al., 2013; Cao et al., 2015). The TCZR system comprises: (i) an insulated temperature-controlled cabinet; (ii) a vertically aligned stainless steel column (internal diameter = 6 mm, length = 360 mm); and (iii) the column mounted travelling cooling zone (TCZ) arrangement, which surrounds a discrete zone of the column. The walls of the column are only 1 mm thick to ensure rapid and homogenous radial heat transfer. With PTFE capped stainless steel adaptors inserted into both ends of the column the internal volume for accommodating the stationary phase can be reduced to 2.83 mL (length = 100 mm). The TCZ is a 'Club sandwich-like' arrangement of three copper blocks and two Peltier elements (Type TB-109-1,4-1,5CH, Kryotherm, St, Petersburg, Russia), flanked top and bottom by aluminium heatsink blocks. By attaching the TCZ to a linear motorized axis (Festo AG, Munich, Germany) controlled by dedicated PC based software (Festo Configuration Tool, FCT) it can be moved along the column in either direction at a velocity of 0.1 to 40 $mm \cdot s^{-1}$. The Peltier elements of the TCZ are connected to a MTTC-1410 thermoelectric temperature controller (Laird Thermal Systems, Morrisville, NC). The temperatures of the cabinet/column and TCZ are monitored in real-time using Pt100 resistance thermometers linked to LabView™ Software (National Instruments, Austin, TX, USA). The TCZR apparatus is controlled by an external computer running LabView software, and Festo control panel, where the TCZ

velocity (v_c), linear motor position, and temperature (Φ) of the cabinet or cooling zone can be measured and modified.

2.8. General description and procedures

All TCZR-HIC experiments were conducted using an ÄKTA Explorer 100 Air chromatography workstation operated using Unicorn 5.1.1 software (GE Healthcare, Uppsala, Sweden). The separation column was packed with Butyl Sepharose 4FF (volume 3.4 mL, height = 114 mm, compression factor 1.052, asymmetry 1.05), or Butyl-650M (volume = 3.4 mL, height = 112 mm, compression factor = 1.052, asymmetry = 1.19).

In all experiments with BSA, 50 mM sodium phosphate buffer pH 7.5 supplemented with 0.5 M AS was used for equilibration, binding, washing and TCZ elution steps. Experiments with Rituximab used a base buffer of 50 mM sodium phosphate buffer pH 7.5 with various AS concentrations (0.125, 0.20, 0.50, or 0.60 M), specified in the results text. Cabinet and TCZ temperatures were fixed at Φ = 40 ± 1 °C and 10 ± 1 °C respectively, unless otherwise stated. The TCZ velocity (*Vc)* was 0.1 mm·s^{-1}, and a constant volumetric flow rate of 0.18 mL·min was used equating to a superficial mobile phase velocity, u, of 38.2 cm/h. Assuming a settled bed voidage, ε_o, of 0.41 for 4% cross-linked Sepharose™ (Stickel and Fotopoulos, 2000) the calculated bed voidage, ε, was ~0.36. Thus, the interstitial velocity, u_i (at u = 38.2 cm/h) was 107.1 cm/h or 0.30 mm·s^{-1}, i.e., 3× faster than v_c (0.1 mm·s^{-1}). The interval between successive TCZ movements was varied by adjusting the start and end positions. For example, at v_c = 0.1 mm·s^{-1}, start and end positions 40 mm either side of the 110 mm high chromatographic bed correspond

to a 31.67 min cycle time (190 mm of travel), whereas 5 mm displaced start and end points reduce the cycle time to 20 min (120 mm travel). Immediately on reaching the end position, the TCZ is rapidly returned to its starting position above the bed in immediate readiness for the next downward pass. The return velocity used in this work of 20 mm·s^{-1} adds an extra 6 s to a 20 min cycle time and 9.5 s to a 31.67 min cycle, giving peak-to-peak separation times of 20.1 min and 31.83 min.

In batch mode TCZR experiments performed with BSA, (0.5 mL of 4 mg·mL^{-1}) was applied to pre-equilibrated beds of Butyl Sepharose 4FF at Φ = 40 °C. The columns were then washed (3 CV) before initiating the first of 7 – 12 sequential movements of the TCZ along the column's full separation length. For all batch experiments with Rituximab, (0.5 mL of 3.2 mg·mL^{-1}) was applied to pre-equilibrated beds of Butyl Sepharose 4FF pre-equilibrated with 0.6 M AS or Butyl 650M pre-equilibrated with 0.125 M AS. The column was washed (2-3 CV) before 5 – 30 sequential movements were performed. On completion of the TCZ's last movement columns were stripped using 20% (*v/v*) ethanol at Φ = 40 °C.

For continuous TCZR-HIC, protein loading and TCZ movements were performed concurrently. For the continuous experiments with BSA, preparations was applied at Φ = 40 °C to fresh, regenerated or fouled (inadequately cleaned) Butyl Sepharose 4FF columns at concentrations of 0.25, 1 and 0.5 mg·mL^{-1} respectively. A minimum of 58 TCZ cycles was conducted at regular intervals (20 or 21.8 min). Loading of BSA was maintained for 190 – 210 mL at which point the flow to columns was switched from BSA in buffer to buffer only whilst continuing TCZ operation for another 6 – 8 cycles, before administering 20% (*v/v*) ethanol to the columns at Φ = 40 °C. Between runs columns

were cleaned with 1 M NaOH, washed with purified water and stored in 20% (*v/v*) ethanol.

For continuous experiments conducted with Rituximab, a feedstock prepared with 0.5 $mg \cdot mL^{-1}$ of Rituximab was applied to a Butyl 650-M column. In this study, an alternate temperature deference was trialled, Φ = 40/10 °C. TCZ movements were done at 20 min intervals. Loading was maintained from 0 – 120 mLs, afterwhich the column was washed with purified water and stripped with 20% (*v/v*) ethanol. In this study, an identical experiment was performed with no TCZ movements, and the data was overlaid, demonstrating the effect of the Peltier element on thermal elution.

Flow exiting all columns was continuously monitored for conductivity and UV absorbance at 280 nm, and all fractions generated during experiments were retained for SEC analysis (**section 2.9**).

2.9. Analysis

Alex Fluor 647 dye and BSA concentrations in samples were determined in a DeNovix DS-11+ UV spectrophotometer (Wilmington, DE, USA) at wavelengths of 650 nm and 280 nm respectively.

CLSM data was analysed using ImageJ2 (Fiji) software (Schindelin et al., 2012). Intensity vs. radial position profiles were extracted and plotted in OriginPro. For ease of visualisation (Crameri et al., 2020) images of individual chromatography beads are shown in the “Hot Cyan” colour scale available in ImageJ Fiji.

After packing and prior to each new TCZR-HIC run bed quality was assessed by comparing peak asymmetry factors (A_s). For this, tracer pulses (50 µL of 0.8 M NaCl) were injected onto Butyl Sepharose 4FF columns operated at 0.18 mL·min^{-1} and employing 0.4 M NaCl as the mobile phase. A minimum of three measurements were performed and A_s was calculated using the ÄKTA Explorer's Unicorn software version 5.1. In all TCZR experiments, regardless of bed history, A_s values were close to 1. Areas under peaks in chromatograms were calculated using OriginPro's Peak Analyser (OriginLab Corporation, Northampton, MA, USA) tool and were subsequently converted to mass (1 mg·mL^{-1} BSA gives a UV 280 signal of 115 mAU, 1 mg·mL^{-1} Rituximab gives a UV 280 signal of 280 mAU).

The compositions of feed solutions and peak fractions collected during TCZR-HIC chromatography were analysed by SEC analysis using a Superdex 200 increase, 300/10 GL column (Cytiva, Marlborough, MA, USA) previously calibrated with Ovalbumin (44 kDa), Conalbumin (75 kDa), Aldolase (158 kDa), Ferritin (440 kDa), Thyroglobulin (669 kDa) and Blue Dextran 2000 (2,000 kDa). Syringe filtered samples were injected onto the column via a 500 µL sample loop. Chromatography was performed at 0.5 mL·min^{-1} using PBS (10 mM phosphate, 137 mM NaCl, 2.7 mM KCl, pH 7.4) as the mobile phase and the UV absorbance of the exiting flow was monitored at 215 and 280 nm. Three elution peaks were observed in BSA feed samples with apparent molecular weights corresponding to monomers, small oligomers (dimers, trimers, and tetramers), and higher molecular weight (HMW) species (larger oligomers and soluble aggregates).

Chapter 3

Integrated system for temperature-controlled fast protein liquid chromatography. Continuous ‘one-column’ ‘low-salt’ hydrophobic interaction chromatography.

3.1. Abstract

The systematic development of a temperature-controlled isocratic process for one-column low-salt hydrophobic interaction chromatography (HIC) of proteins employing a travelling cooling zone reactor (TCZR) system, is described. Adsorption isotherms of BSA to three batches of Butyl Sepharose 4FF in 50 mM sodium phosphate buffer pH7.5 containing 0.5 M AS revealed differences in temperature-dependency of binding. Further binding studies using the 'best' matrix combined with confocal laser scanning microscopy of fluorescently labelled BSA, defined a narrow temperature-dependency window of AS concentrations of 0.3 – 0.75 M appropriate for a process employing 40 °C for binding and 10 °C for elution. In pulse-response HIC studies, BSA in buffer supplemented with 0.5 M AS was applied to a HIC Tricorn 5/50 column immersed in a 40 °C water bath. Rapid transfer of the column to a 10 °C ice bath desorbed >56% of the initially bound BSA in broad strongly tailing elution peak. A bespoke thin-walled stainless-steel column packed with stationary phase mounted with a movable assembly of copper blocks and Peltier elements (travelling cooling zone, TCZ) was used for TCZR-HIC. In pulse-response experiments, BSA applied at 40 °C was eluted from the column by multiple movements of the TCZ down the column at a velocity of 0.1 mm·s^{-1}, with each generating sharp elution peaks dropping in magnitude with every successive pass. Twelve cycles recovered >66% of the loaded BSA, and 86.3% of the applied monomer in 95.3% purity depleted >6-fold in small oligomers (2-4 mer) and nearly 260-fold in higher molecular weight (HMW) species. For continuous TCZR-HIC the cooling zone was moved 49-58 times during uninterrupted loading of BSA feeds at different concentrations (0.25, 0.5 and 1 mg·mL-1) before switching to buffer only accompanied

by further passes of the TCZ. Each movement of the TCZ generated a sharp symmetrical elution peak. At 0.25 mg·mL-1 BSA the height of TCZ elution peaks gradually grew reaching pseudo steady roughly midway (peak 27 out of 49) through the loading phase with no rise in baseline UV280 signal between the peaks, and peak composition remained constant averaging 94.4% monomer, 5.6% 2-4 mer and <0.05% HMW. Monomers were recovered in quantitative yield in the 58 peak elution pool depleted >3.1 fold with respect to 2-4 mer and 92-fold in HMW species cf. the feed (63.6% monomers, 21.8% 2-4 mer, 14.6% HMW). Increasing the BSA feed concentration to 1 mg·mL-1 compromised TCZ elution performance. Early during loading coincident with the largest TCZ elution peak (8 of 58), the UV280 baseline signal gradually rose, elution peaks reduced in size, and monomer purity steadily declined. Eluted monomers were recovered in quantitative yield at 89.6% purity. In TCZR-HIC performed with a fouled HIC column continuously loaded with 0.5 mg·mL-1 BSA and unloaded by 53 TCZ movements the baseline inclined upwards from the outset, elution peaks were wider, and their width grew with continued BSA supply. However, purification performance matched that observed with a clean HIC column supplied with BSA at twice the feed concentration.

3.2. Introduction

Chromatographic operations are indispensable in the downstream processing of biotherapeutics, but their sustainability is coming under increasing scrutiny (Warner and Nochumson, 2003; Nweke et al., 2018; Khanal and Lenhoff, 2021). Adsorption chromatography can be hugely expensive. Traditionally employed approaches exacerbate these costs, and importantly, exhibit poor green credentials. Batchwise single-column operation, for example, is characterised by low productivity, excessive buffer and water consumption and associated levels of waste for disposal post-manufacture (Linke et al., 2012; Müller et al., 2013; Bunnak et al., 2016; Madabhushi et al., 2018; Budzinski et al., 2019; Budzinski et al., 2022). Such concerns drive the bioprocess industry's growing interest in continuous manufacture (Jungbauer et al., 2024). Newer continuous chromatography formats promise significant and well-documented benefits *cf.* batch chromatography, namely increased capacity/resin productivity and process efficiency, lower operational costs, improved scalability, smaller physical footprints and reduced water consumption and environmental impact (Linke et al., 2012; Pietrzykowski et al., 2013; Rathore et al., 2015; Bunnak et al., 2016; Zydney, 2016; Gjoka et al., 2017; Shukla et al., 2017; Madabhushi et al., 2018; Somasundaram et al., 2018; Balfour, 2021; Gerstweiler et al., 2021; Khanal and Lenhoff, 2021; Jungbauer et al., 2024). The transition from batch to continuous chromatography is currently hindered by the latter's greater complexity (Zydney, 2016; Somasundaram et al., 2018). However, a rarely mentioned core problem is that large volumes of different buffers are employed during the sub-steps (equilibrating, washing, eluting, cleaning) with each generating waste. Solutions to this

issue should improve the greenness and sustainability of chromatographic operations employed for biotherapeutics manufacture (Müller et al., 2013; Ketterer et al., 2019).

HIC is powerful and gentle technique for intermediate purification and polishing chromatography of proteins, (Hjertén, 1973; Hjertén, 1981; Perkins et al., 1997; Queiroz et al., 2001; Lienqueo et al., 2007; Shukla et al., 2007b; To and Lenhoff, 2007; Cramer and Holstein, 2011; Fekete et al., 2016) nucleic acids (Hjertén, 1981; Diogo et al., 2000; Diogo et al., 2001) and viruses (Hjertén, 1981; Esquibel-King et al., 1999; Li et al., 2015; Weigel et al., 2019). However, its reliance on very high concentrations of kosmotropic salts (e.g., AS) typically employed to promote binding (Shepard and Tiselius, 1949; Hjertén, 1973; Melander and Horváth, 1977; Melander et al., 1984; Nagrath et al., 2011) creates problems that escalate at manufacturing scales. These include: (i) the costs associated with intermediate sample preparation steps that may be required to reduce the salt concentration before the next process step; (Gagnon, 2000) (ii) AS is highly corrosive to stainless steel equipment; (Bamforth, 1954; Ghose et al., 2013) and that (iii) large amounts of salts, especially AS and potassium phosphate, pose serious environmental concerns that render their disposal in municipal waste water very expensive (Gagnon, 2006).

An obvious solution to the above is to employ suitable replacements for kosmotropic salts. Gagnon (Gagnon, 2000) proposed glycine, but other additives (Arakawa and Timasheff, 1983) also invite attention. Further options are to eradicate (Ghose et al., 2013; Dilks et al., 2023a) or minimise (Chen et al., 2008; Müller and Franzreb, 2012) the reliance of HIC on high concentrations of kosmotropic salts. In the specific case of monoclonal antibodies (mAbs) the triad combination of ‘no-salt HIC, very hydrophobic

stationary phases and flow through operation' represents an attractive option for selective removal of more hydrophobic aggregates from less hydrophobic mAbs; prior optimisation of mobile phase pH is required in each case (Ghose et al., 2013; Dilks et al., 2023a). Müller and Franzreb (Müller and Franzreb, 2012) described a novel and potentially generic solution for intermediate purification by low-salt HIC which involved using temperature to control adsorption-desorption equilibria (see below).

The general effects of temperature on HIC are well known, i.e., high temperatures enhance binding and lower temperatures undermine it, promoting desorption (Hjertén et al., 1974; Geng and Chang, 1990; El Rassi, 1996; Haidacher et al., 1996). It is somewhat surprising, therefore, that there are very few reports on the practical use of temperature modulation in HIC to switch between binding and elution states (Muca et al., 2009a; Muca et al., 2009b; Muca et al., 2010). For example, Muca and coworkers (Muca et al., 2009b) employed step changes in temperature and salt concentration to fractionate a multi-component protein mix of BSA, α-chymotrypsinogen, lysozyme and myoglobin, while Müller and Franzreb's (Müller and Franzreb, 2012) study aimed to use temperature in combination with low salt concentrations to reduce process costs and address the sustainability and green failings of HIC as it is currently practiced. Their approach involved: (i) screening the effect of temperature (10-40 °C) in low AS concentrations (0.1 – 0.5 M) on protein adsorption of BSA to HIC media; (ii) deriving Langmuir and thermodynamic parameters to identify the HIC matrix and AS concentration showing the strongest temperature influence; (iii) performing back-to-back multi-cycle temperature-driven adsorption-desorption runs in a column under isocratic conditions; and (iv)

demonstrating that ‘temperature only’ mediated fractionation of protein mixtures at low salt concentration is possible.

Looking to the long-term future of bioprocess scale adsorption chromatography, we introduced single-column continuous chromatography formats operated under isocratic conditions (Müller et al., 2013; Cao et al., 2015; Ketterer et al., 2019). In these systems stainless-steel columns are mounted with travelling Peltier devices which transiently cool (Müller et al., 2013; Cao et al., 2015), or heat (Ketterer et al., 2019) defined regions or zones of the contained adsorbent bed as they migrate along the length of the column (note, no change in buffer composition is required). In this way discrete ‘local’ changes in bed temperature are used to control adsorption–desorption equilibria; in the standard case, driving elution of bound species from the support into the mobile phase, and exiting the column once the Peltier device passes the column exit (Müller et al., 2013; Cao et al., 2015; Ketterer et al., 2019). This allows for uninterrupted loading of feedstock protein to the column, whilst simultaneously moving the cooling/heating zone along it in repeated fashion. In past demonstrations we employed: (i) thermoresponsive cation exchange media in a travelling cooling zone reactor (TCZR) system for continuous fractionation of a binary mixture of the proteins BSA and bovine lactoferrin; (Cao et al., 2015) and (ii) a commercially available thermoresponsive rProtein A matrix in a travelling heating zone reactor (THZR) system for three different mAb downstream processing applications, i.e., continuous mAb concentration, quasi-continuous mAb purification and quasi-continuous buffer exchange (Ketterer et al., 2019).

In this work we extend the repertoire of travelling cooling systems to HIC of proteins in low-salt buffers building on previous work by Müller and Franzreb (Müller and Franzreb,

2012) employing BSA and Butyl Sepharose 4FF. Specifically, we describe batch binding experiments allied with confocal laser scanning microscopy (CLSM) to confirm optimal conditions for trialling low-salt HIC processes that employ 'cooling only' to effect elution, test the separation concept in pulse-response HIC experiments before transferring to batch and continuous TCZR-HIC to purify BSA monomers from larger and more hydrophobic forms.

3.3. Results and Discussion

In their study Müller and Franzreb (Müller and Franzreb, 2012) screened four differently functionalised HIC media for the binding of BSA at temperatures, Φ, between 10 and 40 °C in a 50 mM sodium phosphate pH 7 buffer variously supplemented with low concentrations (0.1 – 0.5 M) of AS. The authors: (i) noted that temperature-dependency is inversely correlated with hydrophobicity of the matrix; (ii) singled out Butyl Sepharose 4FF as most promising for further investigation of temperature-dependency in HIC; (iii) employed van't Hoff analysis, applied to collected isotherm data, to calculate thermodynamic contributions to BSA binding, highlighting the key import of ΔS *cf.* ΔG and q_{max}; and (iv) Recommended binding (high) and desorption (low) temperatures are ideally selected so that ΔG flips its sign from strongly negative at the higher temperature to positive at the lower temperature.

3.3.1. BSA adsorption on Butyl Sepharose 4FF

Protein binding in HIC is well known to correlate with alkyl chain length and ligand density (Jennissen and Heilmeyer Jr, 1975; Hofstee and Otillio, 1978; Chen et al., 2003; To and Lenhoff, 2007). Müller and Franzreb (Müller and Franzreb, 2012) did not specify

the ligand density (or lot number from which this could be identified) of the Butyl Sepharose 4FF used in their work. In this study, three different lots (designated A – C) with ligand densities ranging from 44 – 50 μmol/mL were screened in batch adsorption isotherms conducted with a range of BSA concentrations (final concentration 7.5 – 0.25 $mg{\cdot}mL^{-1}$) in phosphate buffer containing 0.5 M AS (**Figure 9**, **Table 2**) with two objectives in mind, i.e., identify: (i) the adsorbent best matching the matrix used by Müller and Franzreb (Müller and Franzreb, 2012) for ease of comparison, as the ligand density employed by them is unknown; and more importantly (ii) the matrix displaying the strongest temperature-dependency. Here, temperature-dependency is described by two parameters, i.e., Δq_{Φ}, the difference in binding capacity at 40 °C and 10 °C (Müller and Franzreb, 2012) and k'_{Φ}, the ratio of the initial slopes q_{max}/K_d at 40 °C and 10 °C. At 40 °C BSA binding to all batches of Butyl Sepharose 4 FF (**Figure 9 c**, **Figure 9 f, Figure 9 i**, and, **Table 2**) is very similar (q_{max} = 6.5 – 7 $mg{\cdot}mL^{-1}$, K_d = 0.7 – 1.0 $mg{\cdot}mL^{-1}$, q_{max}/K_d = 7.1 – 9.1). A reduction in temperature to 21 °C substantially weakens binding **Figure 9b**, **Figure 9 e, and, Figure 9 h**,), but the same commonality is retained for batches A–C (q_{max} = 5.0 – 6.35 mg·mL-1, K_d = 2.7 – 3.3 mg·mL-1, q_{max}/K_d = 1.8 – 1.9). Reducing the temperature yet further to 10 °C exposes differences in BSA binding characteristics between the batches (**Figure 9 a**, **Figure 9 d, and, Figure 9 g**). Batch C (50 μmol/mL), likely the most densely derivatised of the four batches, exhibits stronger binding character (e.g., q_{max}/K_d = 1.30 *cf.* 0.8–0.9; **Table 2**), which compromises its temperature-dependency (Δq_{Φ} = 1.1 $mg{\cdot}mL^{-1}$, k'_{Φ} = 7) *Cf.* the rest (Δq_{Φ} = 2.2 – 2.7 $mg{\cdot}mL^{-1}$, k'_{Φ} = 8.7 – 10.8). Batch B was selected for use in all subsequent studies as it displayed the strongest temperature-dependent BSA binding of the three batches of Butyl Sepharose 4FF batch,

closely matching the behaviour previously reported Müller and Franzreb (Müller and Franzreb, 2012) for a different batch of the same matrix.

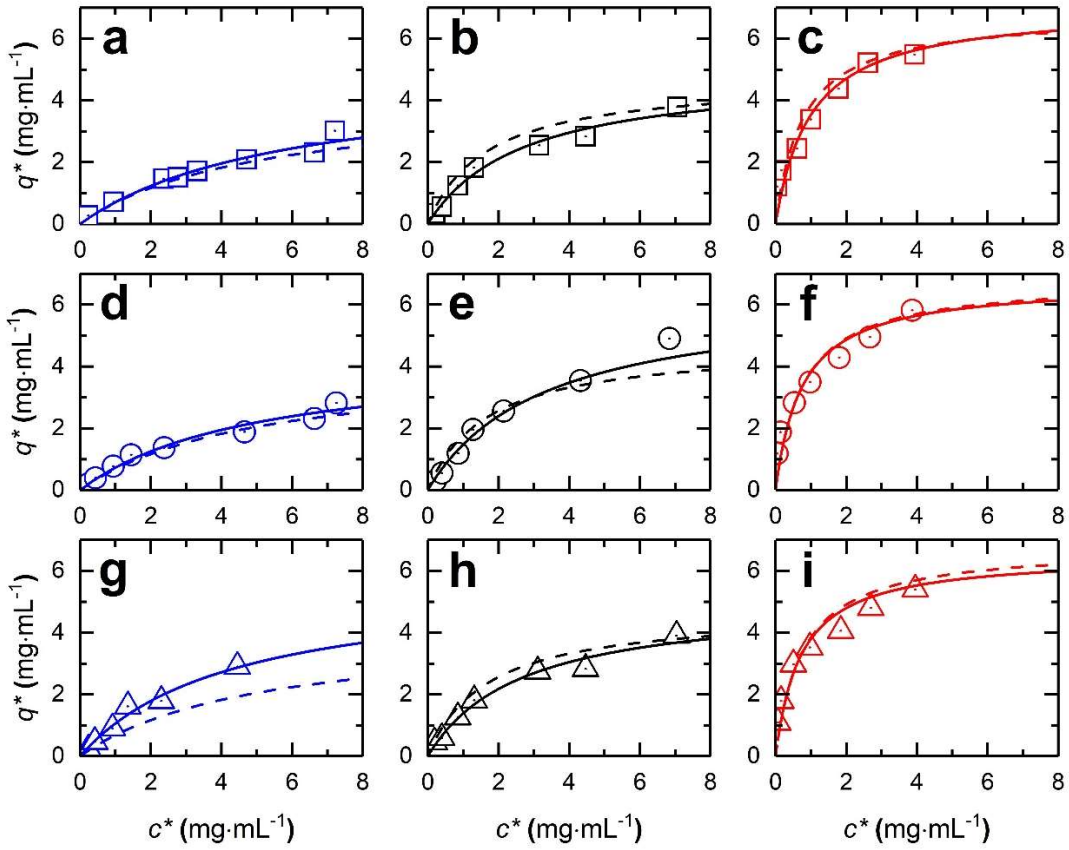

Figure 9: Equilibrium isotherms for the adsorption of BSA to batches A (a – c; open squares), B (d – f; open circles) and C (g – i; open down-triangles) of Butyl Sepharose 4FF tested in this study. The solid lines (blue = 10 ◦C; black = 21 ◦C; red = 40 ◦C) through the data points represent fitted Langmuir curves with parameter values presented in **Table 2** and the dashed lines (blue = 10 ◦ C; black = 25 ◦C; red = 40 ◦C) are simulated Langmuir curves for BSA adsorption to the batch of Butyl Sepharose 4FF employed by Müller and Franzreb (2012).

Table 2: Langmuir parameters for experiments presented in Figure 9.

Batch	Lot number (ligand density)	Φ (°C)	q_{max} (mg·mL^{-1})	K_d (mg·mL^{-1})	R^2	q_{max}/K_d (-)	k'_Φ (-)	Δq_Φ (mg·mL^{-1})
A	10281131 (44 µmol/mL)	10	4.84 ± 0.65	5.88 ± 1.53	0.97	0.82	8.67	2.2
		21	4.95 ± 0.46	2.70 ± 0.58	0.96	1.83		
		40	7.04 ± 0.47	0.99 ± 0.25	0.94	7.11		
B	10309247 (47 µmol/mL)	10	4.40 ± 0.60	5.03 ± 1.22	0.98	0.87	10.16	2.7
		21	6.35 ± 0.77	3.30 ± 0.70	0.99	1.92		
		40	6.72 ± 0.44	0.76 ± 0.20	0.93	8.84		
C	10317570 (50 µmol/mL)	10	5.67 ± 1.20	4.35 ± 1.51	0.98	1.30	6.97	1.1
		21	5.06 ± 0.50	2.65 ± 0.61	0.98	1.91		
		40	6.52 ± 0.40	0.72 ± 0.19	0.93	9.06		
Müller & Franzreb (2012)	Unspecified	10	4.1	5.0	-	0.82	10.78	2.7
		25	4.7	1.67	-	2.82		
		40	6.8	0.77	-	8.84		

3.3.2. Temperature-dependency window for BSA on Butyl Sepharose 4FF

To identify operating windows/limits of temperature-dependency of BSA binding to Butyl Sepharose 4FF the combined influence of AS concentration and temperature was explored in batch binding and CLSM studies. The objective was to identify a salt concentration that demonstrated the greatest difference between temperatures. At a challenge of 20 mg BSA per mL adsorbent in the presence of 0.3 M AS only 9.9 – 20.3% of the protein was adsorbed (**Figure 10 a**). BSA binding capacities were low (1.92, 2.84 and 3.94 mg·mL^{-1} at 10, 21 and 40 °C respectively), but a clear advantage of higher temperature was observed, i.e., the binding capacity at 40 °C was 2.05-fold higher than at 10 °C (**Figure 10 b**; Δq_{Φ} = 2.02 mg·mL^{-1}). With increasing AS concentration capacities rose steeply in roughly linear fashion (**Figure 10 b**). The advantage of high temperature on binding persisted at 0.5 M (6.0 mg·mL^{-1} at 40 °C *cf.* 3.38 mg·mL^{-1} at 10 °C, i.e., 1.78-fold; Δq_{Φ} = mg·mL^{-1}), 0.75 M (9.64 mg·mL^{-1} at 40 °C *cf.* 4.94 mg·mL^{-1} at 10 °C, i.e., 1.95-fold higher; Δq_{Φ} = 4.7 mg·mL^{-1}) and 1 M added salt concentrations (12.72 mg·mL^{-1} at 40 °C *cf.* 8.12 mg·mL^{-1} at 10 °C, i.e., 1.57-fold higher; Δq_{Φ} = 4.6 mg·mL^{-1}) but was lost almost completely at 1.5 M AS (19.68 mg·mL^{-1} at 40 °C *cf.* 19.38 mg·mL^{-1} at 10 °C; Δq_{Φ} = 0.3 mg·mL^{-1}). A similar trend was observed at the higher challenge of 62 mg BSA per mL adsorbent conducted at high added AS concentrations of 1 – 2 M, i.e., capacities increasing with increasing salt and accompanied by gradual loss of temperature-dependency (Δq_{Φ} falling from 5.44 mg·mL^{-1} at 1 M added salt to 2.46 mg·mL^{-1} at 2 M AS). When expressed as percentages of capacities at 40 °C these values of Δq_{Φ} are small, i.e., reflecting binding capacity differences of 21.76% at

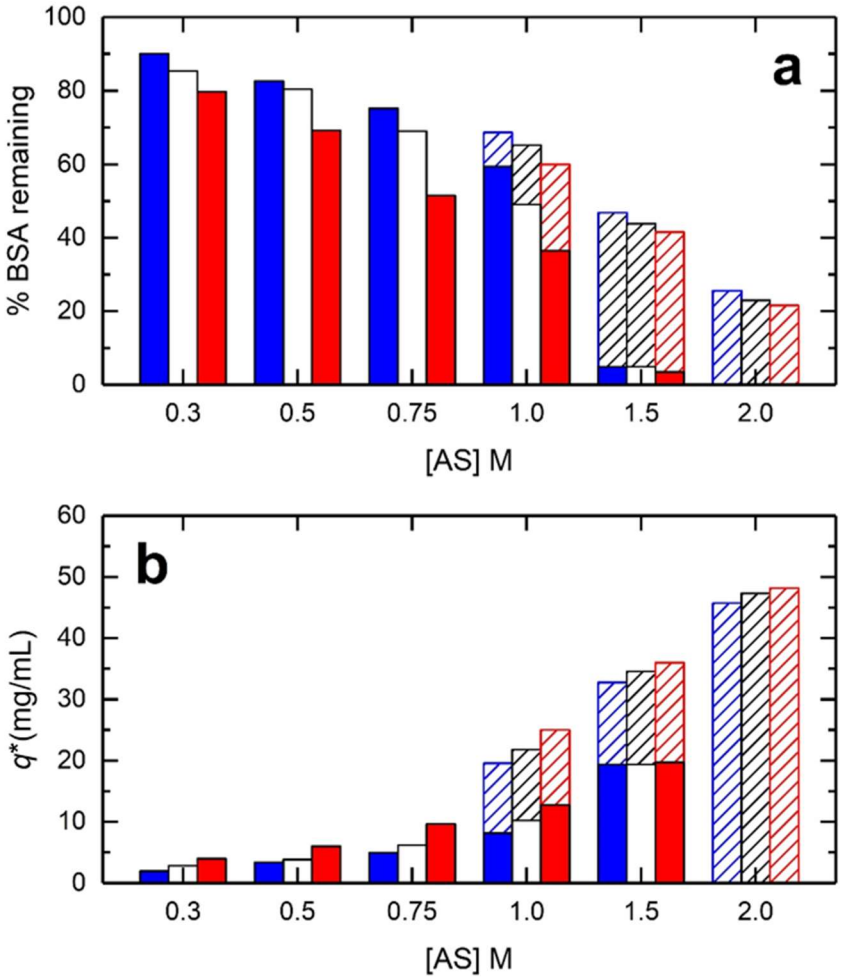

Figure 10: Combined influence of temperature and AS concentration on BSA binding to Butyl Sepharose 4FF at challenges of 20 (filled bars; 0.3 – 1.5 M AS) and 62 (hatched bars; 1–2 M AS) mg BSA per mL of support. Binding temperatures of 40, 21 and 10 ◦C are indicated by red, black, and blue respectively. Panels a and b respectively show the % of BSA remaining in solution and binding capacity plotted against AS concentration.

1 M AS dropping to 5.11% at 2 M added AS. Thus, for the present system (BSA, Butyl Sepharose 4FF) a thermally driven process employing high temperature (40 °C) binding and low temperature (10 °C) for elution is only viable with low AS concentrations (0.3 – 0.75 M). CLSM images arising from equilibrium binding (t = 1.5 h) of Alexa Fluor 647 conjugated BSA to Butyl Sepharose 4FF as functions of temperature (10, 21 and 40 °C) and AS concentration (0.3 – 1.5 M) are shown in **Figure 11**, and the corresponding fluorescence intensity scans are presented in **Figure 12.** The general influence of

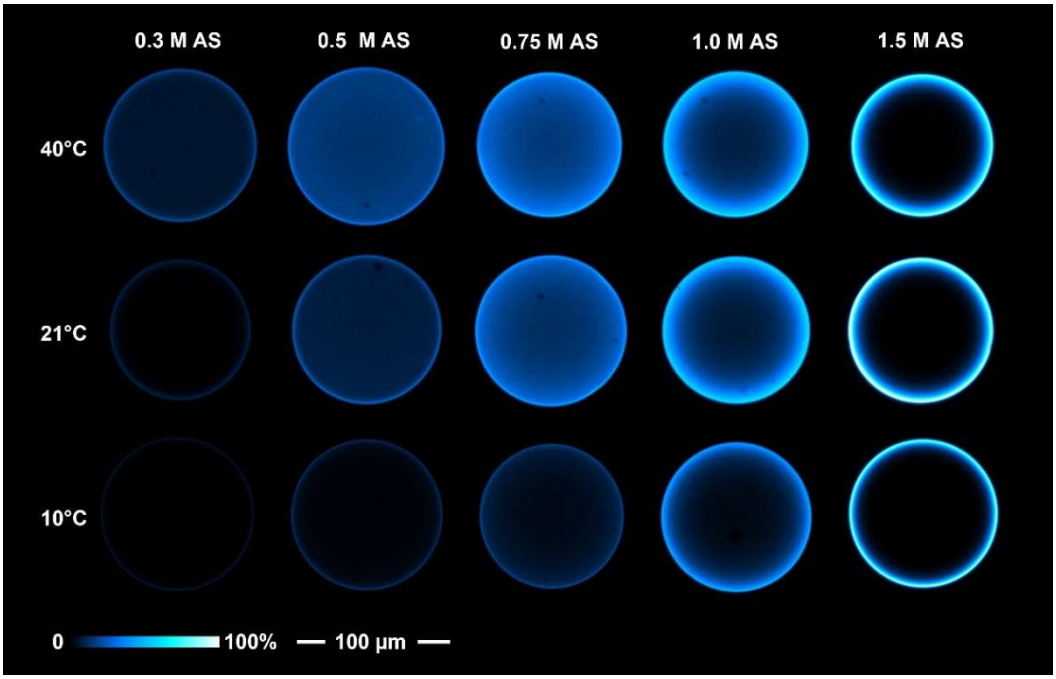

Figure 11: CLSM images of temperature-dependent binding of Alexa Fluor 647-tagged BSA to Butyl Sepharose 4FF beads at AS concentrations of 0.3 – 1.5 M and temperatures of 10, 21 and 40 ◦C. See text for details.

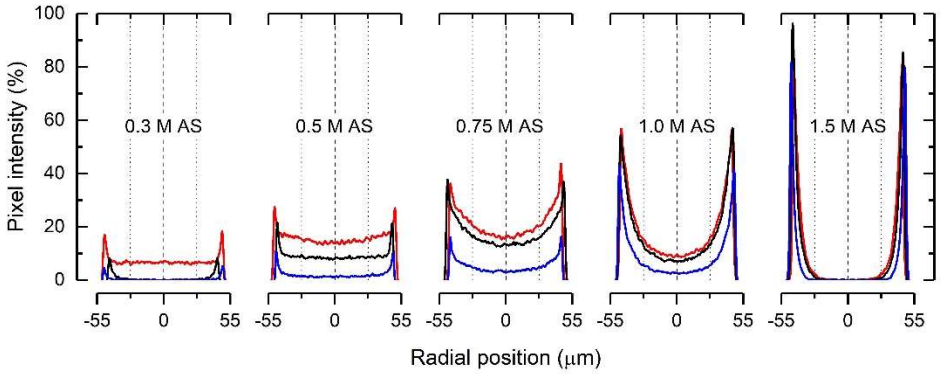

Figure 12: Intensity profiles of beads taken from the left-to-right horizontal midpoint of each bead featured in Figure 11. Pixel intensity represents image brightness, and is the raw output from the CLSM, reported as grey value. The red, black, and blue traces represent binding temperatures of 40, 21 and 10 ◦C respectively.

temperature on fluorescence intensity and intraparticle distribution of adsorbed BSA in Butyl Sepharose 4FF beads can be appreciated at all AS concentrations but is most noticeable below 0.75 M added salt. Temperature plays a secondary role *cf.* salt when high concentrations of the latter (1 and 1.5 M) are employed. Post binding and prior to CLSM analysis samples were washed at the binding temperature. At 10 °C in the presence of 0.3 – 0.75 M AS concentrations and at 21 °C in 0.3 M AS, binding is weak; thus, much of the adsorbed BSA is lost during the wash step and fluorescence is fainter than expected based on scrutiny of **Figure 10 b**. At 40 °C in 0.3 M AS BSA is transported into the centre of the bead (**Figure 11** and **Figure 12**) and raising the salt concentration to 0.5 M increases bead fluorescence uniformly across the bead diameter. At the lower temperatures (21 °C and especially 10 °C) BSA binding is very feeble in 0.3 and 0.5 M AS; the difference in fluorescence (**Figure 11**) and pixel intensity (**Figure 12**) At 40 and 10ºC in 0.5 M added salt is particularly striking and lends support to the selection of this AS concentration for all subsequent work (i.e., pulse-response HIC and TCZR-HIC experiments). Marked and progressive changes in fluorescence intensity and distribution occur as the salt concentration is raised beyond 0.75 M, regardless of temperature, i.e., sharp adsorption fronts develop, separating saturated shells from empty cores, indicating that intraparticle transport of BSA is dominated by hindered pore diffusion (Susanto et al., 2007; Roberts et al., 2020). At these high AS concentrations (>1 M) extensive unfolding, strong binding, and aggregation of BSA in outer regions of the Butyl Sepharose 4FF adsorbent particles (Ueberbacher et al., 2010) blocks the pores preventing further transport to the bead interiors.

3.3.3. Pulse-response HIC

Prior to trialling TCZR-HIC, pulse-response experiments (**Figure 13**) Were conducted using a small glass column packed with Butyl Sepharose 4FF submerged in a water bath held at 40 °C. BSA was supplied as 2 mg pulses (equivalent to 33% of the equilibrium binding capacity of 6 mg·mL^{-1}) to the equilibrated bed at 0.18 mL·min in 50 mM sodium phosphate, pH 7.5 containing 0.5 M AS. The beds were then washed with the same buffer at the same temperature. Under these conditions <20% of the absorbed BSA (**Figure 13, Table** 3), identified by Jungbauer et al. (Jungbauer et al., 2005) as weakly bound native BSA, elutes isocratically as a small broad peak (<3 CV). By contrast retained BSA, elutable by lowering the salt concentration or stripping with 20% (*v/v*) ethanol, is predominantly unfolded (Jungbauer et al., 2005; Ueberbacher et al., 2010; Müller and Franzreb, 2012).

Figure 13 b and **Table 3** show that a substantial fraction (two-thirds) of this tightly bound BSA can be desorbed without change in mobile phase composition, simply by transferring the column to an ice water bath maintained at ~10 °C. Cooling the column in this manner generated a broad strongly tailing elution peak (extending over >6 CV) containing 56% of initially bound BSA. Firmly bound BSA, i.e., that not eluted by cooling, was desorbed from the column in a third sharp peak (23.2% recovered) by stripping with 20% (*v/v*) ethanol. Immediate stripping of the column with 20% (*v/v*) ethanol post isocratic elution (i.e., omitting the cooling step) resulted in a sharp strip peak (**Figure 13 a**) of greater magnitude (87.1% recovery). No further protein was recovered by cleaning the beds with 1 M NaOH.

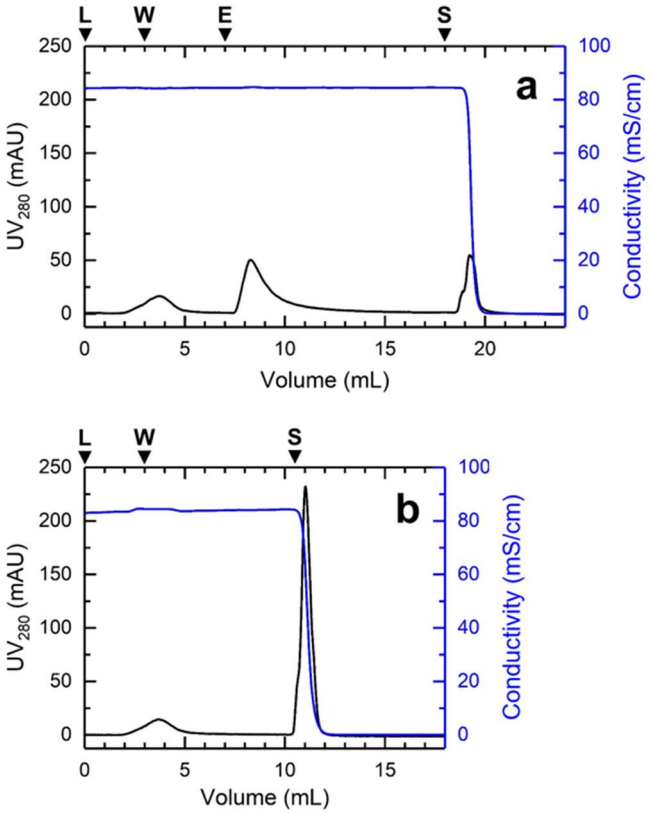

Figure 13: Pulse-response chromatography of BSA on Butyl Sepharose 4FF columns. BSA (2 mg equiv. 33% EBC) was loaded to the columns in sodium phosphate buffer pH 7.5 supplemented with 0.5 M AS at Φ = 40 ◦C and washed at the same temperature. Columns were then: (a) eluted by being immersed in an ice bath (Φ = 10 ◦C) before stripping with 20% (*v/v*) ethanol (Φ = 10 ◦C); or (b) stripped with 20% (*v/v*) ethanol at Φ = 40 ◦C. Loading, wash, elution, and strip phases are indicated arrow heads and the letters L, W, E and S respectively UV absorbance and conductivity traces are respectively indicated by black and blue traces.

Table 3: Evaluation of process performance during pulse response HIC of BSA corresponding to Figure 13.

Experiment	Φ = 40 °C		Φ = 10 °C		% Mass balance
	Eluted (%)	Firmly bound (%)	Eluted (%)	Stripped (%)	
Bath @ 40 °C (Figure 13 a)	16.9	83.1	-	87.1	104.0
Baths @ 40 & 10 °C (Figure 13 b)	17.7	82.3	56.0	23.3	97.0

3.3.4. Batch mode TCZR-HIC of BSA

With the benefits of cooling as a means of elution clearly established, temperatures for binding and elution were transferred to TCZR HIC operation in batch and subsequently continuous modes using 3.4 mL beds of Butyl Sepharose 4FF packed in a thin-walled stainless-steel column (ID = 6 mm), cabinet and TCZ temperature of 40 °C and 10 °C respectively and mobile phase of 0.3 mm·s^{-1} and TCZ velocity of 0.1 mm·s^{-1}. Analogous to pulse-response experiments (**Figure 13**) In batch TCZR-HIC (**Figure 14**), 2 mg BSA were applied to equilibrated beds at 40 °C in 50 mM sodium phosphate pH 7.5 containing 0.5 M AS and the columns were subsequently irrigated with the same buffer at the same flowrate.

The first peak in both chromatograms (**Figure 14 a** & **Figure 14 b**) is of weakly adsorbed native BSA and is much smaller (<3% of the load, **Table 4**) than those observed in the bath pulse-response experiments (<20%, **Figure 13,**

Table 3), and likely relates to the- >3 fold lower BSA loading employed as a percentage of equilibrium binding capacity, i.e., 9.8% *cf.* 33%. Previously, Müller and Franzreb (Müller and Franzreb, 2012) observed that while the degree of BSA unfolding on Butyl Sepharose 4FF columns is practically independent of the amount loaded at temperatures of 10 and 25 °C, at 40 °C the extent of unfolding increases markedly at low BSA loadings; supporting earlier findings from Muca et al. (Muca et al., 2010) that increasing temperature strongly enhances BSA unfolding and retention in HIC. TCZ migration along the column was initiated shortly after weakly bound BSA had eluted from the column, and the first thermally eluted peak was generated as the TCZ passed the column exit. At

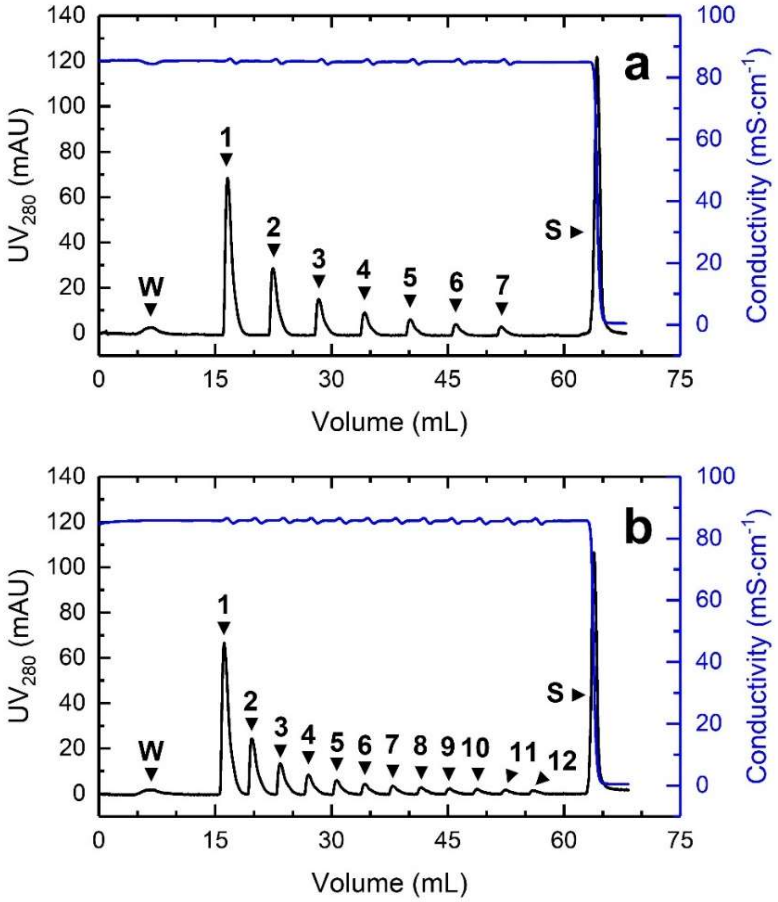

Figure 14: Batch TCZR-HIC chromatograms using Butyl Sepharose 4FF in 0.5 M AS in 50 mM sodium phosphate buffer pH 7.5. Each chromatogram features multiple movements of the TCZ at a velocity vc of 0.1 mm·s^{-1}. Columns were loaded with 2 mg of BSA (0.5 mL of 4 mg·mL^{-1}) and washed at the binding temperature (40 ◦C) prior to initiating the first of seven (a) or twelve (b) sequential movements of the TCZ. Arrow heads with letters or numbers indicate wash (W), TCZ elution (1 – 12) and strip (S) peaks. UV absorbance and conductivity signals are respectively indicated by black and blue traces.

Table 4: Evaluation of process performance for batch TCZR-HIC of BSA corresponding to Figure 14.

Experiment	% BSA recovered				% Mass balance
	Feed (Φ = 40 °C)	Wash (Φ = 40 °C)	TCZ elution cycles (Φ = 10 °C)	Strip (Φ = 10 °C)	
7 × 31.83 min cycles (**Figure 14 a**)	100	2.7	64.4	45.7	112.8
12 × 20.1 min cycles (**Figure 14 b**)	100	2.3	66.1	39.0	107.3

this point the TCZ reverses its direction of travel and is quickly returned (v_c = 20 mm·s^{-1}) to the top of the bed in readiness for its next descent. In the first experiment (**Figure 14 a**) a total of seven THZ movements or cooling cycles were performed. Each travel of the TCZ is accompanied by a sharp elution peak and small blip in the conductivity profile (Ketterer et al., 2019). The size of thermal elution peaks drops with each successive cycles (**Figure 14, Table 4**) as the portion of thermally elutable BSA bound to the bed is progressively reduced with each elution. TCZR mediated elution from Butyl Sepharose 4FF in the stainless-steel column compared favourably with immersion of the whole bed (contained in a glass column) in the 10 °C ice bath. Combined TCZ cycles recovered >64% of the loaded BSA *cf.* 56% by cooling the entire bed. The first TCZ cycle accounted for 48% of the thermally eluted BSA, and each subsequent cycle desorbed diminishing amounts. In the second batch TCZR HIC experiment (**Figure 14 b**) the TCZ 'start' and 'end' positions were adjusted (while maintaining the same v_c of 0.1 mm·s^{-1}) to reduce the cycle time from 31.83 to 20.1 min. In this manner five more travels could be conducted within approximately the same period (i.e., 12 *cf.* 7) reducing the peak-to-peak distance from ~5.8 mL (**Figure 14 a**) to ~3.6 mL (**Figure 14 b**). A small improvement in thermal elution yield of BSA was observed, i.e., twelve combined cooling cycles recovered 66.1% *cf.* 64.4% (**Table 4**). In both runs the first TCZ cycles accounted for nearly 50% of the thermally eluted BSA (48%, **Figure 14 a**, *cf.* 46%, **Figure 14 b**), and each subsequent cycle desorbed decreasing quantities of BSA. Taken collectively it appears that: (i) more than 60% of the BSA retained on Butyl Sepharose 4FF at 40 °C in 0.5 M AS can be recovered by a 30 °C thermal shift to 10 °C; (ii) The TCZR system is able to match/surpass the elution performance achieved by cooling the entire bed; (iii) a

significant portion of BSA (ca. 40%) remains bound after cooling, but is easily recovered by stripping with 20% (*v/v*) ethanol.

3.3.5. SEC analysis of feedstocks and fractions from batch TCZR-HIC of BSA

BSA solutions contain a dynamic mix of interconverting monomeric and multimeric structures of closely related but non-identical molecules; (Madeira et al., 2022; Roberts and Carta, 2023) the amounts of each depend on solvent properties (e.g., buffer pH, salt concentration and type of salt), temperature and protein concentration. To gain a deeper understanding of TCZR-HIC performance, feedstocks and peak fractions were analysed by SEC. The BSA concentration of feedstocks used in chromatographic studies varied between 0.25 to 4 mg·mL^{-1}.

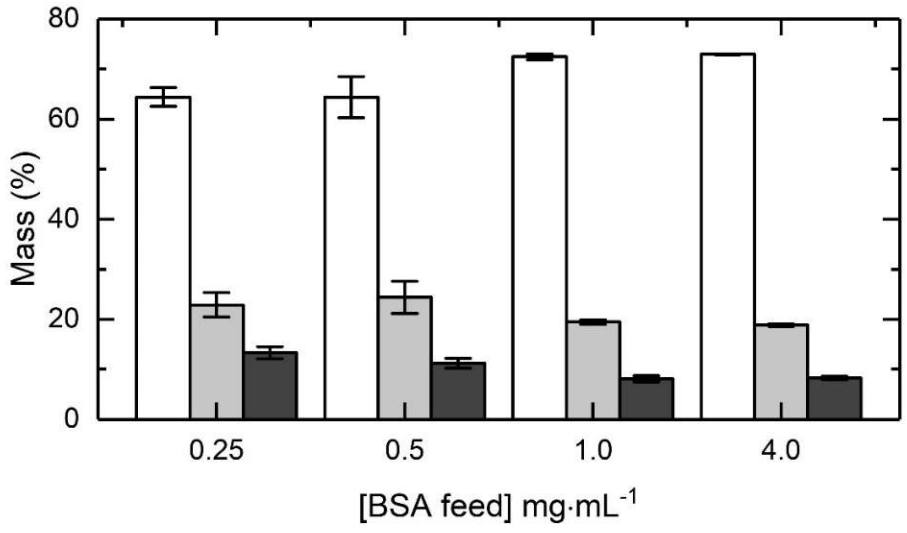

Figure 15: Influence of BSA concentration in the feed on composition determined by SEC. BSA was prepared in 50 mM sodium phosphate supplemented with 0.5 M AS. Key: monomers (white bars); 2–4 mers (pale grey bars); HMW species (dark grey).

Figure 15 shows that the composition remained essentially the same at 1 and 4 mg·mL^{-1} BSA (i.e., 72.4 *cf.* 72.9% monomers; 19.5 *cf.* 18.8% 2-4 mers; 8.1 *cf.* 8.2% HMW), but at lower BSA concentrations (0.25 and 0.5 mg·mL^{-1}) the monomer content dropped to 63.4% at the expense of increased presence of small oligomers (22.9 – 24.4%) and HMW (11.2 – 13.3%). These findings, though initially counterintuitive, accord with observations that aggregation of BSA is more prevalent in dilute solutions, indicating no inherent tendency of the molecule to aggregate (Honda et al., 2000; Borzova et al., 2016; Madeira et al., 2022). Madeira and coworkers (Madeira et al., 2022) hypothesized there were two distinct monomeric forms in solution, one with no tendency to aggregate the other exhibiting increasing aggregation tendency on dilution, and that dilution increases the relative proportion of the latter which in turn drives increased aggregation. **Figure 16 a** and **Table 5** respectively show SEC composition analysis of the feed (4 mg·mL^{-1}) and pooled peak fractions from the TCZR-HIC run in **Figure 14 b**, and key mass balance and purity data for the same experiment. The feed composed <73% monomers, <19% small oligomers and >8% HMW, and the wash peak contained only monomer (**Figure 16 a**). All twelve TCZ eluted peaks were essentially composed of 95% monomers and 5% small oligomers. No significant differences in composition were noted from one TCZ cycle to the next other than trace levels of HMW (0.06 ± 0.01%) detected in the first few TCZ elution cycles, but not in the last seven elution peaks. In stark contrast, 2-4 mer and HMW combined accounted for nearly 45% of the BSA in ethanol strip peak. The mass balance for overall BSA recovery in the experiment closed to >107% (**Table 5**). Monomers in TCZ pool of elution peaks were >95% pure and, based on the improbable assumption of 'no changes in composition' during chromatography, were recovered in 119% yield. The mass balances for recovered small oligomers (86.6%) and HMW (52.4%) did not close.

From this it follows that some portion of oligomeric and higher order BSA desorbed from the column during regeneration with 20% (*v/v*) ethanol is converted back to monomeric form (see **section 3.6**).

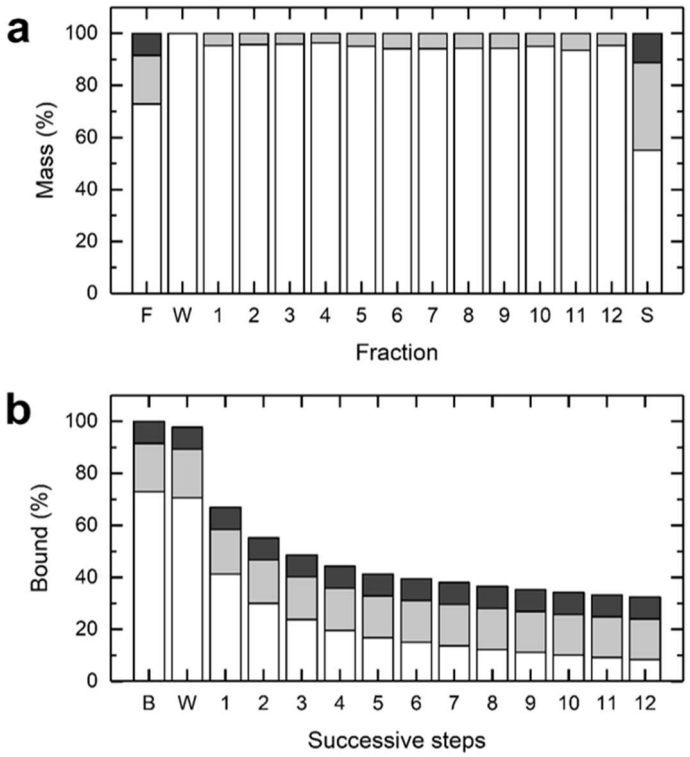

Figure 16: (a) SEC analysis of fractions and (b) calculated changes in mass of adsorbed BSA species during TCZR-HIC (Figure 14 b). Key: feed (F); wash (W); TCZ elution peaks (1 – 12); strip (S); monomers (white bars); 2–4 mers (pale grey bars); HMW species (dark grey)

Table 5: Tracking of BSA monomer, dimer and HMW species during TCZR-HIC on Butyl Sepharose 4FF Figure 14 b.

Fraction	BSA (mg)	BSA composition (%)			BSA composition (mg)			Monomer	DF (-)		
		Monomers	2-4 mers	HMW	Monomers	2-4 mers	HMW	Recovery (%)	PF (-)	2-4mer	HMW
Feed (F)	2.0	72.9	18.7	8.5	1.46	0.37	0.17	100	1.0	1.0	1.0
Wash (W)	0.05	100	0	0	0.05	0	0	3.2	1.37	–	–
Elution pool (1-12 incl.)	1.32	95.3	4.6	0.05	1.26	0.06	<0.001	86.3	1.31	6.12	257
Strip (S)	0.78	55.1	33.6	11.3	0.43	0.26	0.09	29.5	0.76	1.42	1.92
Sum of all fractions	2.15				1.73	0.32	0.09				
% Mass balance	107.3				119.0	86.60	52.4				

3.3.6. Continuous TCZR-HIC

Having established the effectiveness of the TCZ in selectively eluting essentially only monomeric forms whilst accumulating more hydrophobic multimers/HMW aggregates during batch mode HIC, we next employed TCZR-HIC in continuous mode at three different BSA feed concentrations (**Figure 17**) to explore its potential/define its limits as a protein aggregate removal step. In previous work using TCZR and THZR systems respectively configured with smart thermoresponsive cation exchange adsorbents (Cao et al., 2015) and a thermoresponsive rProtein A matrix (Ketterer et al., 2019) we were able to match the rates of the protein loading/binding with those of thermal elution. This resulted in elution peaks reaching a steady maximum height returning to the baseline between peaks. In both studies the travelling devices were operated over 6 – 9 cycles and steady state was typically observed after the 2 – 4 cycles depending on the target protein concentration in the feed. Given the findings from batch experiments, best illustrated by **Figure 16 b**, that tightly binding higher order species accumulate on the column and their binding status is not affected by cooling, at some point during continuous supply of BSA to the bed the column's capacity for 2-4 mer and HMW will be reached, and these species will begin to appear in the exiting flow along with monomer. At this point feeding should stop, so that the column can be regenerated (by stripping with 20% (*v/v)* ethanol followed by NaOH) in readiness for the next round of processing (continuous feeding of BSA and TCZ elution of monomer). It also follows that the working capacity for monomer elution by TCZ cooling must decline at some point during extended operation, meaning that true quasi-steady state operation is not possible. To test the above reasoning in this work feed

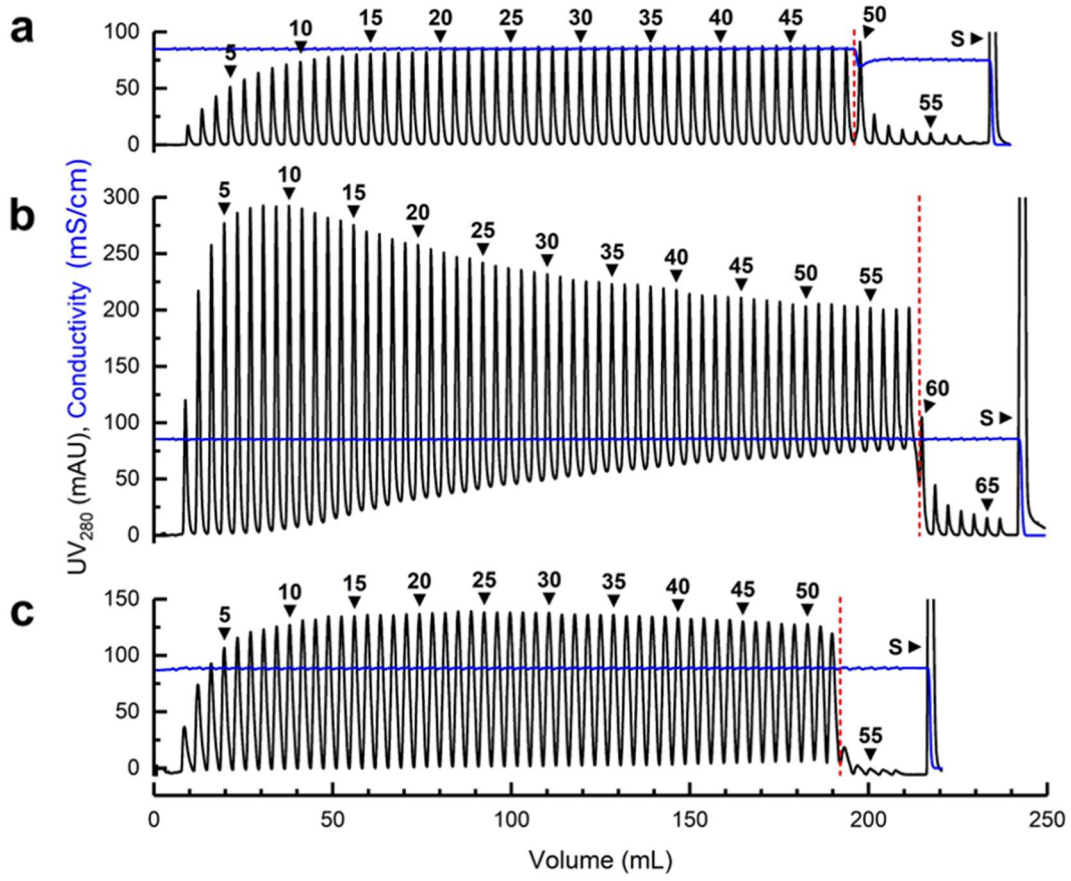

Figure 17: Chromatograms arising from continuous TCZR-HIC tests with Butyl Sepharose 4FF in 0.5 M AS in 50 mM sodium phosphate buffer pH 7.5 employing 58+ movements of the TCZ at a velocity vc of 0.1 mm·s^{-1}. BSA was continuously supplied at: (a) 0.25 mg·mL^{-1} to a fresh column (condition 1); (b) 1 mg·mL^{-1} to a re-generated column (condition 2); and (c) 0.5 mg·mL^{-1} to a fouled column (condition 3). Labelled arrow heads indicate sequential TCZ elution and the ethanol strip (S) peak, and the dashed red lines indicate termination of BSA supply marking the transition from continuous to batchwise operation. The distance travelled by the TCZ was 130 mm (a) or 120 mm (b, c) resulting in a peak-peak cycle times of 21.78 min or 20.1 min respectively. UV absorbance and conductivity signals are respectively indicated by black and blue traces.

was continuously administered at different BSA concentrations (0.25, 1 and 0.5 mg·mL^{-1}) to freshly packed (**Figure 17 a**), regenerated (**Figure 17 b**) or fouled (**Figure 17 c**) beds of Butyl Sepharose 4FF and operation was extended to 58+ travels. Feeding of BSA in buffer (phosphate containing 0.5 M AS) to the beds was maintained for 190 – 210 mL during which the TCZ had moved 49 – 58 times before switching to buffer only. TCZ movements were continued at the same frequency another 5 – 9 times mimicking batch mode operation. Bound BSA not eluted by the TCZ was desorbed after the last movement by stripping with 20% (*v/v*) ethanol.

Comparison of individual eluted peaks within the chromatograms (**Figure 17**) Indicates a certain time is required before maximum peak height/area is reached and that raising the BSA feed concentration speeds its acquisition. For example, at 0.25, 0.5 and 1 mg·mL^{-1} BSA in the feed maximum peak size were reached at peaks 27 (**Figure 17 a**), 23 (**Figure 17 c**) and 8 (**Figure 17 b**) respectively. Other notable aspects discussed below are the UV_{280} baseline signal, eluate composition during the continuous loading-unloading phase, purification performance and mass balance closures, and the width and shape of TCZ elution peaks.

3.3.7. Continuous TCZR-HIC on HIC columns (Conditions 1 & 2)

The baseline signal remained flat for the 'fresh bed + 0.25 mg·mL^{-1} BSA' experiment (condition 1; **Figure 17 a**), during which 49 movements of the TCZ had been completed during the continuous loading-unloading phase followed by a further 8 without feeding (simulating batchwise operation; section 3.4). SEC analysis of every 5th peak (5, 10, 15, 20, 25, 30, 35, 40 and 45) during the continuous loading-unloading part of the run (until

and including peak 49) Confirmed high monomer purity (av. 94.4 ± 0.6%) across all TCZ elution peaks; 2-4 mer and HMW respectively accounted for 5.6 ± 0.6% and <0.05 ± 0.025% of the BSA population (**Figure 18 a**). On terminating the supply of BSA increased levels of 2-4 mer and HMW were detected in peaks 50 (12.1% 2-4 mer, 0.21% HMW) and 55 (16.0% 2-4 mer, 0.38% HMW); thus, monomer purity was noticeably reduced in these fractions (**Figure 18 a**). These reductions can be explained at least in part by a pump valve error which led to dilution of the mobile phase, lowering the conductivity from 85 $mS \cdot cm^{-1}$ to 70 – 76 $mS \cdot cm^{-1}$ (**Figure 17 a**) thereby weakening adsorption of bound 2-4 mer and HMW BSA. As the mass contributions of peaks 50 – 58 were small (1.89 mg) *cf.* all preceding peaks (32.21 mg) monomer purity of the pool dropped only slightly to 92.7% (**Table 6, condition 1**). Of the 48.9 mg BSA applied (31.1 mg monomer, 10.7 mg 2-4 mers, 7.1 mg HMW), 34.1 mg was recovered by the TCZ cooling cycles (31.6 mg of which was monomer), and stripping post TCZ with 20% (*v/v*) ethanol closed the mass balance to >93% (**Table 6, condition 1**). Monomers were recovered in high yield and purity, depleted 3.1-fold with respect to 2-4 mers and 92-fold in HMW species.

Increasing the BSA concentration continuously applied to same column to 1 $mg \cdot mL^{-1}$, after cleaning and re-equilibration (condition 2), compromised TCZ elution performance. Approximately 30 mL (30 mg) into loading, roughly coincident with the 8^{th} travel of the TCZ (which issued the tallest peak in the run at 2.6 mg BSA), the baseline UV signal started drifting upwards, while the peak height diminished, creating a striking chromatographic profile (reminiscent of the dorsal fin of a Sailfish or Marlin). The mass passing in the 'bleed' (area between the original baseline line and the TCZ eluted peaks)

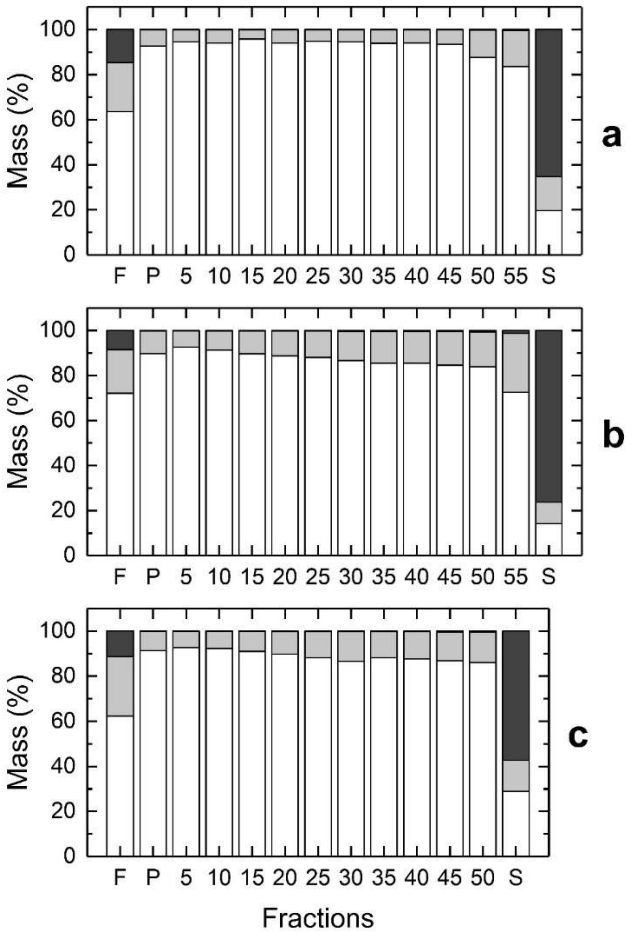

Figure 18: SEC analysis on selected fractions taken during continuous TCZR-HIC of BSA (Figure 17). Fractions were isolated from, (a) fresh (condition 1), (b) regenerated (condition 2) and (c) fouled (condition 3) Butyl Sepharose 4FF columns. Key: feed (F); elution pool (P); selected elution peaks (5 – 55); strip (S); monomers (white bars); 2–4 mers (pale grey bars); HMW species (dark grey bars).

grew throughout the loading phase to represent 45% of the total BSA eluted on completion (TCZ elution peaks accounted for 55% of the total). Note, the rising baseline/increasing bleed does not reflect increasing passive passage of BSA through the bed. Rather it implies bound monomers are displaced back into the mobile phase by more hydrophobic and avidly binding 2-4 mer and HMW BSA species. With gradually

increasing supply to the bed available capacity for adsorbing BSA is consumed by tighter binding species, thus levels of more readily desorbed monomers drop, which accounts for diminishing height of TCZ elution peaks observed through the loading-unloading phase

of **Figure 17 b**. SEC analysis of fractions generated after the 5th travel of the TCZ confirmed gradual reduction in monomer purity primarily at the expense of 2-4 mer, though increasing HMW contamination of the eluate is discernible from peak 20 onwards (**Figure 18 b**). Approximately 214 mg of BSA (72.1% monomers, 19.4% 2-4 mers, 8.5% HMW) was applied in this experiment (**Figure 17 b**; **Table 6**, condition 2) of which >188 mg was eluted (184 mg during feeding, 4.2 mg once feeding had stopped) and a further 23.4 mg was recovered in the 20% (*v/v*) ethanol strip. BSA monomers were recovered in the eluate in high yield but at lower purity (89.6%) *cf.* that observed with the 0.25 mg·mL^{-1} feed (92.7%; **Table 6**, condition 1). For 'clean' beds continuously challenged with BSA at 0.25 and 1 mg·mL^{-1} (**Figure 17 a & Figure 17 b**) mass balances for monomer exceeded 100% (**Table 6, conditions 1 and 2**) while those for 2-4 mers fell far short, i.e., 38.8% (**Table 6, condition 1**) and 51.2% (**Table 6, condition 2**). As noted earlier (**section 3.5**) The process of stripping with ethanol likely dissociates some higher order BSA structures, 2-4 mers in particular, to monomeric forms.

Plots of BSA composition vs accumulated mass of BSA supplied to the HIC columns (**Figure 19**) Provide a clearer picture of how eluate composition changes during continuous TCZR HIC of BSA on Butyl Sepharose 4FF as a function of feed concentration.

At 0.25 mg BSA per mL the composition of the elute remained relatively stable throughout the loading-unloading phase (averaging 94.4% monomer, 5.6% 2-4 mer, <0.05% HMW). For the 1 mg·mL^{-1} condition, monomer accounted for 92.5% of the BSA present in peak 5 (**Figure 19, first point**) and was generated before the baseline began

Table 6: Tracking of BSA monomers, 2-4 mers and HMW species during continuous TCZR-HIC on Butyl Sepharose 4FF (Figure 17). Compositions were determined by SEC analysis (Figure 18). Key: PF = purification factor; DF = depletion factor.

Condition 1: Fresh bed supplied with 0.25 mg·mL^{-1} BSA (Figure 17 a & Figure 18 a)

Fraction	BSA (mg)	BSA composition (%)			BSA composition (mg)			Monomer	DF (-)		
		Monomer	2-4 mer	HMW	Monomer	2-4 mer	HMW	Recovery (%)	PF (-)	2-4 mer	HMW
Feed (F)	48.9	63.6	21.8	14.6	31.1	10.7	7.1	100	1.0	1.0	1.0
Elution pool (P)	34.1	92.7	7.1	<0.2	31.6	2.4	0.05	101.6	1.46	3.07	92.1
Strip (S)	11.5	19.7	15.0	65.3	2.3	1.7	7.5	7.3	0.31	1.45	0.22
Sum of all fractions	45.6				33.9	4.1	7.5				
% Mass balance	93.1				108.9	38.8	105.6				

Condition 2: Regenerated bed supplied with 1.00 mg·mL^{-1} BSA (Figure 17 b & Figure 18 b)

Fraction	BSA (mg)	BSA composition (%)			BSA composition (mg)			Monomer	DF (-)		
		Monomer	2-4 mer	HMW	Monomer	2-4 mer	HMW	Recovery (%)	PF (-)	2-4 mer	HMW
Feed (F)	213.7	72.1	19.4	8.5	154.0	41.4	18.3	100	1.0	1.0	1.0
Elution pool (P)	188.2	89.6	10.1	<0.3	168.7	19.0	0.5	109.5	1.24	1.92	30.5
Strip (S)	23.4	14.2	9.6	76.2	3.3	2.2	17.8	2.2	0.20	2.02	0.11
Sum of all fractions	211.6				172.0	21.2	18.4				
% Mass balance	99.00				111.7	51.2	100.6				

Condition 3: Fouled bed supplied with 0.50 mg·mL^{-1} BSA (Figure 17 c & Figure 18 c)

Fraction	BSA (mg)	BSA composition (%)			BSA composition (mg)			Monomer	DF (-)		
		Monomer	2-4 mer	HMW	Monomer	2-4 mer	HMW	Recovery (%)	PF (-)	2-4 mer	HMW
Feed (F)	96.1	62.4	26.3	11.3	60.0	25.3	10.9	100	1.0	1.0	1.0
Elution pool (P)	112.4	91.3	8.5	<0.2	102.7	9.6	0.2	171.2	1.46	3.09	59.5
Strip (S)	10.2	29.0	13.7	57.3	3.0	1.40	5.8	4.9	0.46	1.92	0.20
Sum of all fractions	122.6	62.4			105.6	11.0	6.0				
% Mass balance	127.6	91.3			176.1	43.4	55.6				

to rise (**peak 8; Figure 17 b**). Thereafter the contribution of monomers in elution fractions fell steadily to reach <84% at peak 50 (**Figure 19,** last data point), paralleling the increasing appearance of 2-4 mer and HMW species (**Figure 19;** >15% and >0.6% respectively) and rising baseline 'bleed' and shrinking 'monomer-rich' peaks observed in **Figure 17 b**.

Realistically, at any given BSA feed concentration continuous operation of TCZR-HIC should continue to the point where the baseline starts to rise, as this point should coincide with deterioration of performance, e.g., marked by a drop in monomer purity (**Figure 18 & Figure 19**), whereupon the bed should be regenerated before initiating the next round of continuous TCZR HIC. That point was after only ~30 mg had been applied (~10 mg BSA per mL ofmonomer.1 mg·mL^{-1} (**Figure 17 b**) but was not reached at 0.25 mg·mL^{-1}

(**Figure 17 a**), signifying in this case, a safe/conservative loading capacity of >50 mg or 17 mg of BSA per mL of matrix, per operating cycle, featuring >50 movements of the TCZ with each unloading 0.7 – 0.8 mg of >94% pure monomer.

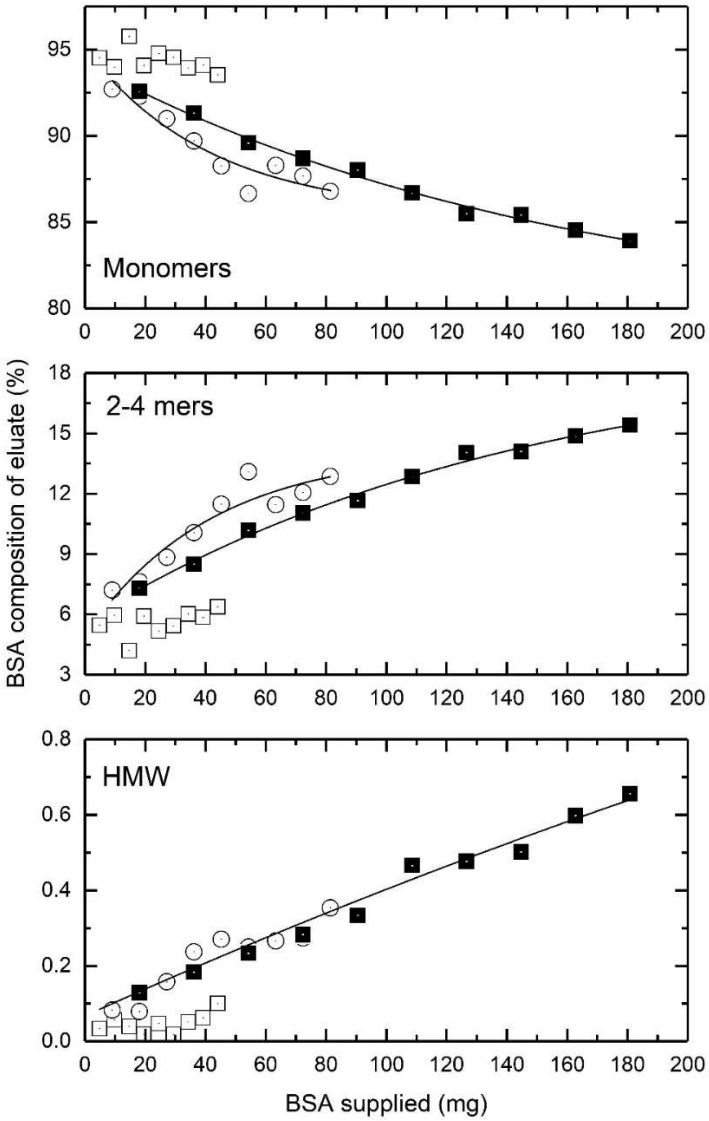

Figure 19: BSA eluate composition vs. BSA supplied during continuous TCZR-HIC of BSA (Figure 17, loading phase only). Key: fresh column fed with 0.25 mg·mL^{-1} BSA (open squares); regenerated column fed with 1 mg·mL^{-1} BSA (filled squares); fouled column fed with 0.5 mg·mL^{-1} BSA (open circles).

3.3.8. Continuous TCZR-HIC on a fouled HIC column

The chromatogram for continuous TCZR-HIC of BSA at 0.5 mg·mL^{-1} on a fouled bed of Butyl Sepharose 4FF (i.e., one previously exposed to 100 mg of BSA, cleaned and stored in 20% (*v/v*) ethanol, but not subjected to 1 NaOH) appears superficially similar to those conducted with freshly cleaned beds of the same matrix, with maximum peak heights roughly correlating with BSA feed concentration and gradually decreasing peak magnitude after the 23rd pass of the TCZ (**Figure 17 c**). However, there are salient differences, i.e., the UV_{280} baseline rises continuously from the outset (reaching 8 mAU at ~190 mL accounting for 11.5 mg or 10.2% of the BSA eluted), and the TCZ elution peaks are much wider/less sharp, and their width gradually increases as more BSA is supplied to the bed (**Figure 20**). For example, for the clean columns full-width-at-half-maximum (FWHM) values during loading remain relatively constant at 0.76 ± 0.01 mL and 0.84 ± 0.02 mL at 0.25 mg·mL^{-1} and 1 mg·mL^{-1} respectively. For the fouled column FWHM starts at 1.42 mL for the first elution peak and climbs to a maximum of 1.99 mL for the 53rd. On switching to batch operation FWHM drops steeply in all cases consistent with reduced mass in the elution peaks. In total, 96.1 mg of BSA was supplied to the fouled column (**Table 6, condition 3**), 112.4 mg was collected in the elution pool (of which 102.7 mg was monomer representing a >1.7 increase *cf.* the feed) and 10.2 mg in the strip fraction, i.e., considerably more came off the column than was applied (mass balance = 127.6%) reflecting that BSA accumulated on the column in previous trial runs (not shown) appeared in the exiting flow of the run in **Figure 17 c**. The impact of this 'extra source' of BSA on eluate composition can be seen in **Figure 18 c & Figure 19**. Monomer purity in the eluate from the fouled column fed with 0.5 mg·mL^{-1} deteriorated

more readily than for the clean column fed with twice the BSA concentration in plots of composition vs. BSA supplied (**Figure 19**), largely due to enhanced levels of 2-4 mers.

For example, monomer purities dropped below 90% after supply of just 25 mg BSA to the fouled column (condition 3) *cf.* >50 mg to the clean column (condition 2), but the gap between the two conditions appears to close at higher BSA supply, i.e., beyond ~70 mg. Hence, the fouled column fed with 0.5 $mg \cdot mL^{-1}$ BSA delivered comparable purification performance (**Table 6, condition 3**) To that of the freshly regenerated bed of identical matrix operated with twice the BSA concentration (**Table 6, condition 3**).

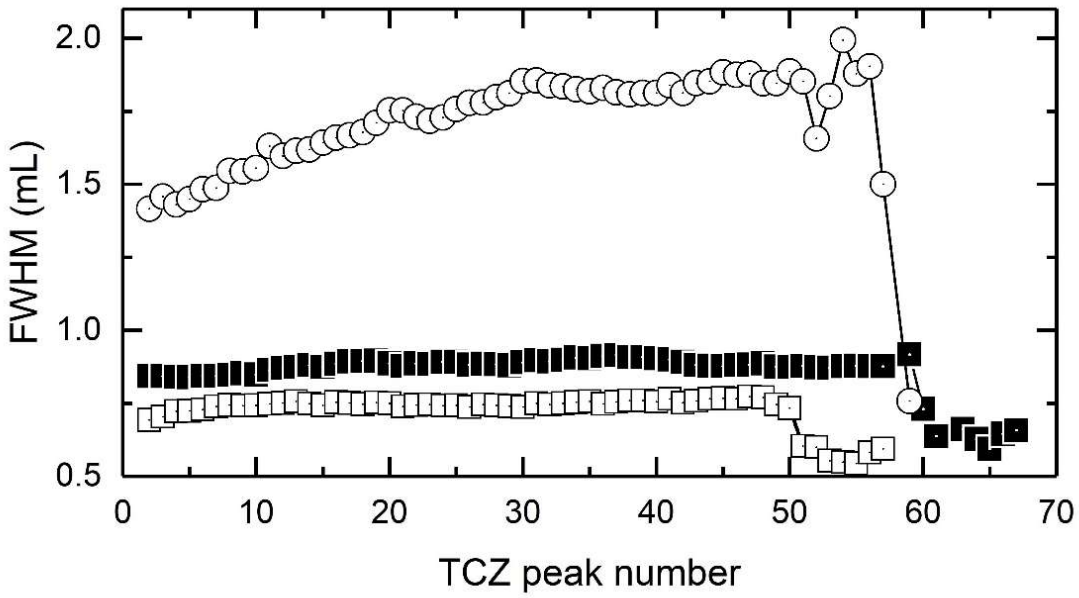

Figure 20: Peak width vs. TCZ peak number during continuous TCZR-HIC of BSA (Figure 17). Key: fresh column fed with 0.25 $mg \cdot mL^{-1}$ (open squares); regenerated column fed with 1 $mg \cdot mL^{-1}$ BSA (filled squares); fouled column fed with 0.5 $mg \cdot mL^{-1}$ (open circles).

3.4. Conclusions

In earlier work, Müller and Franzreb (Müller and Franzreb, 2012) showed how temperature alone could be used to control the sorption behaviour of BSA in HIC. Novel TCZR/THZR systems capable of performing continuous temperature-controlled adsorption chromatography in a single column were subsequently developed and trialled for protein fractionation by ion exchange (Müller et al., 2013; Cao et al., 2015) and affinity separation (Ketterer et al., 2019).

In this study the systematic advance of continuous low-salt TCZR-HIC for the separation of protein monomers from higher order species is demonstrated. Suitable conditions for temperature reversible binding of BSA to Butyl Sepharose 4FF without any modulation of buffer composition were identified, from batch binding and CLSM studies mapping AS concentration and temperature combined, and confirmed in pulse-response temperature switching experiments, before successfully transferring to TCZR-HIC, first in batch and subsequently in continuous operating modes.

SEC analysis of BSA in TCZ eluted peaks generated during continuous TCZR-HIC revealed they were substantially purified with respect to monomer. In the best case (condition 1 employing the lowest BSA feed concentration of 0.25 $mg \cdot mL^{-1}$) continuous TCZR-HIC operated at >17 mg BSA applied per mL of bed delivered monomeric BSA of >94% purity substantially depleted in higher order structures (5.6% 2-4 mer, <0.05% HMW) *cf.* the initial feed (63.6% monomer, 21.8% 2-4 mer, 14.6% HMW), but raising the BSA feed concentration applied impaired both operational capacity and purity profile.

Ultimately, two factors compromise the effective use of continuous TCZR-HIC in this work, namely: (i) the low protein binding capacity of Butyl Sepharose 4FF and other traditional HIC media, especially at low ionic strengths; (Susanto et al., 2007; Müller and Franzreb, 2012) and (ii) The high content of strongly binding higher order species in BSA feeds, which accounted for 23 – 36.4% of the mass depending on the concentration employed. The low binding capacity issue calls for the development of new high-capacity media with heightened sensitivity to temperature (Cao et al., 2015; Mata-Gómez et al., 2016; Tan et al., 2018; Tan et al., 2020). Aggregate levels in mAbs post-capture are typically an order of magnitude lower than for BSA (Gabrielson et al., 2007; Vázquez-Rey and Lang, 2011), and must be reduced to <1% in final mAb formulations (Moussa et al., 2016). It follows that TCZR-HIC might be attractive for the removal of trace level soluble aggregates from mAbs. Monoclonal antibodies are significantly more thermostable than BSA (Michnik, 2002; Brader et al., 2015; Kohli et al., 2015; Molodenskiy et al., 2017; Garidel et al., 2020; Sert et al., 2022) meaning that higher temperatures could be used to enhance binding at low salt concentrations.

Chapter 4

Application of an integrated system for temperature-controlled fast protein liquid chromatography for 'one-column' 'low-salt' hydrophobic interaction chromatography for polishing monoclonal antibodies.

4.1. Abstract

Further optimisation of a temperature-controlled isocratic process employing the Travelling Cooling Zone Reactor (TCZR) for 'one-column' 'low-salt' hydrophobic interaction chromatography (HIC) with Rituximab, a commercially relevant monoclonal antibody, is presented. Adsorption isotherms for Rituximab were determined using several commercial HIC resins, namely Butyl Sepharose 4 FF, Butyl 650M, Butyl 650S, Phenyl 650M, and Phenyl 650S, in 50 mM sodium phosphate buffer, pH 7.5, supplemented with 0.1–0.75 M AS. Temperature-dependent binding was observed for all Butyl ligands to varying extents, while the Phenyl ligands exhibited no detectable temperature responsiveness.

Temperature ranges and AS concentrations were systematically manipulated to identify optimal conditions during pulse-response HIC studies using a Tricorn 5/50 column immersed in a temperature-controlled water bath. Two conditions were selected for TCZR testing: Butyl Sepharose 4 FF with 0.5 M AS; and Butyl 650M with 0.125 M AS. Results indicated that Rituximab's physicochemical properties make it less amenable to thermally driven HIC than BSA. Both batch and continuous operations were demonstrated, though antibody retention and elution challenges persisted, underscoring the need for higher binding and lower elution temperatures and reduced salt dependency.

Future work should focus on re-engineering the TCZR system to allow greater temperature differentials for binding and elution to be achieved, exploring alternative HIC, mixed mode or temperature-sensitive smart polymer resins and further scouting of buffer salts and concentrations.

4.2. Introduction

The global market for mAbs continues to grow, with year-over-year growth of 13.8% (Shaikh and Jaiswal, 2018; Stratis, 2023). To accommodate the increasing demand, industrial investment has predominantly focused on expanding large-scale, capital-intensive production facilities. However, competitive pressures necessitate reducing manufacturing costs due to: (i) the emergence of biosimilars (Sarpatwari et al., 2015); (ii) intensifying global competition (Shukla et al., 2017); and (iii) the proliferation of single-use technologies, lowering the entry barrier (Shulka and Gottschalk, 2013). The industry has a growing interest in continuous processing to alleviate these pressures, which offers several advantages over batch operations, notably in terms of cost reduction, which have been previously mentioned (**Chapter 1** & **Chapter 3**). Several studies examining continuous processing specifically for mAbs report substantial cost saving, efficiency and buffer consumption advantages (Xenopoulos, 2013; Walther et al., 2015; Xenopoulos, 2015; Pollock et al., 2017; Hummel et al., 2019; Gupta et al., 2021; Mahal et al., 2021). Despite the well-documented benefits of transitioning to continuous processing, adoption within the industry has been notably slow (Jungbauer, 2013; Rathore et al., 2015; Xenopoulos, 2015; Pollock et al., 2017; Shukla et al., 2017; Hummel et al., 2019).

Continuous downstream processing continues to offer a significant operational and technical challenge. Several significant barriers persist, including high capital costs, mechanical complexity, and the operational challenges associated with current continuous chromatography technologies such as SMB and PCC. Additionally, batch chromatography methods are heavily reliant on protein A affinity chromatography due to its high selectivity and capacity, which incurs significant expenses due to the elevated

cost of recombinant Protein A resins. To ensure viral clearance and facilitate elution, low pH hold steps are commonly employed for viral inactivation, although these conditions can inadvertently induce aggregation in pH-sensitive mAbs (Ejima et al., 2007; Mazzer et al., 2015; Jin et al., 2019; Walchli et al., 2020). Furthermore, conventional systems generate substantial volumes of environmentally hazardous waste, primarily as a result of extensive buffer consumption and the stringent cleaning-in-place protocols required to maintain operational efficiency (Ho et al., 2010; Kokai-Kun, 2022a; Kokai-Kun, 2022b). To date, effective and widely adopted solutions to these challenges remain elusive.

As a response to these limitations, the study in this chapter investigates the utility of TCZR-HIC as a potential alternative to the conventional mAb purification platform process. Unlike other continuous multi-column systems, TCZR-HIC represents a simplified, single-column format for downstream processing, employing a temperature-controlled adsorption mechanism that eliminates low-pH elution buffers, which are known to induce protein aggregation (Vázquez-Rey and Lang, 2011; Madadkar et al., 2017). By leveraging temperature modulation rather than pH shifts, this approach could provide a more cost-effective and less aggregation-prone purification strategy for large-scale mAb purification. Additionally, the elevated binding temperature provided by the TCZR enables low-salt HIC to be performed, minimising salt usage and improving the sustainability of the technique.

Previous research has explored various strategies to enhance the sustainability of HIC in mAb purification. One approach involved utilising pH modulation instead of high concentrations of salt to regulate adsorption/desorption equilibria (Ghose et al., 2013). In their study Ghose and colleagues employed pH adjustments instead of kosmotropic salt

manipulation to control adsorption and desorption. The authors demonstrated that a comparable degree of HMW species removal could be achieved with a highly hydrophobic Hexyl 650C column, without the inclusion of kosmotropic salts, thereby reducing overall salt consumption and mitigating the environmental impact associated with traditional HIC processes. Binding of mAbs to the HIC resins without kosmotropic salt was highly pH-dependent. Furthermore, aggregate removal performance was inversely correlated with column loading (mg protein·mL^{-1} resin), where lower column loading resulted in greater monomer purification.

A subsequent study by Dilks et al. (2023) expanded on this concept using six mAbs and achieved effective aggregate removal using a Capto Phenyl (High Sub) column without kosmotropic salt and confirmed the same column loading and pH trends (Dilks et al., 2023b). The HMW reduction achieved was dependent on feedstock concentration (6–24 mg·mL^{-1}), with greater removal observed with more dilute feedstocks, and greater residence times (1.2–12 min). Antibody isoelectric focusing point (the pH at which a protein carries no net charge) influenced the optimal mobile phase pH for aggregate removal, with superior performance being achieved when the antibody net charge was close to zero.

Building on the low-salt approaches pioneered by Dilks et al. and Ghose et al., and the work presented in **Chapter 3**, which demonstrated the potential of continuous TCZR-HIC using BSA as a model protein, this chapter evaluates the feasibility of continuous TCZR-HIC for mAbs. **Chapter 3** demonstrated that by employing temperature differences to modulate adsorption and desorption equilibria, it was possible to develop a continuous, ‘one-column’ ‘low-salt’ HIC process, eliminating the need for both high-

salt buffers typically used in conventional HIC. Here, we extend those findings to a more complex and commercially relevant application, assessing whether temperature modulation alone can provide a cost-effective and sustainable platform for large-scale polishing of mAbs.

4.3. Results and Discussion

4.3.1. Temperature-dependent solubility of Rituximab in ammonium sulphate.

Kosmotropic salts such as AS enhance interactions between proteins and hydrophobic resins; however, they also promote protein precipitation at higher concentrations by preferentially enhancing water-water hydrogen bonds vs. water-protein interactions. Due to this effect, it is critical to establish the solubility of Rituximab in the temperature range of interest (40, 21, and 4 °C) in the presence of AS, before beginning TCZR-HIC method development.

To determine the solubility profile of Rituximab in AS, aliquots of Rituximab were mixed with an increasingly concentrated gradient of AS (0.65–1.20 M). Rituximab forms visible white precipitates, thus the solubility threshold was determined by measuring absorbance in the visible range (400–700 nm). Percentage transmittance was calculated from absorbance data obtained from a 96 well-plate reader.

A photograph of the 96-well plate is shown **Figure 21 a**, showing the formation of a cloudy precipitate at higher AS concentrations. The transmittance data is presented in **Figure 21 b-e**. Solubility data for 40, 21 and 4 °C is presented in red, black, and blue,

respectively. Transmittance rapidly decreases once Rituximab is no longer soluble at the indicated salt concentration. Rituximab remained soluble in AS concentrations up to 0.8 M. Curiously, the solubility of Rituximab was slightly lower at 40 °C, than 10 or 4 °C. According to classical solubility, protein solubility typically increases with higher temperature, but the presence of kosmotropic salt may disrupt hydration shell more at elevated temperature. This may explain the change in solubility between temperatures. These results demonstrate that Rituximab remains soluble up to, 0.8 M AS, thereby setting an upper limit for HIC salt screening.

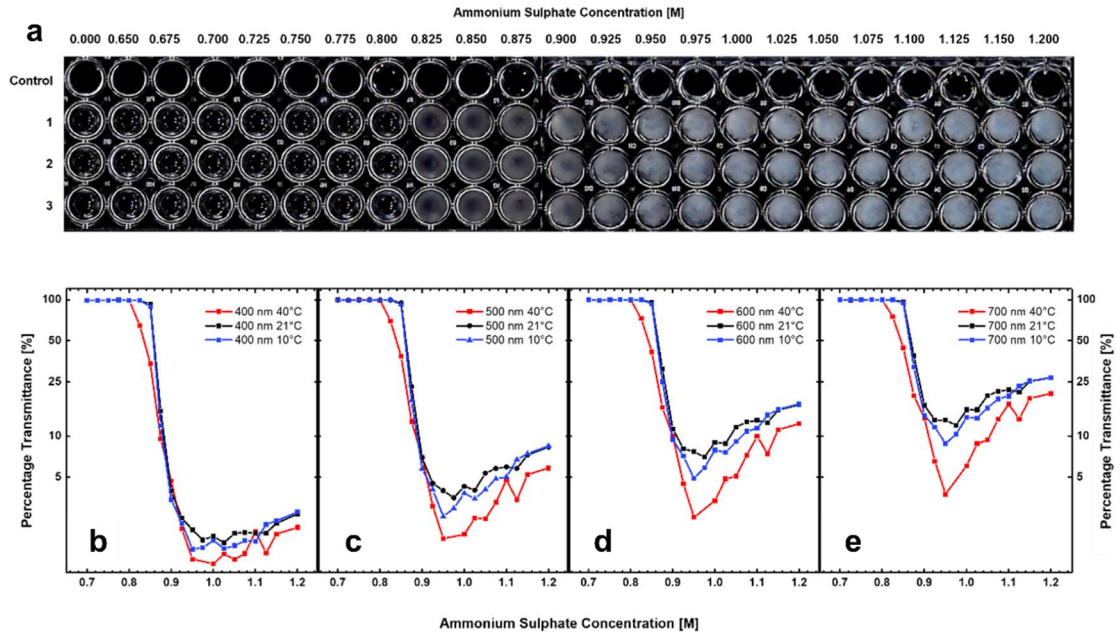

Figure 21: Rituximab solubility in an increasing gradient of AS. (a) Photograph of a 96 well plate, demonstrating the solubility of Rituximab in AS. Rituximab remains soluble in ≤0.8 M AS. Above these concentrations the kosmotropic salt causes Rituximab to precipitate, visible as a white deposit. (**b-e**) The light transmittance through the 96 well plate was measured across the visible spectrum (400, 500, 600 and 700 nm) in a 96 well plate reader.

4.3.2. Comparison of Rituximab batches for TCZR-HIC development.

To develop a robust protocol for temperature-controlled zone reactor hydrophobic interaction chromatography (TCZR-HIC), it was essential to characterise the starting materials thoroughly. This section evaluates two distinct Rituximab batches supplied by Lonza, which underwent different downstream processing approaches. A detailed comparison using HIC gradients and SEC was undertaken to evaluate hydrophobicity and aggregate profiles, critical for their suitability in TCZR-HIC studies.

One batch, Rituximab (ProA), originated from a neutralised Protein A eluate without further polishing, while the other, Rituximab (IEX), was subjected to additional ion-exchange (IEX) polishing. These contrasting preparation methods were anticipated to result in differences in product quality, particularly in aggregate content and molecular profile.

SEC was employed to quantify monomer and aggregate content, while HIC gradients assessed hydrophobicity profiles. Comparative SEC traces, normalised to the total chromatographic area for direct comparison, are shown in **Figure 22 a**. Peak integration revealed that Rituximab (IEX) contained 0.5% HMW species, compared to 3.9% in Rituximab (ProA). This aligns with the preparation methods, as IEX polishing effectively reduces aggregate content. The higher HMW species in Rituximab (ProA) provide a stringent test for TCZR-HIC's capability to reduce aggregate levels. Consequently, Rituximab (ProA) was selected for TCZR-HIC experiments, while Rituximab (IEX) was reserved for batch binding studies.

To confirm comparable hydrophobicity between the batches, an HIC gradient experiment was conducted using a 1 mL Butyl Sepharose 4FF column equilibrated with 0.750 M AS. A shallow gradient (from 0 to 0.75 M AS over 37.5 mL) ensured fine resolution. Overlaying the chromatograms with the gradient profile (**Figure 22 b**) highlights that both batches exhibited similar peak shapes, retention times, and UV intensities, confirming consistent hydrophobicity profiles.

These results demonstrate that while Rituximab (ProA) and Rituximab (IEX) exhibit comparable hydrophobicity, Rituximab (ProA)'s elevated aggregate content offers a more challenging substrate for polishing. This characteristic made it the preferred candidate for TCZR-HIC optimisation, with Rituximab (IEX) retained for complementary batch binding studies.

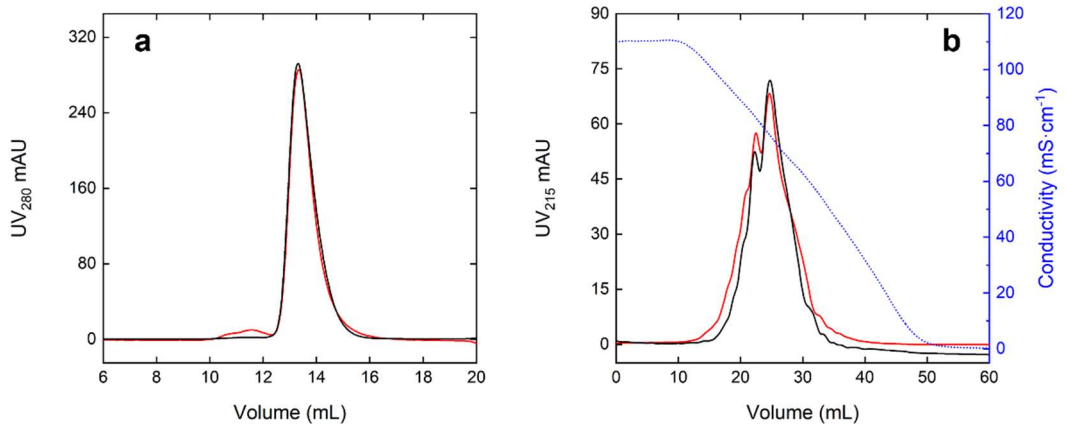

Figure 22: Comparative SEC and HIC analysis of two Rituximab preparations, Rituximab (ProA) and Rituximab (IEX). (a): SEC analysis of Rituximab (ProA, red trace) and Rituximab (IEX, black trace), scaled to equal chromatographic area to facilitate direct comparison. Integration revealed 0.5% HMW species in Rituximab (IEX) compared to 3.9% in Rituximab (ProA), reflecting the impact of IEX polishing. (b): HIC analysis of Rituximab (ProA) and Rituximab (IEX) using a 1 mL Butyl Sepharose 4FF column. A shallow gradient (0.750 – 0.00 M AS) was applied over 40 mL, as shown by the dotted blue conductivity trace.

4.3.3. Acid-Induced Aggregation for TCZR-HIC Polishing Studies.

To evaluate the aggregate polishing capabilities of TCZR-HIC, a reliable method for generating soluble aggregates without precipitation was developed. Acid-induced aggregation, a phenomenon associated with the low-pH viral inactivation step in mAb manufacturing, was selected as the model system due to its industrial relevance and controllability.

Low-pH environments disrupt the secondary and tertiary structures of proteins by inducing protonation of negative amino acid side chains, such as glutamine and aspartic acid. Protonation neutralises negatively charged residues, destabilising critical salt bridges. For example, those stabilising the CH2-CH3 interface in mAbs and interrupting hydrogen bonding networks that maintain the native protein structure (Ejima et al., 2007; Shukla et al., 2007a; Latypov et al., 2012; Mazzer et al., 2015). This destabilisation increases molecular flexibility and exposes hydrophobic residues buried within the protein core, facilitating hydrophobic interactions that drive aggregation. Notably, aggregation often proceeds via distinct structural mechanisms in different protein domains. For mAbs, CH2 domains are particularly susceptible to low-pH-induced perturbation, with unfolding preceding that of the CH3 domain (Latypov et al., 2012). This stepwise denaturation process exacerbates the exposure of aggregation-prone regions and primes proteins for multimeric interactions. Thermal aggregation, another mechanism frequently employed to model protein aggregation, occurs due to heat-induced protein unfolding. However, it was excluded in this study as it poorly reflects the conditions encountered during mAb manufacturing and is less representative of the stresses relevant to industrial workflows.

A 1 $mg \cdot mL^{-1}$ solution of Rituximab (IEX) was exposed to 50 mM sodium citrate (pH 3.2) or 50 mM glycine-HCl (pH 2.0) for 2 or 24 h to induce aggregation. Following incubation, samples were filtered to remove insoluble aggregates and subsequently analysed by SEC. The percentage of monomers and HMW species was calculated from peak areas and is presented in **Figure 23**.

Untreated Rituximab (IEX) contained 0.5% HMW species by total area (**Figure 23**, black trace). Exposure to sodium citrate (pH 3.2) resulted in a modest increase in HMW content without significantly disrupting the monomer peak (**Figure 23**, dark blue trace). After 2 h, HMW species accounted for 7.0% of the total peak area. In contrast, glycine-HCl (pH 2.0) was employed as an extreme aggregation scenario, leading to substantial aggregation. After 2 and 24 h of incubation (**Figure 23**, blue and green trace respectively), the proportion of HMW species increased to 84.4% and 84.3%, respectively. Despite similar HMW percentages, the chromatograms for the 24-hour exposure showed further degradation, as evidenced by additional changes in peak shape (**Figure 23**). Additionally, neutralisation of glycine-HCl treated samples post-aggregation resulted in precipitation, highlighting a limitation of this method for generating purely soluble aggregates.

These results confirm that a 2 hour exposure to sodium citrate (pH 3.2) is suitable for producing soluble acid-induced aggregates. This method provides a reproducible system for evaluating TCZR-HIC performance. In contrast, glycine-HCl produced higher aggregation but also generated insoluble aggregates, making it less practical for TCZR-HIC studies. Thus, the sodium citrate approach was selected as the preferred method for assessing TCZR-HIC efficacy in mAb aggregate polishing.

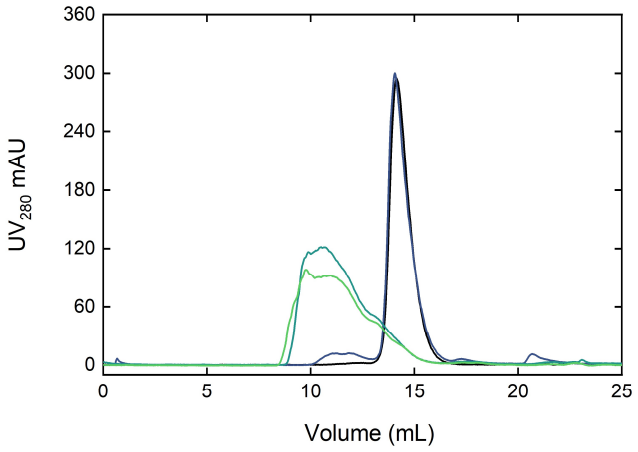

Figure 23: SEC analysis of Rituximab samples subjected to various low-pH treatments. The chromatograms display traces for untreated Rituximab (black), sodium citrate-treated samples at pH 3.2 (dark blue), and glycine-HCl-treated samples at pH 2.0 for 2 h (light blue) and 24 h (green). Elution profiles were monitored by UV absorbance at 280 nm, with volume ranges corresponding to HMW species and monomers indicated on the x-axis.

4.3.4. The effect of temperature and salt on the binding of Rituximab to hydrophobic resins.

To assess the potential of hydrophobic resins for temperature modulated binding to BSA, Müller and Franzreb first assessed a variety of resins, at a range of AS concentrations and temperatures (Müller and Franzreb, 2012). Binding strength was quantified by measuring bound protein after incubation for 90 min. These studies would later inform the work performed in **Chapter 3**. A similar strategy was adopted here for Rituximab. This study aimed to screen different AS concentrations to identify the optimal conditions for temperature-dependent binding and elution of Rituximab with Butyl Sepharose 4FF by exposing small volumes of resin to Rituximab at temperatures between 10 and 40 °C. Resins and salt concentrations that demonstrated substantial differences in binding strength were selected for TCZR-HIC experiments. Butyl Sepharose 4FF was selected to

continue previous work documented by Müller and Franzreb (2012), and in **Chapter 3**. Four additional resins were also screened to be tested alongside Butyl Sepharose 4FF, namely Butyl-650M, Butyl-650S, Phenyl-650M, Phenyl-650S. This study was expanded to include resins with Phenyl ligands, as well as smaller particle sizes and pore sizes. A comparison of the various resins is presented in **Figure 24** and **Figure 25.**

First, the temperature-dependent binding of Rituximab to Butyl Sepharose 4FF was evaluated. As in **Chapter 3** and in Müller and Franzreb, temperature-dependency is described by Δq_{Φ}, which quantifies the difference in the Langmuir model parameter, q_{max}, between temperatures, and k'_{Φ}, the ratio of initial slopes q_{max}/K_d at 40 and 10 °C respectively (Müller and Franzreb, 2012). The data is presented in **Figure 24 a-f**. At 0.30 M AS (panel a), Rituximab exhibited negligible binding, preventing reliable model fitting.

Lower salt concentrations (<0.5 M AS) exhibited poor binding performance, with minimal protein adsorption across all temperatures, thus limiting the potential for temperature modulation. Across 0.5–0.75 M AS, the ratio of the initial slopes k'_{Φ}, is always > 1, indicating the tightness of binding increases with temperature **Figure 24 b-f** (k'_{Φ} = *6.49, 3.58, 1.07, 5.93* for 0.5–0.75 M respectively, presented in **Table 7**). While the binding capacity, q_{max}, was lower at 0.5 M compared to 0.75 M, the increased sensitivity to temperature was the primary factor for selecting a salt concentration. Although Δq_{Φ} values, which describe the difference in q_{max} between 40 °C and 10 °C, also suggest temperature-dependent behaviour, they are less reliable due to limitations in Langmuir model fitting, especially in conditions of weaker binding affinity. This occurs due to the extrapolation of q_{max} to infinite protein concentrations, consequently these

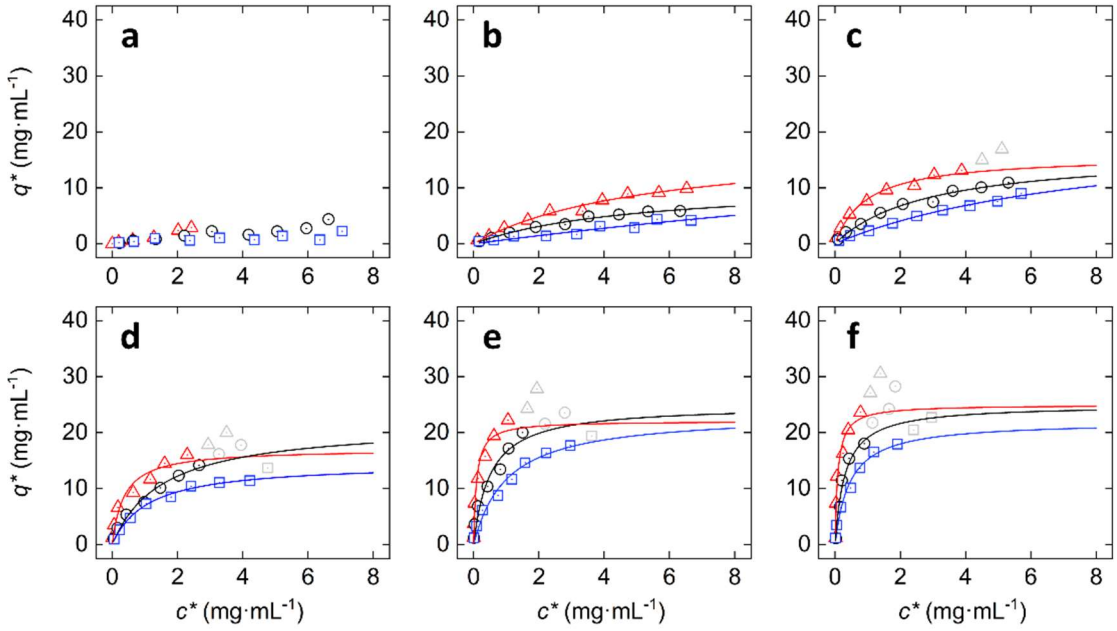

Figure 24: Langmuir adsorption isotherms depicting the temperature-mediated binding of Rituximab to Butyl Sepharose 4FF under varying AS concentrations. Each panel (a-f) corresponds to a different AS molarity: (**a**) 0.30 M, (**b**) 0.40 M, (**c**) 0.50 M, (**d**) 0.60 M, (**e**) 0.70 M, and (**f**) 0.75 M. Adsorption data were collected at three distinct temperatures: 40 °C (red triangles), 21 °C (black circles), and 10 °C (blue squares). The solid curves represent Langmuir model fits, while grey markers denote outliers excluded to enhance the model's accuracy.

Table 7: Langmuir parameters derived from equilibrium binding data presented in Figure 24. The table presents the AS concentration, the binding temperature (Φ), saturated binding capacity (q_{max}), dissociation constant (K_d), and, alongside the q_{max}/K_d ratio, the slope ratio (k'_Φ), and the difference in q_{max} between temperatures (Δq_Φ). These parameters describe the affinity of the solute for the stationary phase.

AS [M]	Φ (°C)	q_{max} (mg·mL^{-1})	K_d (mg·mL^{-1})	q_{max}/K_d	k'_Φ	Δq_Φ (mg·mL^{-1})
0.75	40	24.96	0.09	289.59		
0.75	21	24.94	0.31	80.47	5.93	2.97
0.75	10	21.99	0.45	48.87		
0.7	40	22.06	0.9	24.52		
0.7	21	24.88	0.5	49.77	1.07	-1.37
0.7	10	23.43	1.02	22.97		
0.6	40	17.06	0.36	47.39		
0.6	21	21.61	1.54	14.03	3.58	2.49
0.6	10	14.57	1.1	13.24		
0.5	40	15.71	0.96	16.37		
0.5	21	16.43	2.85	5.77	6.49	-5.67
0.5	10	21.38	8.48	2.52		
0.4	40	18.05	5.41	3.34		
0.4	21	10.94	5.04	2.17	4.34	-11.52
0.4	10	29.57	38.51	0.77		

values can be unrealistically elevated in cases where the binding data isn't sufficient to generate an accurate fit. Based on these findings, 0.5 M AS was selected for subsequent Rituximab binding studies using Butyl Sepharose 4FF, as it provided the greatest temperature-dependent change in binding strength.

Secondly, the temperature-dependent binding of Rituximab to four TOSOH Biosciences' TOYOPEARL HIC resins, specifically Butyl-650M, Butyl-650S, Phenyl-650M, and Phenyl-650S, was evaluated in this study. These four resins were selected so two ligand chemistries (Butyl and Phenyl) could be compared, in combination with two particle sizes (65 μm "M" and 35 μm "S" variants) to optimise surface area for hydrophobic interactions. Based on fluorescent binding data presented in **Chapter 3**, the majority of temperature-dependent binding appears to occur near the particle outer surface; thus, it is hypothesised that resins with greater surface area will exhibit an enhanced thermoresponsive effect, and likely, greater binding capacities. Müller and Franzreb (2012) previously reported that Phenyl-functionalised resins exhibited low temperature sensitivity ($\Delta q_{\Phi} < 2$ across all AS concentrations). If a similar observation is made here with TOYOPEARL Phenyl resins, the ligand chemistry can likely be identified as the determining factor in the absence of temperature-dependent behaviour, ruling out other bead properties as causal factors. Additionally, the TOYOPEARL resins feature a methacrylate polymer base matrix, which enhances resistance to compression and may facilitate greater flow rates relative to the agarose-based resins.

The binding data is presented in **Figure 25 a-j**. Non-Langmuir binding, identified as a second rise in q^* after the initial slope, was excluded to improve the fit (hollow data points). At 0.3 M AS, the temperature-dependent effect was minimal in Phenyl resins,

therefore the binding data was fitted to a convergent model (purple trace). Temperature significantly influenced the binding characteristics of Butyl-650M and Butyl-650S (**Figure 25 a-f**), resulting in distinct differences in q_{max} and K_d. As expected, binding affinity, measured as q_{max}/K_d, was enhanced at higher AS concentrations and temperatures. The difference in binding affinity between temperatures, $k'_{\Phi,}$ was maximised at 0.3 M AS for both Butyl-650M and Butyl-650S (k'_{Φ} = 16.0, and 17.1 respectively, presented in **Table 8**). Consistent with the hypothesis, TOYOPEARL's higher butyl ligand density resulted in greater q_{max} values compared to Butyl Sepharose 4 FF at equivalent salt concentrations (40 °C 0.5 M AS q_{max} = 28.8 and 28.2, vs. 15.71 for 650M, 650S, and Butyl Sepharose 4FF respectively). Thus, the TOSOH resins functionalised with Butyl ligands provided a greater temperature sensitivity, and higher capacities with lower salt concentrations. Despite the smaller particle size of Butyl-650S, the maximum capacity q_{max} was very similar, despite the greater surface area available for binding.

In contrast to the Butyl resins, the Phenyl resins show no temperature-dependent variation in binding, as illustrated by the overlapping Langmuir model fits (purple curves) applied to the data from 0.3 M AS (**Figure 28 g** and **i**).This behaviour was also observed by Müller and Franzreb, who observed that Phenyl Sepharose 6FF demonstrated low temperature sensitivity. These results underline the distinct mechanisms of adsorption: temperature-mediated hydrophobic interactions for Butyl ligands and purely salt-driven hydrophobic interactions for Phenyl ligands. The data generated at 0.3 M AS could be modelled with a convergent fit, highlighting the absence of a temperature-induced effect.

This lack of temperature sensitivity likely arises from the Phenyl ligand's aryl structure with an aromatic ring. Furthermore, given that the same ligand structure produces similar

results across different base matrices and particle sizes, it is probable that the intrinsic structure of the Phenyl ligand limits thermoresponsive behaviour.

One metric, $\Delta q\Phi$, calculated as the difference in q_{max} between temperatures, generated negative results in instances of weak binding. Extrapolated qmax values from 10 °C were greater than those at 40 °C. This is not due to greater binding at a lower temperature, but rather an artefact of the qmax extrapolation method, which assumes an infinite protein supply. As a consequence, datasets with weak initial binding result in an overestimation of the plateau (q_{max}) compared to datasets with tighter binding. This occurs because the extrapolation model relies on assumptions of saturation that break down when protein binding is minimal, amplifying noise and introducing significant error. Therefore, $\Delta q\Phi$ is not reliable under conditions of weak protein binding.

These findings indicate that Butyl-650M and Butyl-650S outperform Butyl Sepharose 4 FF across all metrics, demonstrating a larger temperature-dependent binding strength difference while requiring lower AS concentrations. The Phenyl resins, lacking thermoresponsive properties, will not be used in TCZR-HIC experiments. TCZR-HIC experiments will now focus on Butyl Sepharose 4FF, to compare to **Chapter 3**, and Butyl-650M due to (i) optimal pressure-flow characteristics relative to the S variant, (ii) excellent k'_{Φ} of 16.0, (iii) lower AS requirement compared to Butyl Sepharose 4FF, and (iv) higher binding capacity at 40 °C.

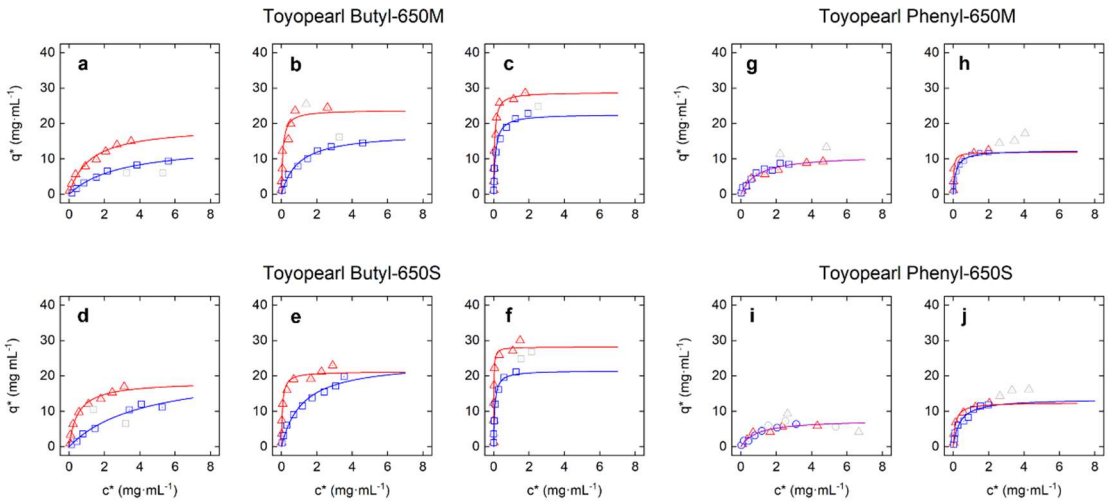

Figure 25: Equilibrium adsorption isotherms for TOSOH TOYOPEARL Butyl and Phenyl resins under varying AS concentrations and temperatures. Panels (a–f) display data for Butyl-650M and Butyl-650S resins at AS concentrations of 0.1 M, 0.3 M, and 0.5 M, evaluated at 40 °C (red triangles) and 10 °C (blue squares). Solid lines represent Langmuir model fits to the red and blue data points, while grey points were excluded to enhance the accuracy of the fit.

Table 8: Langmuir parameters for the isotherms presented in Figure 25. Langmuir parameters for Butyl-650M, Butyl-650S, Phenyl-650M, and Phenyl-650S are all presented. Convergent fits are listed under a single AS concentration.

Hydrophobic Resin	AS [M]	Φ (°C)	q_{max} (mg·mL^{-1})	K_d (mg·mL^{-1})	q_{max}/K_d	k'_{Φ}	Δq_{Φ} (mg·mL^{-1})
Butyl-650M	0.5	40	28.8	0.1	576	2.8	6.2
	0.5	10	22.6	0.1	205.7		
	0.3	40	23.8	0.1	297.5	16	6.3
	0.3	10	17.5	0.9	18.6		
	0.1	40	19.3	1.2	16.6	3.3	4.9
	0.1	10	14.4	2.9	5		
Butyl-650S	0.5	40	28.2	0.1	563.4	1.8	6.7
	0.5	10	21.5	0.1	307.1		
	0.3	40	21.2	0.1	353.3	17.1	-3
	0.3	10	24.2	1.2	20.7		
	0.1	40	18.4	0.5	36.9	7	-3.7
	0.1	10	22.1	4.2	5.3		
Phenyl-650S	0.5	40	12.5	0.1	103.8	2.8	-1
	0.5	10	13.5	0.4	36.6		
	0.3	Shared fit	7.6	0.9	8.4	-	-
Phenyl-650M	0.5	40	11.9	0	396.7	4.8	-0.5
	0.5	10	12.4	0.2	82.7		
	0.3	Shared fit	11.1	0.9	12.3	-	-

4.3.5. Pulse-Response HIC with Butyl Sepharose 4FF.

Before progressing to TCZR-HIC experiments, pulse-response experiments were conducted, using a scaled-down glass-column temperature-controlled with a water bath. A water bath maintained at the binding temperature was used to simulate the heated cabinet of the TCZR, while a water bath maintained at 10 °C was used to simulate the travelling cooling zone. Immersion of the column from one temperature controlled environment to another allowed for rapid temperature manipulation of the stationary phase.

A series of pulse-response studies was first conducted on Butyl Sepharose 4FF at 0.5 M AS, identified as the optimal salt concentration for temperature-modulated HIC in static binding studies. Rituximab was applied in 1.6 mg pulses via a 500 µL sample loop to a bed (Φ = 40 °C) equilibrated in 0.5 M AS, 50 mM sodium phosphate, pH 7.5, at 0.18 $mL \cdot min^{-1}$. The column was subsequently washed with protein-free equilibration buffer to remove loosely bound protein. **Figure 26 a** shows a significant UV baseline signal following washing, indicating substantial loss of loosely bound Rituximab, consistent with weak solute-ligand interactions. Peak integration reveals this baseline accounted for 81.5% of bound protein (**Table 9**), i.e., the solute-ligand interaction strength at the binding temperature is insufficient for robust antibody retention. In studies with BSA, this step resulted in a minor loss (approx. 20%) of loosely bound protein, consistent with prior findings (Jungbauer et al., 2005), and also observed in **Chapter 3**. As most of the protein had already been removed, the cooling step was omitted, and the column was stripped with 20% (*v/v*) ethanol, successfully removing the remaining Rituximab. The binding studies presented in previous sections, (**Figure 24 c)** determined that 0.5 M AS

was optimal under static conditions, however, under dynamic conditions, antibody retention is the limiting factor.

To improve retention, the binding temperature was increased to 50 °C (**Figure 26 b**). This adjustment reduced the baseline signal post-wash, with only 12.0% of Rituximab being loosely bound and removed, as shown by the lower UV absorbance. The subsequent cooling step at 10 °C resulted in the elution of 77.0% of the protein, while 20% (*v/v*) ethanol stripped an additional 10.9%, confirming improved retention at higher temperatures.

Increasing the binding temperature further to 60 °C (**Figure 26 c**) showed complete retention, with no detectable protein loss during washing. However, the ethanol stripping phase showed abnormalities in the UV trace, likely due to partial ethanol vaporisation within the system at elevated temperatures. As a result, this experiment was not replicated with a cooling step.

Finally, raising the AS concentration to 0.6 M AS and keeping the temperature at 40 °C (**Figure 26 d**) increased Rituximab retention, with only 2.6% lost during washing. To initiate elution, the column was then immersed in a water bath (Φ = 10 °C). Thermal elution was successful, however, rather than the sharp narrow elution peak observed with BSA in **Chapter 3**, a broad elution peak was observed, lasting 40 CVs. In contrast, in the pulse response studies performed with BSA, thermal elutions peaked in UV absorbance within 1 CV, and returned to baseline after 7 CVs. Despite the elongated elution time, thermal elution removed 62.3% of bound Rituximab, slightly more than the 56.0% of bound BSA removed under identical conditions in **Chapter 3**.

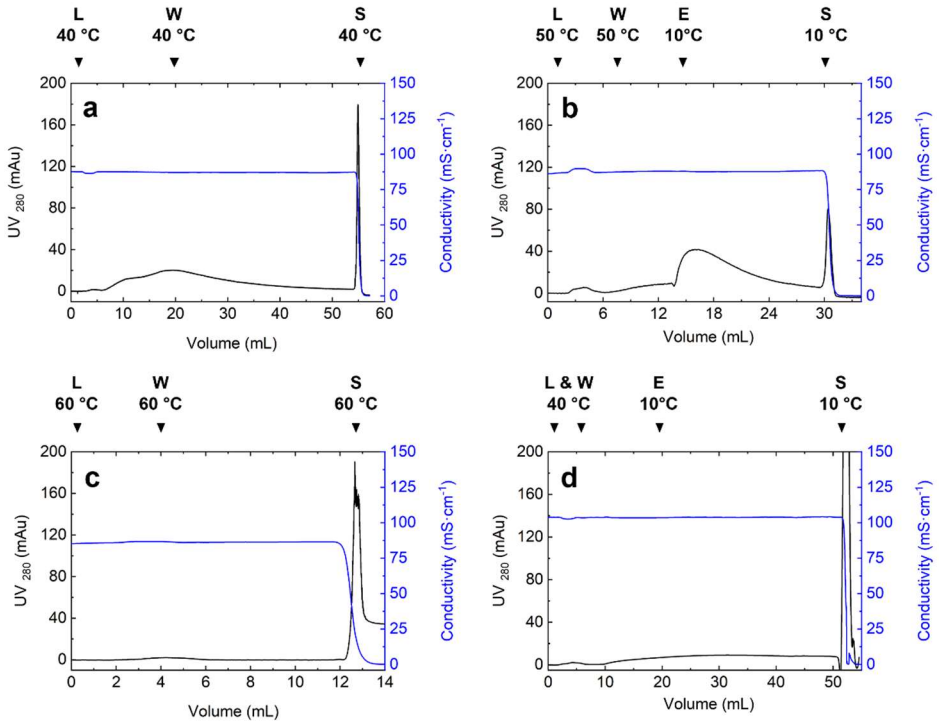

Figure 26: Pulse-response HIC of Rituximab on Butyl Sepharose 4FF under different binding conditions. (a) Binding at 40 °C with 0.5 M AS; **(b)** Binding at 50 °C with 0.5 M AS: Rituximab application, washing, cooling to 10 °C for elution, and ethanol stripping; **(c)** Binding at 60 °C with 0.5 M AS: Rituximab application and washing steps followed by ethanol stripping without cooling; **(d)** Binding at 40 °C with 0.6 M AS: Rituximab application, washing, cooling to 10 °C for elution, and final ethanol stripping. Each panel shows UV absorbance at 280 nm (black line, left y-axis) and conductivity (blue line, right y-axis) as a function of elution volume (mL), with distinct phases marked by changes in signal intensity and conductivity. Letters denote loading (L), washing (W), thermal elution (E), and ethanol strip (S).

Table 9: Tabulated outcomes of pulse-response HIC experiments for Rituximab on Butyl Sepharose 4FF under varying AS concentrations and binding temperatures. Columns indicate the AS concentration and binding temperature (Φ), the amount of Rituximab loaded (mg), and the percentage of protein that was loosely bound, firmly bound, eluted at 10 °C, and stripped with 20% (*v/v*) ethanol. The % Mass balance column provides the total recovery of protein across each condition, accounting for loosely bound, eluted, and stripped fractions.

Trace	AS [M]	Binding Φ (°C)	Loaded (mg)	Loosely bound (%)	Firmly bound (%)	Φ = 10 °C		Mass balance (%)
						Eluted (%)	Stripped (%)	
Figure 26 a	0.5	40	1.6	81.5	18.5	-	18.8	100.3
Figure 26 b	0.5	50	1.6	12.0	88.0	77.0	10.9	99.9
Figure 26 c	0.5	60	1.6	0	100	-	-	-
Figure 26 d	0.6	40	1.6	2.6	97.4	62.3	36	100.9

The column was immediately stripped with 20% (*v/v*) ethanol resulting in a sharp strip peak. Although this approach removed more bound protein, the prolonged elution peak suggests that the solute-ligand interaction at Φ = 10 °C remains too strong for efficient desorption.

These results demonstrate that the optimal salt concentration for TCZR-HIC lies between 0.5 and 0.6 M AS. At the lower salt concentration, the binding strength was insufficient at Φ = 40 °C, while increasing the kosmotropic salt resulted in hydrophobic interactions too strong for efficient elution at Φ = 10 °C. Increasing the binding temperature improves antibody retention predictably, however, may cause issues with certain solvents used during HIC.

4.3.6. Pulse-Response HIC with Butyl-650M.

Additional pulse-response studies were conducted on the Butyl-650M matrix, selected for the reduced particle size and greater k'_{Φ} relative to Butyl Sepharose 4FF (k'_{Φ} = 16 at 0.3 M AS, see **Table 8**). Although initial screening predicted that 0.3 M AS would offer the greatest performance, a range of AS concentrations (0–0.3 M AS) were screened to assess the influence of salt on temperature mediated adsorption and desorption.

To improve on the results presented in **Figure 26**, a standardised procedure was established. For each trace, Rituximab (1.6 mg) was loaded onto a column equilibrated at Φ = 40 °C. Weakly bound proteins were removed during the initial flow-through. After 12 mL of flow through, the column was transferred to a water bath maintained at Φ = 10 °C, initiating temperature-induced elution. The resulting chromatograms, shown in

Figure 27 a-f, where the black trace represent Φ = 40 °C, while the blue trace represents Φ = 10 °C.

The results demonstrate that low AS concentrations (e.g., 0, and 0.05 M), yielded insufficient Rituximab retention at the binding temperature, Φ = 40 °C, as indicated by an increase in the UV absorbance before 12 mL. Intermediate AS concentrations (0.1–0.125 M) improved retention and produced sharper, more defined elution peaks at 10 °C. Elevated AS concentrations (0.15–0.3 M) further enhanced antibody retention but produced broader elution peaks, suggesting that the increased binding strength diminished elution efficiency due to slower desorption rates. An intermediate AS concentration of 0.125 M was identified as an optimal compromise, offering sufficient retention at 40 °C without significant peak broadening at 10 °C. As tabulated in **Table 10**, This condition provided 11.8% loss of antibody due to retention, but demonstrated 76.1% recovery during the thermal elution, with a relatively small quantity being recovered by regeneration with 20% *(v/v)* ethanol.

Further pulse response experimentation was performed with a different binding and elution temperature scheme, (Φ = 35 and 5 °C) tested with AS concentrations of 0.125 and 0.2 M to assess the reproducibility of observed trends. A lower binding and elution temperature scheme was selected to explore whether retention or peak broadening could be enhanced at intermediate and high AS levels. The data is presented in **Figure 28.** When comparing antibody retention at 0.125 M AS (**Figure 27 d** vs. **Figure 28 a),** the 5 °C reduction in binding temperature resulted in noticeably lower antibody retention at 35 °C. Peak integration of the retention area indicates that binding at 40 °C resulted in 88.2% of bound protein retained, compared to 65.8% of bound protein.

Further comparisons of the data are presented in **Table 10**, for example, the elution and retention profile of 0.2 M AS (**Figure 28 b**), and 0.15 M AS (**Figure 27 e)** are highly comparable, (95.3 and 95.5% tightly bound, and 79.7 and 80.8% thermally eluted). These findings suggest that a 5 °C decrease in binding temperature yields an effect on binding strength comparable to a reduction of 0.05 M AS in the mobile phase composition.

The total amount of protein eluted (loosely bound + thermally eluted) decreased as the AS concentration increased (**Table 10**), resulting in increased protein recovered by the 20% (*v/v*) ethanol strip. This necessitates careful optimisation of operational conditions to balance retention, elution efficiency, and total yield. These data indicate that the physicochemical properties of Rituximab may render it less amenable to thermally driven HIC.

Prior studies with BSA by Müller and Franzreb (2012), and expanded upon in **Chapter 3**, demonstrated effective reversible binding of BSA to Butyl Sepharose 4FF at 0.5 M AS (Müller and Franzreb, 2012). For Rituximab, although favourable binding was observed under static conditions, pulse-response data suggest that the difference in binding strength between 40 °C and 10 °C is substantially smaller for Rituximab, creating a narrower range of conditions for a $\Delta\Phi$ 30 °C difference to be effective. Using an alternative temperature scheme did not change these observations. This limitation might be overcome by implementing a larger temperature deference, as a greater thermal differential should result in an increased change in the retention factor, as described by **Equation 1**. To evaluate the viability of this approach, a study was conducted to determine the maximum temperature difference that the TCZR could achieve.

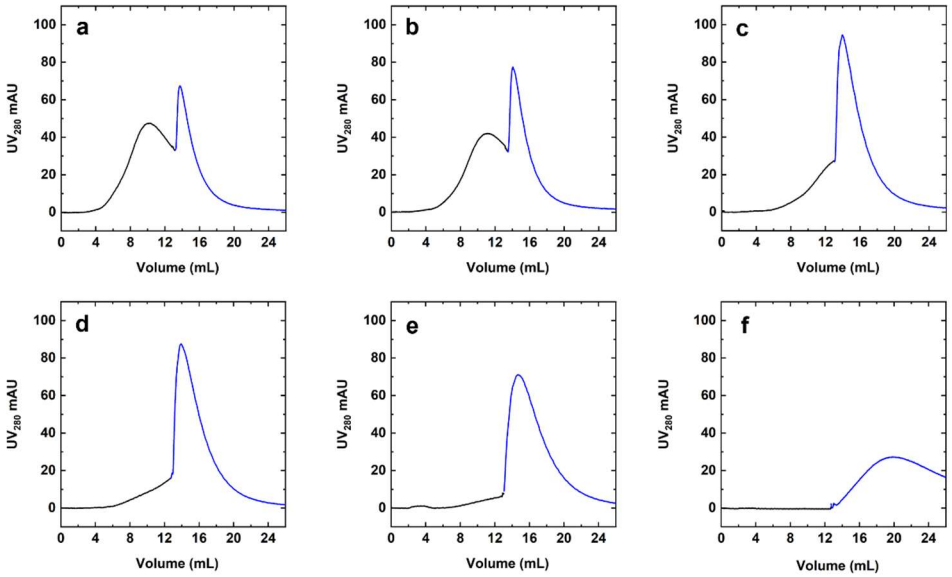

Figure 27: Pulse-response studies performed with Butyl-650M at two temperatures (*Φ* = 40 and 10 °C), across a range of AS concentrations. Panels (a–f) represent individual AS concentrations: (a) 0 M, (b) 0.05 M, (c) 0.1 M, (d) 0.125 M, (e) 0.15 M, and (f) 0.3 M. Each panel shows two temperature conditions: the black line corresponds to the binding phase at 40 °C, and the blue line represents the elution phase at 10 °C. The chromatograms illustrate Rituximab retention and elution behaviour at the binding and elution temperatures as a function of AS concentration. Conductivity for each salt concentration was constant for the duration of each experiment, after which a strip with 20% ethanol (*v/v*) strip was performed (not presented).

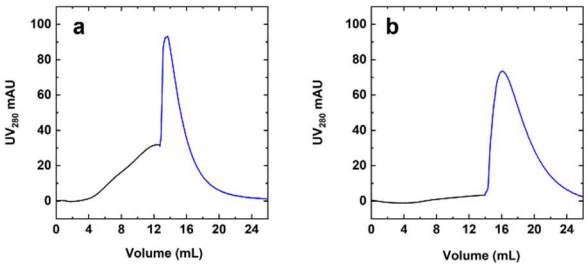

Figure 28: Further pulse-response experimentation at alternative temperatures (*Φ* = 35 and 5 °C). (a) 0.125 M, (b) 0.2 M. Both show two temperatures: the black line corresponds to the binding phase at 35 °C, and the blue line represents the elution phase at 5 °C.

Table 10: Analysis of process performance during pulse response HIC of Rituximab, presented in Figure 27 and Figure 28.

Φ (°C)	Figure	AS [M]	Eluted (%)	Tightly Bound (%)	Thermally Eluted (%)	Total Eluted (%)	Strip (%)
40 & 10	Figure 27 a	0	57.6	42.4	41.1	98.7	1.3
	Figure 27 b	0.05	48.9	51.1	48.7	97.5	2.5
	Figure 27 c	0.1	19.6	80.4	74.6	94.2	5.8
	Figure 27 d	0.125	11.8	88.2	76.1	87.9	12.1
	Figure 27 e	0.15	4.7	95.3	79.7	84.4	15.6
	Figure 27 f	0.3	0.0	100.0	66.5	66.5	33.5
35 & 5	Figure 28 a	0.125	34.2	65.8	62.1	96.2	3.8
	Figure 28 b	0.2	4.5	95.5	80.8	85.3	14.7

4.3.7. Assessing the TCZR maximum thermal performance.

The limited window for effective on/off binding between temperatures with Rituximab could be expanded by increasing the temperature difference. To assess whether the TCZR could generate and maintain a gradient beyond $\Delta\Phi$ = 30 °C, several modifications were made to the system; (i) the cabinet was insulated with dense foam to minimise heat loss, (ii) the cooling zone was insulated to separate the hot cabinet air from the copper block, (iii) the Peltier element was operated at full capacity (target Φ = -10 °C). The cabinet temperature was incrementally increased by 1 °C (20–50 °C) and, after a 5-minute equilibration period, temperatures were recorded at the TCZ, within the cabinet, and at the upper and lower heat blocks. As presented in **Figure 29**, the top panel indicates that the TCZ temperature difference reaches a maximum of Δ30.52 °C achieved at a cabinet temperature of 49 °C. The bottom panel further illustrates that below a cabinet temperature of 33 °C, cooling efficiency degrades, resulting in a minimum temeprature difference of $\Delta\Phi$ = 27.01 °C at a cabinet temperature of 21 °C. Between 33 °C and 50 °C, however, the TCZ maintains a relatively stable temperature difference, averaging $\Delta\Phi$ = 29.49 °C.

These results demonstrate the TCZR is already operating at maximum capacity, and a greater temperature difference is not possible without substantial modifications to the system. These modifications could include: (i) increasing cooling power or (ii) enhancing system efficiency through improved insulation or optimised heat transfer mechanisms. Since improving the Peltier element, controller, or power delivery system is not within the project's scope, TCZR-HIC experimentation will proceed with a $\Delta\Phi$ = 30 °C difference.

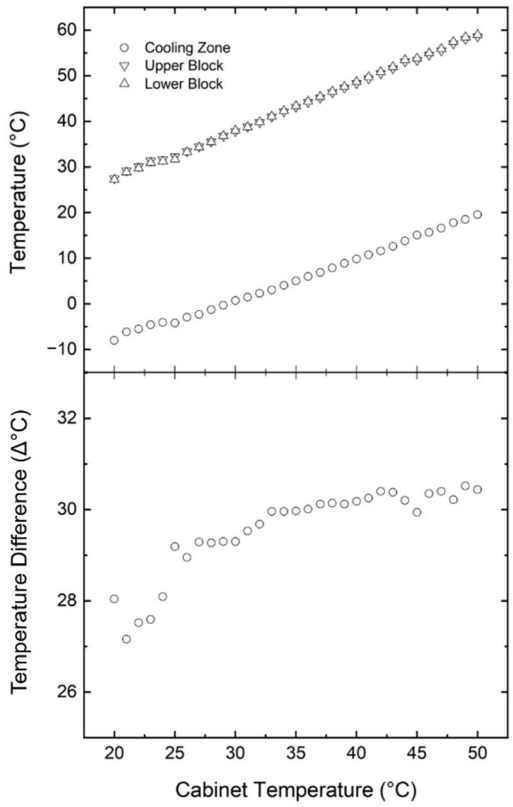

Figure 29: Thermal performance of the Travelling Cooling Zone Reactor (TCZR) under varying cabinet temperatures. (Top) Temperature profiles of the cooling zone, upper heat block, and lower heat block as a function of cabinet temperature, with the Peltier element set to a target temperature of -10 °C. (Bottom) Temperature difference ($\Delta\Phi$ °C) between the cabinet and cooling zone, illustrating the TCZR's inability to sustain a stable gradient above $\Delta\Phi$ = 30 °C.

4.3.8. Batch mode TCZR-HIC of Rituximab with Butyl Sepharose 4FF.

To validate the applicability of the pulse response studies, a batch TCZR-HIC experiment was conducted. The pulse-response studies accurately predicted TCZR-HIC if specific criteria are met: (i) limited elution should be evident at 0.6 M AS, with each TCZ travel at Φ = 10 °C, and; (ii) limited antibody retention should be observed at 0.5 M AS at Φ =

40 °C. Meeting these conditions would establish the pulse-response HIC studies as a reliable preliminary screening tool for TCZR-HIC.

To assess this, the TCZR was packed with 3.4 mL of Butyl Sepharose 4FF. The column was equilibrated with 0.6 M AS, and 2 mg of Rituximab was applied to the column. After applying 15 mL of binding buffer to remove loosely bound proteins, seven movements of the TCZ were performed. The resulting chromatogram is presented in **Figure 30 a**. Under these conditions, the thermal elution peaks were only discernible at 215 nm, indicating that the binding strength at 0.6 M AS and $\Phi = 10$ºC was too strong for efficient desorption (as accurately predicted by pulse response experiments). While UV 280 nm is more standard for protein quantification, UV 215 nm was employed here for higher sensitivity, as Rituximab absorbs approximately 20-fold more at 215 nm than at 280 nm. Each TCZ movement generated incrementally larger peaks; however, these were only detectable at 215 nm.

To reduce binding strength and achieve a greater yield at $\Phi = 10$ °C, the AS concentration was decreased from 0.6 M to 0.5 M (95 – 87 $mS \cdot cm^{-1}$). This adjustment was intended to increase each elution peak's height by weakening the binding strength at the elution temperature. The resulting chromatogram (**Figure 30 b**) shows 33 cycles at the lower salt concentration, producing 33 elution peaks of varying size. Although this adjustment led to larger elution peaks visible at 280 nm, antibody retention issues identified in the pulse response studies were also observed here. Peak heights were greatest in the middle of the chromatogram and were proportional to the UV baseline. These findings validated that water bath experiments can accurately predict binding and elution conditions within the TCZR. Peak shape is similar to those observed in previous TCZR and THZR studies

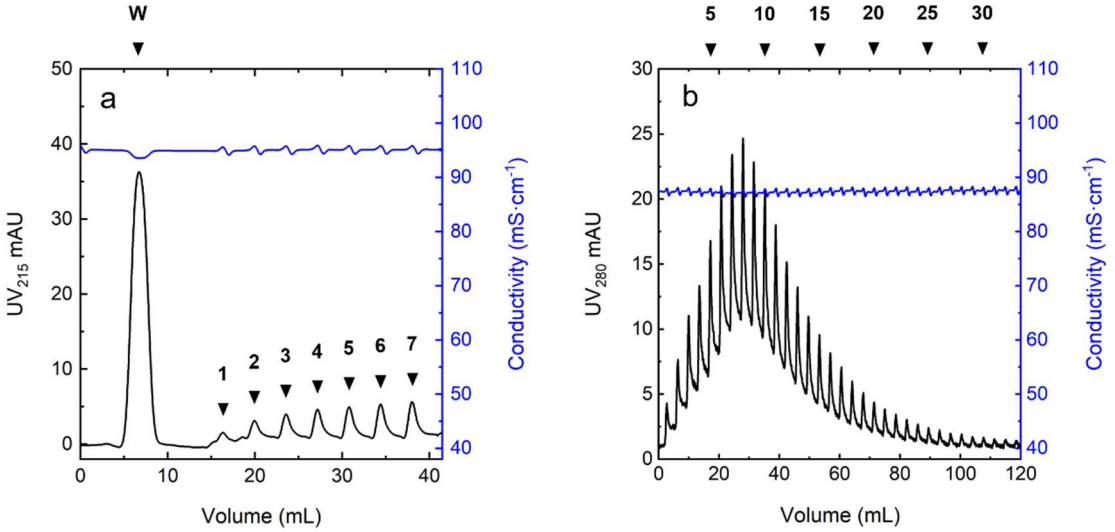

Figure 30: A batch TCZR-HIC experiment with Butyl Sepharose 4FF. (**a**) the first half of the experiment, where seven thermally mediated elutions (1-7) are only detectable by UV_{215} are plotted on the left Y axis. Rituximab absorbs UV_{215} 20 times more than UV_{280}. (**b**) the second half of the experiment, where, without regenerating the column, the AS concentration was lowered to 0.5 M AS and thermal elutions continued (5 – 30). Significantly more protein was detected, therefore UV_{280} is presented on the left Y axis.

(Müller et al., 2013; Cao et al., 2015; Ketterer et al., 2019) though the rising UV baseline is atypical.

Peak integration analysis determined that thermally eluted peaks accounted for just 0.53 mg, or 27.0% of the loaded protein, while 73.0% remained loosely bound, contributing to the rising UV baseline signal. For BSA in previous **Chapter 3** experiments, thermal elution was expected to release at least 60% of bound protein, without retention issues.

These results confirm that temperature-mediated HIC can effectively process Rituximab, but the optimal salt concentration lies between 0.5–0.6 M AS. Rather than conducting additional salt concentration screens with Butyl Sepharose 4FF, the investigation shifted to exploring whether Butyl-650M, which features a greater ligand density, and smaller particle size, would provide better results.

4.3.9. Batch mode TCZR-HIC of Rituximab with Butyl-650M.

Two batch TCZR-HIC experiments were conducted at 0.125 M AS to investigate the influence of temperature on retention, peak shape, and polishing efficiency. The experiments utilised two paired temperature conditions: binding at 40 °C and elution at 10 °C (hereafter denoted as '40/10'), and binding at 35 °C and elution at 5 °C ('35/5'). Both ranges utilise the maximum temperature difference achievable by the TCZR ($\Delta\Phi$ = 30 °C). A Rituximab feedstock (6 mg, 0.125 M AS) was applied to a 3.4 mL Butyl 650M column. The resulting chromatograms for both temperature sets are presented in **Figure 31 a,** and **Figure 31 b.**

Both experiments feature 17 movements of the travelling cooling zone reactor, resulting in 17 thermally eluted peaks. The effect of binding temperature on antibody retention is clear, as evidenced by a rising UV baseline. At a binding temperature of 40 °C, 4.77 mg of Rituximab remained bound to the column, compared to 3.47 mg at the decreased 35 °C binding temperature **Table 11**. This is evidenced by the increased baseline in **Figure 31 b** compared to **Figure 31 a**, a result that agrees with the pulse-response studies. This improvement can be attributed to the increased strength of the hydrophobic interactions at 40 °C. In both studies, the initial thermal elution peaks were small, gradually increasing in size. The direct proportionality between peak height and the UV baseline increase suggests that the thermal effect exerted by the TCZR contributes minimally to changes in the binding strength of Rituximab bound to the Butyl-650M matrix. By peak 8, differences in peak height were negligible, consistent with the $\Delta\Phi$ = 30 °C difference applied in both cases.

Total protein eluted by movements of the TCZ differed between studies. As a percentage of bound protein, elution efficiency was greater with the Φ = 35/5 °C range than the Φ = 40/10 °C range (52.1% vs. 30.6%). This is due to the greater binding strength imposed by the elevated binding temperature and is corroborated by previous pulse-response observations.

Although the current TCZR-HIC setup shows limitations in achieving on-off binding with a $\Delta\Phi$ = 30 °C difference, its potential for aggregate removal warrants further assessment. SEC analysis of the collected elution fractions, pooled across all peaks, and compared to the feedstock highlights the potential of TCZR-HIC for polishing **Table 12**. As expected, binding and elution at 40 and 10 °C demonstrated superior removal of HMW species. At these temperatures, thermally eluted peaks were entirely devoid of Rituximab aggregates. The TCZR's ability to produce concentrated peaks offers advantages over traditional aggregate removal processes used in mAb downstream processing, such as flow-through-HIC, particularly if a larger temperature difference could be exploited.

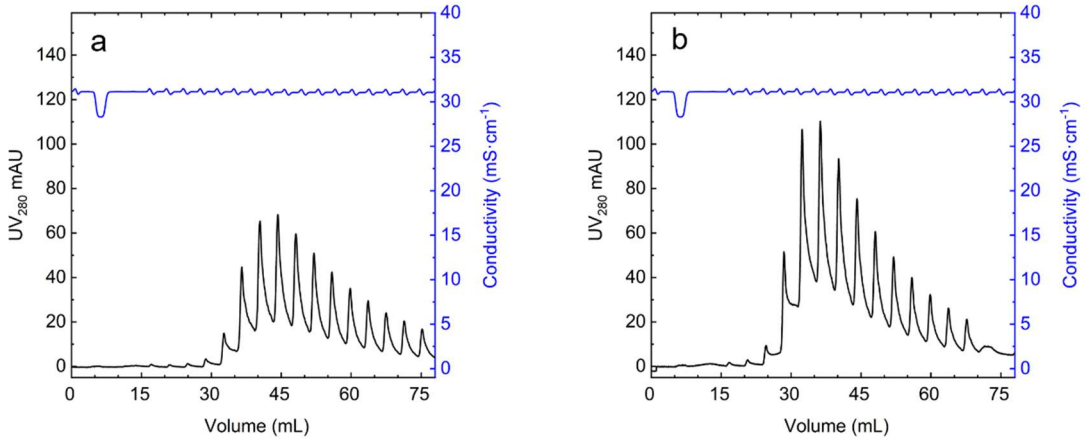

Figure 31: Batch mode TCZR-HIC performed with Butyl-650M at 0.125 M AS, contrasting the effect of two different temperature ranges on Rituximab retention and elution. (a) Chromatogram obtained with the TCZR-HIC system operated at Φ = 40/10 °C, demonstrating 15 cycles of thermal elution; (b) Chromatogram obtained under identical conditions but at the Φ = 35/5 °C temperature range. Black traces represent the UV absorbance at

280 nm (left y-axis), while blue traces represent conductivity (right y-axis). Both temperature schemes utilise the maximum temperature difference achievable by the TCZR ($\Delta\Phi$ = 30 °C).

Table 11: Evaluation of Batch TCZR-HIC performance with Butyl-650M at 0.125 M AS. The table summarises the quantity of loaded protein, bound protein, unbound protein, protein eluted by the TCZ, protein present in the 20% ethanol (*v/v*) strip, and the mass balance. An air-bubble was present during the ethanol strip during the experiment presented in **Figure 31 a**, preventing the accurate calculation of the strip peak. Values were calculated by peak area integration.

Figure Φ (Bindng/Elution)	Loaded (mg)	Bound (mg)	Unbound (mg)	TCZ Elution (mg)	Strip (mg)	Recovery (mg)	Mass Balance (%)
Figure 31 a Φ = 40/10	6.0	4.77	1.23	1.46	-	-	-
Figure 31 b Φ = 35/5	6.0	3.47	2.53	1.81	1.57	5.91	98.5 %

Table 12: SEC analysis of the feedstock and thermally eluted peaks from TCZR-HIC runs conducted at two temperature ranges; Φ = 40/10 °C and Φ = 35/5 °C. The table summarises the percentage composition of aggregates (HMW species) and monomers in the feedstock compared to the thermally eluted fractions for each temperature scheme, highlighting the enhanced aggregate removal at the Φ = 40/10 °C range.

Figure Φ (Bindng/Elution)	Oligomer	Feedstock	Thermally Eluted Peaks	Monomer PF	HMW DF
Figure 31 a Φ = 40/10	HMW Monomer	6.8% 93.2%	<0.1% >99.9%	- 1.07	> 68
Figure 31 b Φ = 35/5	HMW Monomer	5.8% 94.2%	4.4% 95.6%	- 1.01	1.31 -

Composition determined by SEC analysis. Key: PF = Purification Factor, DF = Depletion Factor

Additionally, due to the lower concentrations of kosmotropic salts used because binding is enhanced by the elevated cabinet temperature, this offers lower disposal costs, and reduced burden on downstream buffer exchange and formulation steps.

The small elution yield experienced in the first few TCZ movements is a phenomenon not previously observed in **Chapter 3**, and appears to be unique to Rituximab. This observation, coupled with the quantity of protein failing to bind to the column, suggests that the effect of the TCZ is relatively small. To further assess this, a continuous

experiment was conducted, and the data overlaid. The same procedure would be followed, one with TCZ movements and one without, simulating a flowthrough HIC procedure.

4.3.10. Continuous mode TCZR-HIC of Rituximab with Butyl-650M.

Building on previous work in **Chapter 3** with BSA, where TCZR-HIC demonstrated effective continuous mode operation with varying feedstock concentrations, we aimed to assess similar efficacy with Rituximab. In **Chapter 3**, lower concentrations (e.g., 0.25 $mg \cdot mL^{-1}$), the UV trace could return to baseline between TCZ cycles, and the TCZR maintained polishing effectiveness even with heavily fouled resin, demonstrating effective operation under challenging circumstances. With these findings as a foundation, we tested whether TCZR-HIC could maintain Rituximab's retention and release dynamics effectively under continuous operation.

For this study, a Butyl-650M packed column within the TCZR, applying 0.50 $mg \cdot mL^{-1}$ of Rituximab feedstock. A binding temperature of 35 °C and an AS concentration of 0.2 M was selected based on preliminary pulse-response experiments, which suggested these conditions are a viable alternative to the Φ = 40/10 °C, 0.125 M previously trialled in batch mode, with greater binding strength and greater elution yield. Two studies were conducted, one with continuous TCZ cycles, the TCZ disengaged.

The overlay is presented in **Figure 32** with the baseline trace (red) indicating a breakthrough curve at approximately 30 mL of flow-through. The corresponding DBC at 10% breakthrough was calculated to be 5.6 mg protein·mL $resin^{-1}$. Forty-four movements of the TCZ were conducted. Initial movements resulted in minimal protein elution, however elution peak size increases at peak 12, before reaching steady state operation at

18. Notably, the thermally eluted peaks closely tracked the overlaid breakthrough curve with no TCZ movements, suggesting that the TCZR is not achieving a strict on/off binding mechanism, in contrast to previous results with BSA. Instead, it appears that the TCZR is enabling a form of desorption synchronised with the breakthrough, confirming that temperature modulation may be insufficient alone to fully control Rituximab retention under these conditions. A detailed assessment of **Figure 32** shows that the $\Delta\Phi$ = 30 °C temperature difference (35/5 °C range) is inadequate for effective temperature-mediated HIC with Rituximab, as evidenced by the amount of protein that was unbound, and remained bound after TCZ cycling until removed by the strip (**Table 13**). The binding strength differential achieved in this setup is minimal, resulting in a narrow operational window where temperature-based modulation significantly influences binding affinity. The trough between peaks is lower than that of the breakthrough line (red), due to the enhanced binding conveyed by the flanking heat sinks, which were not engaged in the overlaid breakthrough. This experiment definitively demonstrates that the success observed in **Chapter 3** cannot be replicated with the current $\Delta\Phi$ = 30 °C difference.

Despite the minimal protein elution, the experiment produced good HMW removal, as tabulated in **Table 14**, underscoring the systems polishing potential. Despite the sub-optimal conditions, a depletion factor of 7.43 was achieved, and thermally eluted peaks were 99.4% monomer. This replicates the SEC analysis findings of **4.3.9**, which found temperature mediated HIC was able to remove virtually all HMW species, under the right conditions. This combined with the continuous load-and-elute capabilities of the system, and the possibility of concentration and minimal kosmotropic salt usage gives the system a niche, however intriguing potential for mAb polishing.

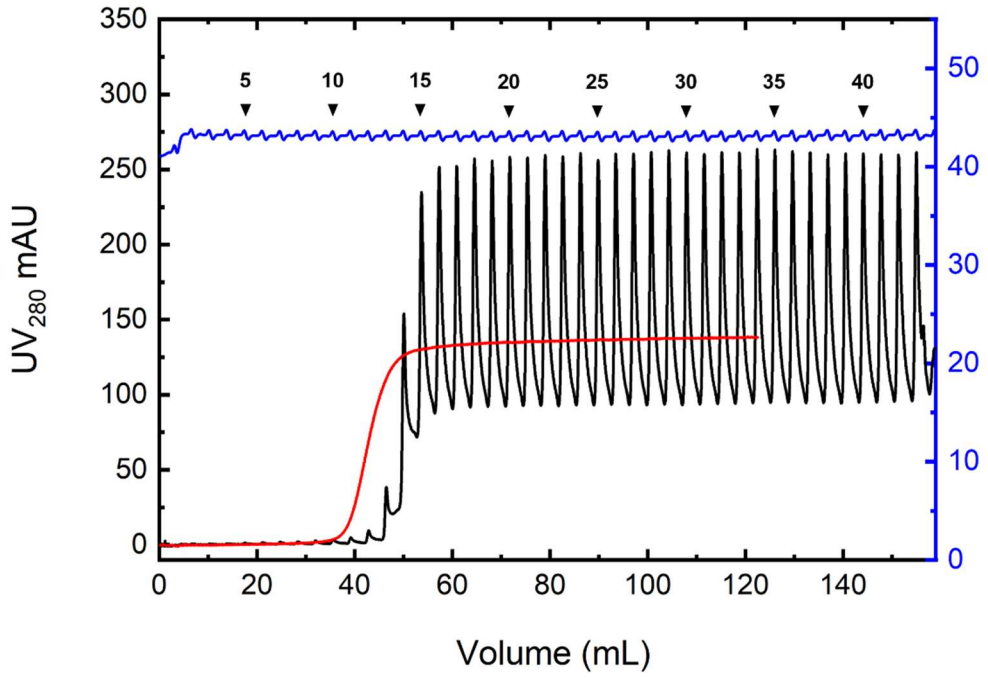

Figure 32: Chromatogram of continuous TCZR-HIC, performed with Butyl-650M, in 0.2 M AS in 50 mM sodium phosphate buffer pH7. Forty-four movements of the TCZ were performed, at a velocity of 0.1 mm·s^{-1}. UV absorbance, conductivity, and baseline UV without TCZ movements in a separate experiment are presented in black, blue, and red, respectively. Rituximab was constantly supplied at 0.5 mg·mL^{-1} to a fresh column. The cycle time was 1 cycle every 20.1 min, and the travel distance was 120 mm.

Table 13: Peak integration data extracted from Figure 32. Percentages are relative to the total loaded protein (90 mg). "Unbound " corresponds to proteins contributing to the rising UV trace baseline. "TCZ Elution " represents proteins were removed by TCZ movements, and residual proteins were washed out using 20% ethanol (Strip). A final cleaning-in-place (CIP) step with 1 M NaOH ensured complete column regeneration. Mass balance demonstrates slight over-recovery.

Units	Load	Bound (% of Load)	Unbound (% of Load)	TCZ Elution (% of Bound)	Strip	CIP (NaOH)	Mass Balance (%)
mg	90	51.0	40.6	19.3	15.0	16.7	101.8%
Percentage of Load	100	55.7%	44.3%	-	-	-	
Percentage of Bound	-	-	-	37.9%	29.3%	32.8%	

Table 14: Tabulated peak area data from SEC analysis of the feedstock, thermally eluted peaks, and strip presented in Figure 32.

Oligomer	Feedstock	Thermally Eluted Peaks	Strip
Monomer	94.8%	99.4%	90%
HMW Aggregates	5.2%	0.7%	10%

4.4. Conclusion

The results generated with Rituximab in this chapter, while showing some promise, are not as compelling as those observed with BSA in **Chapter 3**. The application of TCZR-HIC to Rituximab revealed a much narrower window of opportunity for effective operation, driven by its more constrained retention behaviour and binding characteristics.

Specifically, the current TCZR system generates a maximum temperature difference of $\Delta\Phi$ = 30 °C, restricting its ability to elute less thermally-responsive proteins, such as Rituximab. This narrower operational range highlights the necessity of achieving a greater temperature difference than is currently possible with the existing TCZR system. Without this capability, the method struggles to fully exploit temperature differences to drive effective retention and desorption for Rituximab, limiting its overall performance.

Despite these challenges, the system demonstrates significant promise for polishing applications. SEC analysis revealed a substantial reduction in aggregates in thermally eluted Rituximab peaks, with aggregate content reduced from 6.8% to >0.1% in batch operation, and 5.2% to 0.7% under continuous operation. The system's ability to polish Rituximab to this level compares favourably with other polishing approaches, such as flowthrough HIC. These results underscore the potential utility of TCZR-HIC as a final polishing step, especially given its ability to operate with reduced AS concentrations and without additional buffer exchange steps. The system also offers simultaneous polishing and concentration, further increasing its versatility and reducing the number of unit operations required.

A notable advantage of TCZR-HIC compared to flowthrough HIC the temperature control enables operation with lower salt concentrations. This reduction in AS usage has both environmental and operational benefits, including less buffer consumption, reduced waste generation, and lower costs associated with downstream processing. Additionally, with the right temperature range, the TCZR system concentrates monomers during thermal elution, providing a dual benefit of polishing and concentration in a single step. The reduced salt usage also alleviates pressure on subsequent buffer exchange steps, potentially eliminating the need for these steps entirely and further simplifying downstream workflows.

However, the limited temperature differential achievable with the current thermal control system remains a major constraint. While binding issues with Rituximab could theoretically be resolved by expanding the temperature gradient, for example, operating at $\Phi = 60$ °C for binding and $\Phi = 5$ °C for elution, power, and design limitations of the TCZR prevent such configurations. Additionally, the use of commercially available resins not specifically tailored for temperature-based chromatography restricts the system's potential. Without significant upgrades to both resin design and the TCZR system, the technique is likely to remain a niche curiosity rather than a mainstream bioprocessing method.

To unlock the full potential of temperature-mediated HIC, future work should prioritise the development of new resin formulations with optimised HIC ligands, re-engineering the system to support a broader temperature range, and exploring alternative kosmotropic salts to improve retention and desorption dynamics. Such innovations are required in the

continued development of TCZR-HIC, enabling enhanced product purity, operational efficiency, and reduced manufacturing complexity for mAbs like Rituximab.

In conclusion, while temperature-mediated HIC for Rituximab currently faces notable limitations its advantages, such as reduced salt requirements, simultaneous polishing and concentration, and continuous operation, make it a promising candidate for niche applications. With targeted innovations in resin design and system upgrades, TCZR-HIC has the potential to evolve into a highly effective tool for next-generation downstream processing, combining environmental sustainability with operational efficiency.

Chapter 5

Conclusions and Future Work

5.1. Conclusions & Future Work

Continuous processing, widely regarded as the future of bioprocessing, offers enhanced efficiency, reduced costs, and a smaller environmental footprint compared to traditional batch methods. These advancements are increasingly vital as the bioprocessing industry strives to meet the growing need for sustainable and scalable downstream processing techniques. Recent global events, such as the COVID-19 pandemic, have highlighted the urgency for rapid and high-yield therapeutic production to address surging global demands. Against this backdrop, temperature-controlled chromatography emerges as a promising alternative, combining operational efficiency with both environmental and economic sustainability.

In this thesis, the objective was to explore and expand the applications of the bespoke TCZR chromatography system for HIC. By leveraging the TCZR's unique temperature-based elution mechanism, which decouples binding strength from mobile phase composition, this work aimed to achieve continuous protein processing in a single column. This approach enables simultaneous loading and elution from the same column, delivering a capability unmatched by conventional chromatographic systems.

In **Chapter 3**, the feasibility of TCZR-HIC was rigorously evaluated using BSA, a well-characterised model protein. This chapter successfully demonstrated the fundamental capabilities of the TCZR system. Firstly, preliminary batch binding experiments and pulse-response temperature switching trials established operational parameters with Butyl Sepharose 4FF resin (**3.3.1, 3.3.3**). These trials demonstrated the robust

temperature-mediated binding and desorption of BSA, forming the basis for continuous TCZR operation.

Secondly, CLSM imaging revealed that binding was confined to the outer periphery of the beads, highlighting the need for small particles with large pore size to maximise available surface area, and aid poor mass-transfer into the centre of the bead (**3.3.2)**.

Thirdly, with the operational parameters established, two batch TCZR-HIC experiments demonstrated batch mode operation, producing first seven, and then twelve peaks in the two studies; decreasing in size as the bound protein was depleted (**3.3.4**).

Fourth, three continuous TCZR-HIC experiments demonstrated continuous operation under a variety of conditions. Initially with a dilute feedstock, showing a best-case scenario for the systems capabilities (**3.3.7, Condition 1**). Following this, experiments with a high concentration feedstock demonstrated the progressive overload of the columns working-capacity (**3.3.7, Condition 2**). The available monomer-binding capacity of the column was steadily reduced as it was consumed by an accumulation of HMW species. The system still demonstrated excellent polishing capabilities, even under overloaded conditions. After this, an intermediate concentration feedstock was applied to a fouled column, further demonstrating impressive purification performance under fouled conditions (**3.3.8**).

The system achieved over 94% monomer recovery and a six-fold reduction in high-molecular-weight aggregates, meeting regulatory standards for therapeutic product quality. Although binding capacities at the reduced salt concentration are low, the system was remarkably effective at aggregate removal, underscoring the system's suitability as

a polishing step in large-scale bioprocessing workflows (**3.3.8**). This was all achieved while using a lower salt concentration than would otherwise be used, due to the elevated binding temperature. The ability to perform isocratic separations with reduced salt concentrations further enhances its appeal as a greener alternative to conventional methods.

Building on the foundational work in **Chapter 3**, **Chapter 4** focused on applying the TCZR-HIC system to Rituximab, a widely used therapeutic mAb. This exploration highlighted the protein-specific nature of TCZR-HIC and its dependence on target-specific physicochemical properties.

While **Chapter 3** leveraged the work of Müller and Franzreb 2012, and 2013 as predicate work, **Chapter 4** required additional molecule specific characterisation and optimisation. The key findings were: (i) The solubility of Rituximab in AS was established at < 0.8 M AS, providing a wide range of possible salt concentrations (0 – 0.8 M AS) to explore (**4.3.1**); (ii) Two batches of Rituximab, manufactured to different purities, were compared for their HMW content and hydrophobicity. These batches had similar hydrophobicity when assessed on a HIC gradient, however one had significantly more HMW species, which was subsequently reserved for TCZR-HIC polishing studies (**4.3.2**); (iii) A reliable method for generating soluble aggregates was established, which could be employed for future polishing studies (**0**); (iv) static binding studies with five-resins including Butyl Sepharose 4FF, and four other resins designed to capitalise on the CLSM observations from **Chapter 3,** (**3.3.2**); these resins were optimised to have a small particle size, and large a pore sizes to maximise outer-surface area and internal mass-transfer. Phenyl resins exhibited no temperature sensitivity, whereas Butyl resins demonstrated temperature

sensitive behaviour, possibly due to Phenyl being an aryl group with an aromatic ring, unlike Butyl, which is an alkyl group (**0**); (v) In pulse-response studies, conducted in a waterbath, Rituximab required a greater than 30 °C temperature difference for effective binding and elution, evidenced by binding trials above 40 °C (**4.3.5**). Adjusting the salt concentration in a range, and trialling a different resin did improve yields, however, came at the cost of poor antibody retention. An alternative temperature range, Φ = 35/5 °C, was also trialled, yielding similar results (**4.3.6**). These observations underscore the need for a >30 °C temperature difference. (vi) Modifications to the TCZR internal cabinet and thermal blocks were unable to increase the available temperature difference. Without substantial re-engineering the system is unable to achieve a >30 °C difference, so the work proceeded with a $\Delta\Phi$ = 30 °C temperature difference, acknowledging that this is sub-optimal (**4.3.7**). (vii) Batch and continuous operation were demonstrated, however the predicted antibody retention issues observed during the pulse-response studies were successfully replicated, demonstrating that although the principle works, the available system could not generate a sufficient temperature difference, demonstrated with batch, (**4.3.8, 4.3.9**), and continuous (**4.3.10**) operation. (viii) Despite yield challenges, the TCZR system excelled in aggregate removal, achieving a five-fold reduction in high-molecular-weight species compared to the initial feed (**4.3.10**). This result achieves the quality control requirements for commercially available Rituximab, which state >97.77% by HPLC on certificates of analysis, (MedChemExpress, 2025), and reinforces the system's potential as an advanced polishing tool.

The ability to selectively retain aggregates while also concentrating the feedstock into sharp elution peaks represents a major advantage over conventional modalities, such as

flowthrough-HIC. This mode of operation combines polishing, concentration and reduces the burden for buffer exchange by employing less salt. With a sufficiently high binding temperature, this could possibly be performed in a very mild formulation buffer, removing the necessity for buffer exchange as well, as even with Φ = 40 °C, a very low concentration of salt was required (0.125 M). Water bath studies demonstrated that widening the temperature difference to conditions such as 60 °C for binding and 5 °C for elution could address the limitations encountered with Rituximab. Such conditions would enable effective on/off binding, enhancing both yield and purity. These findings highlight the molecule-specific challenges and opportunities associated with TCZR-HIC. They also reinforce the importance of optimising resin properties and temperature difference to accommodate the diverse characteristics of target proteins.

Collectively, the results of **Chapters 3** and **Chapter 4** reveal both the strengths and limitations of temperature-controlled chromatography. Key benefits include high-resolution separation, continuous operation, and effective aggregate removal, attributes directly aligned with the bioprocessing industry's goals for greener, leaner, and more scalable systems. However, the system's effectiveness is highly dependent on the target protein's physicochemical properties, necessitating careful optimisation for each application. Additionally, by relying on a single column, the rate of loading must equal the rate of elution, otherwise the column becomes saturated, allowing unbound protein through as observed with the rising UV baseline in **3.3.7**. The thermally-mediated nature also limits the column width that can be employed, as the mechanism of elution relies on efficient thermal transfer into the centre of the bed.

The limitations discussed herein can likely be addressed by increasing several ways. Firstly, increasing the cooling capacity of the central copper block by upgrading to larger Peltier elements, more robust power delivery systems, and better controllers could achieve broader temperature differences, enabling more effective separation for challenging molecules like Rituximab. Second, improving thermal efficiency by insulating the copper block from the heated cabinet, using higher-performance thermal interface materials to aid thermal transfer between the Peltier element and the heatsinks, or alternative heatsink technologies (e.g., heat pipes or vapour chambers). These upgrades would improve thermal transfer from the Peltier element to the flanking heatsinks. An alternative approach involving a water-cooled insulated copper block could achieve temperature differences exceeding 30 °C while maintaining energy efficiency. Coolants such as ethylene glycol could enable near-zero operation, expanding TCZRs operational window. Such a design would likely forfeit the "peak sharpening" effect inherent to Peltier-driven systems, which enhances resolution by promoting adsorption immediately after cooling. This may result in less-well defined peaks, and decreased resolution.

Future work has many options for advancing TCZR technology. Future studies could explore TCZR-HIC's applicability to other therapeutic proteins, such as bispecific antibodies, antibody-drug conjugates, and fusion proteins. These targets present unique purification challenges that could benefit from TCZR's high-resolution capabilities. Antibody-drug conjugates in particular represent an intriguing target, as the molecule's hydrophobicity is greatly determined by the antibody-drug ratio. Integration of the TCZR system with other continuous processing steps such as perfusion bioreactors, continuous

centrifugation, or continuous capture chromatography could create end-to-end study, demonstrating TCZR-HIC in a truly continuous context.

This thesis underscores the potential of temperature-controlled chromatography in modern bioprocessing. While the technology is not universally applicable, its ability to provide sustainable operation, high-resolution separation, and effective aggregate removal represent an attractive alternative unit-operation. By addressing the challenges outlined in this research, particularly in thermal management and scalability, future iterations of TCZR systems could unlock even broader adoption in industrial bioprocessing. Ultimately, this work contributes to the ongoing evolution of bioprocessing technologies, paving the way for greener, more efficient, and highly adaptable solutions to meet the demands of a rapidly changing global landscape.

Appendices

Appendix A

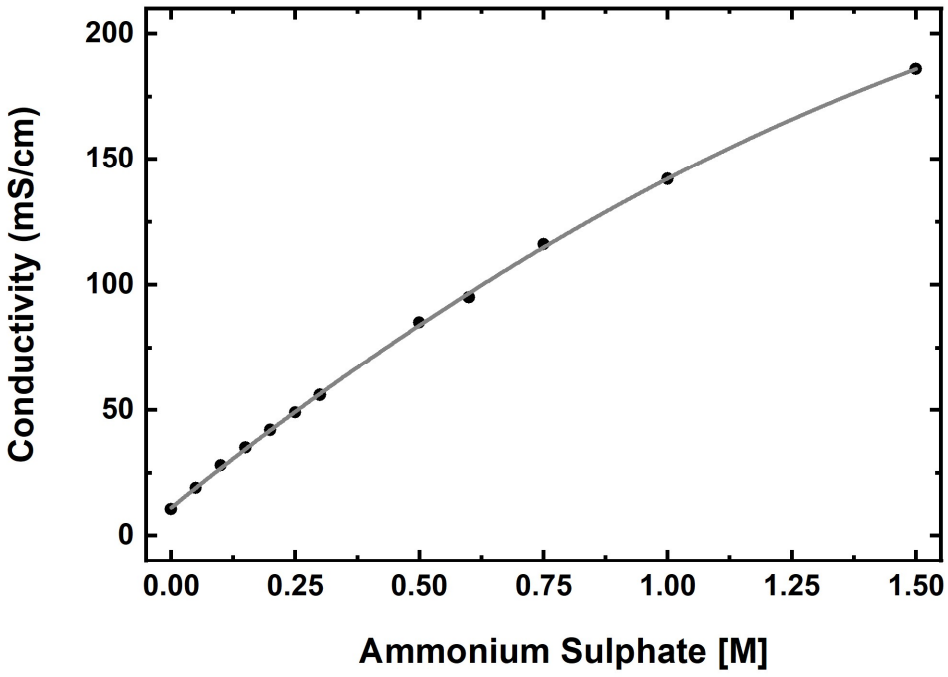

Figure 33: AS Conductivity curve used to quality control buffers. AS in 50 mM Phosphate buffer (pH 7) was prepared carefully at a range of AS concentrations: [0.00, 0.05, 0.10, 0.15, 0.20, 0.25, 0.30, 0.50, 0.60, 0.75, 1.00, 1.50 M AS + 50 mM Phosphate Buffer]. The conductivity measured by the AKTA was recorded and plotted. The resulting relationship was non-linear and was used to quality control all buffers that contained AS to ensure accuracy; subsequent buffers were adjusted to within 0.5 mS/cm of the curve. All buffers were made and measured at room temperature.

Table 15: Polynomial fit applied to the data presented in **Figure 33**.

Fit	Polynomial Cubic
Equation	$y = a + bx + cx^2 + dx^3$
A	11.16
B	160.29
C	-29.48
D	0.22
R^2	0.99

Appendix B

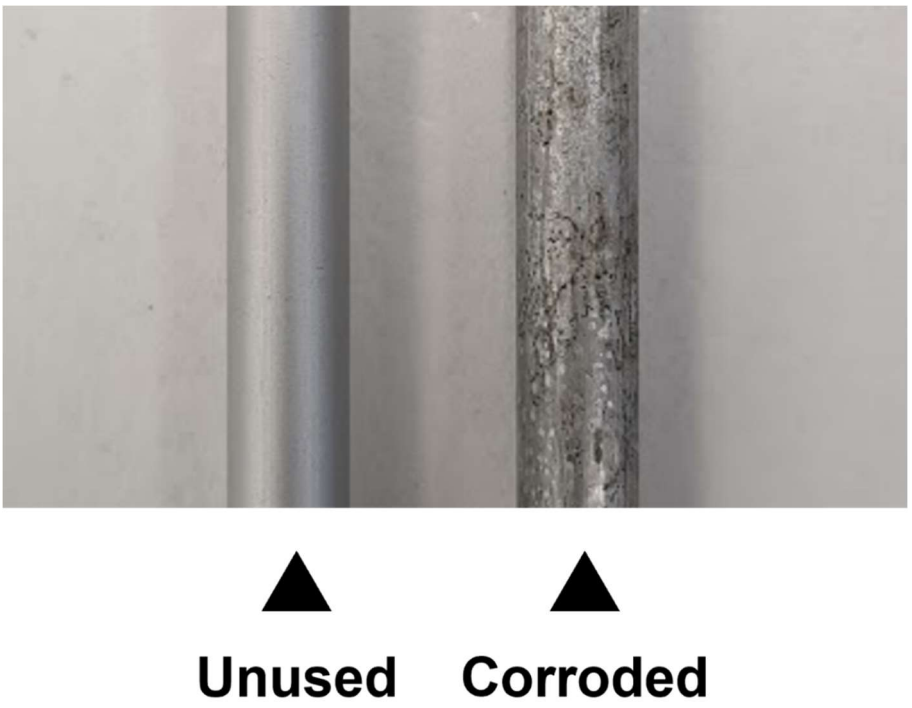

Figure 34: Comparison of anodised aluminium inner column inserts. The unused insert (left) remains free of corrosion, while the used insert (right) exhibits extensive corrosion damage. This degradation is attributed to galvanic corrosion, an electrochemical process facilitated by the contact of dissimilar metals in the presence of an electrolyte. The corrosion rate is influenced by the nature of the electrolyte and the difference in standard reduction potentials (SRPs) between the metals. The less noble metal, characterised by a lower SRP, corrodes preferentially. In this case, the AS -based mobile phase used during TCZR-HIC likely accelerated this effect due to its corrosive properties.

Appendix C

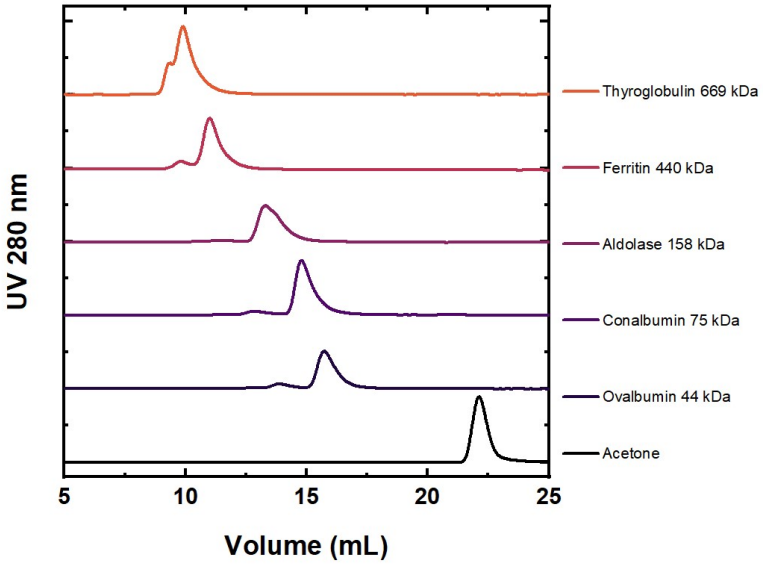

Figure 35: Overlaid traces from SEC calibration. The retention of Thyroglobulin (669 kDa), Ferritin (440 kDa), Aldolase (158 kDa), Conalbumin (75 kDa), Ovalbumin (44 kDa), and Acetone was used to calibrate the SEC column.

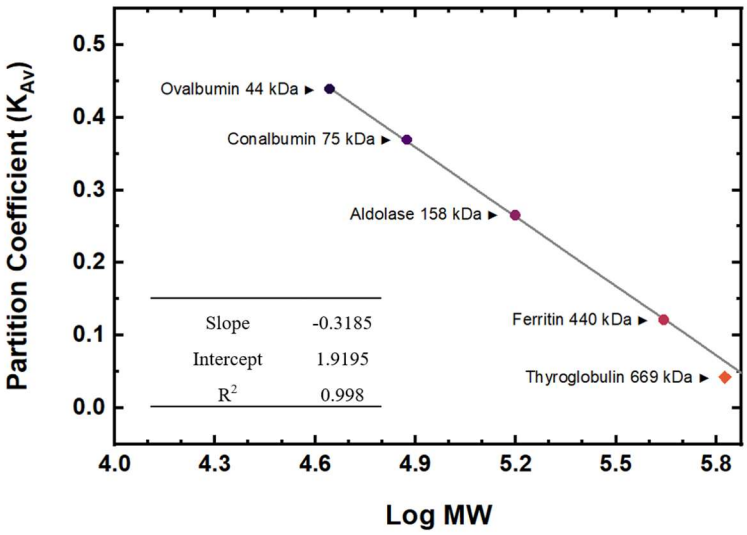

Figure 36: Partition Coefficient vs. Log MW of tested calibration standards. A linear fit is applied to protein standards that fit within the Superdex 200 increase 300/10 exclusion range (Coloured dots and trace). Thyroglobulin 669 kDa falls outside of this range but has been plotted for completeness, thus has not been included in the linear fit (Orange Dimond).

Appendix D

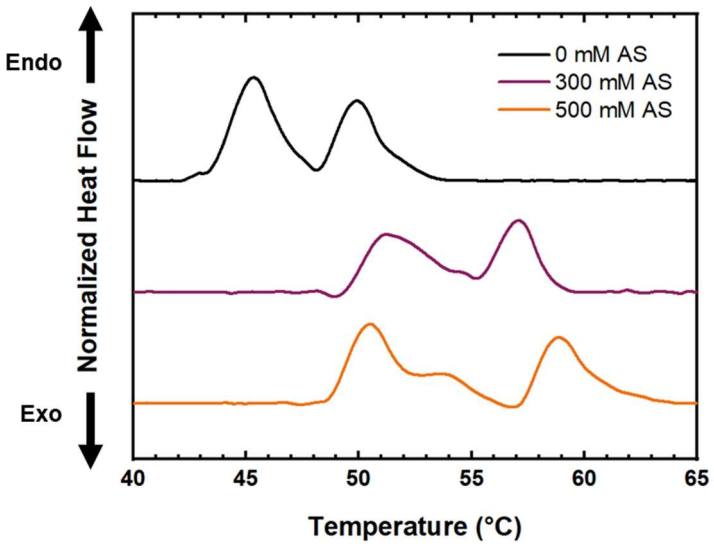

Figure 37: Differential scanning calorimetry (DSC) thermograms of BSA, (1 mg/mL) in 50 mM phosphate buffer with AS concentrations of 0 mM, 300 mM, and 500 mM. The thermograms display endothermic (endo) heat flow during a temperature ramp from 40 °C to 65 °C, showing two distinct melting transitions that correspond to the sequential unfolding of BSA's domains. The curves are normalised for comparison. Increasing AS concentrations shift the melting transitions to higher temperatures, indicating stabilisation of BSA's structure by AS. Endothermic peaks correspond to the disruption of secondary and tertiary structure, involving the breaking of hydrogen bonds, hydrophobic interactions, and van der Waals forces. The observed transitions provide insights into the thermal stability and unfolding behaviour of BSA under varying AS conditions.

Table 16: Tabulated thermogram data of BSA (1 mg/mL) in three AS solutions at 0.00 M, 0.30 M, and 0.50 M concentrations. The thermograms depict endothermic (endo) heat flow during heating from 40 °C to 65 °C, highlighting two distinct melting transitions.

BSA [1 mg/mL]				
Solvent	T_{onset}	T_{M1}	T_{M2}	T_{End}
0.0 M AS	42.1 °C	45.3 °C	49.9 °C	54.0 °C
0.3 M AS	48.1 °C	51.3 °C	57.1 °C	59.7 °C
0.5 M AS	47.2 °C	50.5 °C	58.9 °C	64.0 °C

References

AFABLE, M. G., SHAIK, M. & SUGIMOTO, Y. et al. (2011) Efficacy of rabbit anti-thymocyte globulin in severe aplastic anemia. *Haematologica*, 96, p. 1269.

AKIBA, H. & TSUMOTO, K. (2015) Thermodynamics of antibody–antigen interaction revealed by mutation analysis of antibody variable regions. *J. Biochem.*, 158(1), pp. 1–13.

ALAS, S. & BONAVIDA, B. (2001) Rituximab inactivates signal transducer and activation of transcription 3 (**STAT3**) activity in **B-non-Hodgkin's** lymphoma through inhibition of the interleukin 10 autocrine/paracrine loop and results in down-regulation of **Bcl-2** and sensitization to cytotoxic drugs. *Cancer Res.*, 61, pp. 5137–5144.

ANGELO, J., PAGANO, J. & MÜLLER-SPÄTH, T. et al. (2018) Scale-up of twin-column periodic counter-current chromatography for mAb purification. *Bioproc. Int.*, 16, pp. 28–37.

ANICETO, J. P. S. & SILVA, C. M. (2014) Simulated moving bed strategies and designs: from established systems to the latest developments. *Sep. Purif. Rev.*, 44(1), pp. 41–73.

ARAKAWA, T. & TIMASHEFF, S. N. (1983) Preferential interactions of proteins with solvent components in aqueous amino acid solutions. *Arch. Biochem. Biophys.*, 224, pp. 169–177.

BABCOCK, J. J. & BRANCALEON, L. (2013) Bovine serum albumin oligomers in the e-and b-forms at low protein concentration and ionic strength. *Int. J. Biol. Macromol.*, 53, pp. 42–53.

BALFOUR, H. (2021) Continuous biomanufacturing–where are we now? *Eur. Pharm. Rev.*, 26, pp. 12–15.

BALKANI, S., SHAMEKHI, S. & RAOUFINIA, R. et al. (2016) Purification and characterization of bovine serum albumin using chromatographic method. *Adv. Pharm. Bull.*, 6(4), pp. 651–654.

BAMFORTH, A. (1954) Corrosion problems of ammonium sulphate manufacture. *Anti-Corros. Methods Mater.*, 1, pp. 31–35.

BANSODE, V., GUPTA, P., KATEJA, N. & RATHORE, A. S. (2022) Contribution of protein A step towards cost of goods for continuous production of monoclonal antibody therapeutics. *J. Chem. Technol. Biotechnol.*, 97, pp. 2420–2433.

BARNARD, G. C., KULL, A. R. & SHARKEY, N. S. et al. (2010) High-throughput screening and selection of yeast cell lines expressing monoclonal antibodies. *J. Ind. Microbiol. Biotechnol.*, 37, pp. 961–971.

BARTH, H. G., JACKSON, C. & BOYES, B. E. (1994) Size exclusion chromatography. *Anal. Chem.*, 66, pp. 595–620.

BAYER, V. (2019) An overview of monoclonal antibodies. *Semin. Oncol. Nurs.*, 35, p. 150927.

BEHRING, E. V. (1890) Untersuchungen ueber das zustandekommen der diphtherie-immunität bei thieren. *Drucke 19. Jh.* (Historical reference).

BENDER, J. & WOLK, B. (1998) Putting a spin on CHO harvest: centrifuge technology development. *Paper presented at the ACS Meeting, Boston, MA.*

BERDICHEVSKY, M., D'ANJOU, M. & MALLEM, M. R. et al. (2011) Improved production of monoclonal antibodies through oxygen-limited cultivation of glycoengineered yeast. *J. Biotechnol.*, 155, pp. 217–224.

BERGANTINI, L., D'ALESSANDRO, M. & CAMELI, P. et al. (2020) Effects of rituximab therapy on **B-cell** differentiation and depletion. *Clin. Rheumatol.*, 39, pp. 1415–1421.

BERLIER, J. E., ROTHE, A. & BULLER, G. et al. (2003) Quantitative comparison of long-wavelength alexa fluor dyes to cy dyes: fluorescence of the dyes and their bioconjugates. *J. Histochem. Cytochem.*, 51, pp. 1699–1712.

BESSELINK, T., JANSSEN, A. & BOOM, R. (2015) Isolation of bovine serum albumin from whey using affinity chromatography. *Int. Dairy J.*, 41, pp. 32–37.

BHATTACHARYA, A. A., GRUNE, T. & CURRY, S. (2000) Crystallographic analysis reveals common modes of binding of medium and long-chain fatty acids to human serum albumin. *J. Mol. Biol.*, 303, pp. 721–732.

BIO-RAD (2016) *Protein A antibody purification handbook* [online]. Bio-Rad Laboratories. Available from: https://www.bio-rad-antibodies.com/static/2015/proteus/protein-a-handbook.pdf [Accessed 25 August 2024].

BIOSPACE (2022) Biopharmaceuticals market size to hold USD 856.1 bn by 2030 [online]. Biospace.com. Available from: https://www.biospace.com/article/biopharmaceuticals-market-size-to-hold-usd-856-1-bn-by-2030/ [Accessed 30 May 2023].
BIOSPACE (2024) Pharmaceutical market size to hit around USD 2,832.66 bn by 2033 [online]. Biospace.com. Available from: https://www.biospace.com/pharmaceutical-market-size-to-hit-around-usd-2-832-66-bn-by-2033 [Accessed 26 August 2024].
BISHOP, A. L., SCHILD, S. & PATIMALLA, B. et al. (2010) Mucosal immunization with vibrio cholerae outer membrane vesicles provides maternal protection mediated by antilipopolysaccharide antibodies that inhibit bacterial motility. *Infect. Immun.*, 78, pp. 4402–4420.
BLOOMFIELD, V. (1966) The structure of bovine serum albumin at low pH. *Biochemistry*, 5, pp. 684–689.
BOBALY, B., BECK, A. & VEUTHEY, J. L. et al. (2016) Impact of organic modifier and temperature on protein denaturation in hydrophobic interaction chromatography. *J. Pharm. Biomed. Anal.*, 131, pp. 124–132.
BOES, M. (2000) Role of natural and immune **IgM** antibodies in immune responses. *Mol. Immunol.*, 37, pp. 1141–1149.
BORZOVA, V. A., MARKOSSIAN, K. A. & CHEBOTAREVA, N. A. et al. (2016) Kinetics of thermal denaturation and aggregation of bovine serum albumin. *PLoS One*, 11(4), p. e0153495.
BRADER, M. L., ESTEY, T. & BAI, S. et al. (2015) Examination of thermal unfolding and aggregation profiles of a series of developable therapeutic monoclonal antibodies. *Mol. Pharm.*, 12(4), pp. 1005–1017.
BRÄUNINGER, A., GOOSSENS, T., RAJEWSKY, K. & KÜPPERS, R. (2001) Regulation of immunoglobulin light chain gene rearrangements during early b cell development in the human. *Eur. J. Immunol.*, 31, pp. 3631–3637.
BRODSKY, Y., ZHANG, C., YIGZAW, Y. & VEDANTHAM, G. (2012) Caprylic acid precipitation method for impurity reduction: an alternative to conventional chromatography for monoclonal antibody purification. *Biotechnol. Bioeng.*, 109, pp. 2589–2598.
BROWN, M. C. (2008) Antibodies: key to a robust lateral flow immunoassay. In: **WONG, R. & TSE, H. (eds.)** *Lateral flow immunoassay.* New York: Humana Press, pp. 1–16.
BRUSOTTI, G., CALLERI, E. & COLOMBO, R. et al. (2018) Advances on size exclusion chromatography and applications on the analysis of protein biopharmaceuticals and protein aggregates: a mini review. *Chromatographia*, 81, pp. 3–23.
BUCHACHER, A., IBERER, G. & JUNGBAUER, A. et al. (2001) Continuous removal of protein aggregates by annular chromatography. *Biotechnol. Prog.*, 17, pp. 140–149.
BUDZINSKI, K., BLEWIS, M. & DAHLIN, P. et al. (2019) Introduction of a process mass intensity metric for biologics. *New Biotechnol.*, 49, pp. 37–42.
BUDZINSKI, K., CONSTABLE, D. & D'AQUILA, D. et al. (2022) Streamlined life cycle assessment of single use technologies in biopharmaceutical manufacture. *New Biotechnol.*, 68, pp. 28–36.
BUNNAK, P., ALLMENDINGER, R. & RAMASAMY, S. V. et al. (2016) Life-cycle and cost of goods assessment of fed-batch and perfusion-based manufacturing processes for mAbs. *Biotechnol. Prog.*, 32, pp. 1324–1335.
BURNOUF, T. (2007) Modern plasma fractionation. *Transfus. Med. Rev.*, 21(2), pp. 101–117.
BURTON, D. R. & WOOF, J. M. (1992) Human antibody effector function. *Adv. Immunol.*, 51, pp. 1–84.
CAMBIER, J. C., GAULD, S. B., MERRELL, K. T. & VILEN, B. J. (2007) B-cell anergy: from transgenic models to naturally occurring anergic b cells? *Nat. Rev. Immunol.*, 7, pp. 633–643.
CAMPODÓNICO, V. L., LLOSA, N. J. & GROUT, M. et al. (2010) Evaluation of flagella and flagellin of pseudomonas aeruginosa as vaccines. *Infect. Immun.*, 78, pp. 746–755.
CAO, P. (2015) *Smart adsorption materials and systems for recovery of high value protein products.* PhD Thesis. University of Birmingham.
CAO, P., MÜLLER, T. K. & KETTERER, B. et al. (2015) Integrated system for temperature-controlled fast protein liquid chromatography. II. optimized adsorbents and 'single column continuous operation'. *J. Chromatogr. A*, 1403, pp. 118–131.
CARTA, G. & JUNGBAUER, A. (2020) *Protein chromatography: process development and scale-up.* Hoboken: John Wiley & Sons.
CHEN, C., WONG, H. E. & GOUDAR, C. T. (2018) Upstream process intensification and continuous manufacturing. *Curr. Opin. Chem. Eng.*, 22, pp. 191–198.

CHEN, J., TETRAULT, J. & LEY, A. (2008) Comparison of standard and new generation hydrophobic interaction chromatography resins in the monoclonal antibody purification process. *J. Chromatogr. A*, 1177, pp. 272–281.
CHEN, W.-Y., HUANG, H.-M., LIN, C.-C. & LIN, F.-Y. (2003) Effect of temperature on hydrophobic interaction between proteins and hydrophobic adsorbents: studies by isothermal titration calorimetry and the van't hoff equation. *Langmuir*, 19, pp. 9395–9403.
CLYNES, R. A., TOWERS, T. L., PRESTA, L. G. & RAVETCH, J. V. (2000) Inhibitory fc receptors modulate in vivo cytotoxicity against tumor targets. *Nat. Med.*, 6, pp. 443–446.
COHN, E. J., STRONG, L. E., HUGHES, W. L. et al. (1946) Preparation and properties of serum and plasma proteins. iv. a system for the separation into fractions of the protein and lipoprotein components of biological tissues and fluids. *J. Am. Chem. Soc.*, 68, pp. 459–475.
CRAMER, S. M. & HOLSTEIN, M. A. (2011) Downstream bioprocessing: recent advances and future promise. *Curr. Opin. Chem. Eng.*, 1, pp. 27–37.
CRAMERI, F., SHEPHARD, G. E. & HERON, P. J. (2020) The misuse of colour in science communication. *Nat. Commun.*, 11, p. 5444.
CUMMINS, P. M., ROCHFORT, K. D. & O'CONNOR, B. F. (2017) Ion-exchange chromatography: basic principles and application. In: **WALLS, D. (ed.)** *Protein chromatography: methods and protocols.* New York: Springer, pp. 209–223.
CYTIVA (2020) Butyl sepharose 4 fast flow, octyl sepharose 4 fast flow, hydrophobic interaction resin, instructions for use [online]. Available from: https://d3.cytivalifesciences.com/prod/IFU/71500240.pdf [Accessed 14 June 2023].
CYTIVA (2021) Vol. 1: antibodies – affinity chromatography [online]. Available from: https://cdn.cytivalifesciences.com/api/public/content/digi-11660-pdf [Accessed 25 August 2024].
CYTIVA (2024) Size exclusion chromatography, principles and methods [online]. Available from: https://cdn.cytivalifesciences.com/api/public/content/digi-11639-pdf [Accessed 28 July 2024].
DENIZLI, A. (2011) Plasma fractionation: conventional and chromatographic methods for albumin purification. *Hacet. J. Biol. Chem.*, 39, pp. 315–341.
DILKS, A. T., GILCHRIST, J. & LAM, Y. et al. (2023a) Considerations for operational space definition and optimization of a no-salt flowthrough hydrophobic interaction chromatography purification step. *Biotechnol. Prog.*, 39, p. e3351.
DILKS, A. T., GILCHRIST, J. & LAM, Y. et al. (2023b) Considerations for operational space definition and optimization of a no-salt flowthrough hydrophobic interaction chromatography purification step. *Biotechnol. Prog.*, 39, p. e3351.
DIOGO, M. M., QUEIROZ, J. A. & PRAZERES, D. M. (2001) Studies on the retention of plasmid dna and escherichia coli nucleic acids by hydrophobic interaction chromatography. *Bioseparation*, 10, pp. 211–220.
DIOGO, M. M., RIBEIRO, S. & QUEIROZ, J. A. et al. (2000) Scale-up of hydrophobic interaction chromatography for the purification of a dna vaccine against rabies. *Biotechnol. Lett.*, 22, pp. 1397–1400.
DIXON, M. & WEBB, E. C. (1961) Enzyme fractionation by salting-out: a theoretical note. *Adv. Protein Chem.*, 16, pp. 197–219.
DUNKELBERGER, J. R. & SONG, W. C. (2010) Complement and its role in innate and adaptive immune responses. *Cell Res.*, 20, pp. 34–50.
DUONG-LY, K. C. & GABELLI, S. B. (2014) Salting out of proteins using ammonium sulfate precipitation. *Methods Enzymol.*, 541, pp. 85–94.
EJIMA, D., TSUMOTO, K. & FUKADA, H. et al. (2007) Effects of acid exposure on the conformation, stability, and aggregation of monoclonal antibodies. *Proteins*, 66, pp. 954–962.
EL RASSI, Z. & CRAMER, S. M. (1996) Recent progress in reversed-phase and hydrophobic interaction chromatography of carbohydrate species. *J. Chromatogr. A*, 720, pp. 93–118.
ER-EL, Z., ZAIDENZAIG, Y. & SHALTIEL, S. (1972) Hydrocarbon-coated sepharoses: use in the purification of glycogen phosphorylase. *Biochem. Biophys. Res. Commun.*, 49, pp. 383–390.
ESQUIBEL-KING, M. A., DIAS-CABRAL, A. C., QUEIROZ, J. A. & PINTO, N. G. (1999) Study of hydrophobic interaction adsorption of bovine serum albumin under overloaded conditions using flow microcalorimetry. *J. Chromatogr. A*, 865, pp. 111–122.
EWONDE, R. E., LINGG, N., EßER, D. & EELTINK, S. (2022) A protocol for setting-up robust hydrophobic interaction chromatography targeting the analysis of intact proteins and monoclonal antibodies. *Anal. Sci. Adv.*, 3, [page range not provided].

FANALI, G., DI MASI, A. & TREZZA, V. et al. (2012) Human serum albumin: from bench to bedside. *Mol. Aspects Med.*, 33, pp. 209–290.
FARID, S. S. (2007) Process economics of industrial monoclonal antibody manufacture. *J. Chromatogr. B*, 848, pp. 8–18.
FEKETE, S., BECK, A., VEUTHEY, J.-L. & GUILLARME, D. (2015) Ion-exchange chromatography for the characterization of biopharmaceuticals. *J. Pharm. Biomed. Anal.*, 113, pp. 43–55.
FEKETE, S., VEUTHEY, J.-L., BECK, A. & GUILLARME, D. (2016) Hydrophobic interaction chromatography for the characterization of monoclonal antibodies and related products. *J. Pharm. Biomed. Anal.*, 130, pp. 3–18.
FORTHAL, D. N. (2014) Functions of antibodies. *Microbiol. Spectr.*, 2, p. AID-0019-2014.
FUJISAWA, H. (2008) Neutrophils play an essential role in cooperation with antibody in both protection against and recovery from pulmonary infection with influenza virus in mice. *J. Virol.*, 82, pp. 2772–2783.
GABRIELSON, J. P., BRADER, M. L. & PEKAR, A. H. et al. (2007) Quantitation of aggregate levels in a recombinant humanized monoclonal antibody formulation by size-exclusion chromatography, asymmetrical flow field flow fractionation, and sedimentation velocity. *J. Pharm. Sci.*, 96, pp. 268–279.
GAGNON, P. (2000) Use of hydrophobic interaction chromatography with a non-salt buffer system for improving process economics in purification of monoclonal antibodies. *Paper presented at the Waterside Conference on Monoclonal and Recombinant Antibodies, Miami, Florida, USA, 30 April–3 May 2000.*
GAGNON, P. (2006) Polishing methods for monoclonal igg purification. In: **SHUKLA, A. A., ETZEL, M. R. & GADAM, S. (eds.)** *Process scale bioseparations for the biopharmaceutical industry.* Boca Raton: CRC Press.
GALLI, S. J. & TSAI, M. (2012) IgE and mast cells in allergic disease. *Nat. Med.*, 18, pp. 693–704.
GARIDEL, P., EIPERLE, A., BLECH, M. & SEELIG, J. (2020) Thermal and chemical unfolding of a monoclonal igg1 antibody: application of the multistate zimm-bragg theory. *Biophys. J.*, 118, pp. 1067–1075.
GAY, D., SAUNDERS, T., CAMPER, S. & WEIGERT, M. (1993) Receptor editing: an approach by autoreactive b cells to escape tolerance. *J. Exp. Med.*, 177, pp. 999–1008.
GEISBERGER, R., LAMERS, M. & ACHATZ, G. (2006) The riddle of the dual expression of igm and igd. *Immunology*, 118, pp. 429–437.
GENG, X. & CHANG, J. (1990) Study of the retention mechanism of proteins in hydrophobic interaction chromatography. *J. Chromatogr. A*, 507, pp. 1–23.
GERSTWEILER, L., BI, J. & MIDDELBERG, A. P. J. (2021) Continuous downstream bioprocessing for intensified manufacture of biopharmaceuticals and antibodies. *Chem. Eng. Sci.*, 231, p. 116272.
GHOSE, S., TAO, Y., CONLEY, L. & CECCHINI, D. (2013) Purification of monoclonal antibodies by hydrophobic interaction chromatography under no-salt conditions. *Mabs*, 5, pp. 795–800.
GIRARD, V., HILBOLD, N. J. & NG, C. K. et al. (2015) Large-scale monoclonal antibody purification by continuous chromatography, from process design to scale-up. *J. Biotechnol.*, 213, pp. 65–73.
GJOKA, X., GANTIER, R. & SCHOFIELD, M. (2017) Transfer of a three step mAb chromatography process from batch to continuous: optimizing productivity to minimize consumable requirements. *J. Biotechnol.*, 242, pp. 11–18.
GOLDSTEIN, G. (1987) Monoclonal antibody specificity: orthoclone okt3 t-cell blocker. *Nephron*, 46(suppl 1), pp. 5–11.
GOODYEAR, C. S. & SILVERMAN, G. J. (2003) Death by a b cell superantigen: in vivo vh-targeted apoptotic supraclonal b cell deletion by a staphylococcal toxin. *J. Exp. Med.*, 197, pp. 1125–1139.
GOYON, A., EXCOFFIER, M. & JANIN-BUSSAT, M.-C. et al. (2017) Determination of isoelectric points and relative charge variants of 23 therapeutic monoclonal antibodies. *J. Chromatogr. B*, 1065, pp. 119–128.
GREEN, A. A. & HUGHES, W. L. (1955) Protein fractionation on the basis of solubility in aqueous solutions of salts and organic solvents. In: **COLOWICK, S. P. & KAPLAN, N. O. (eds.)** *Methods in Enzymology.* Vol. 1. New York: Academic Press, pp. 67–90.
GRINBERG, N., BLANCO, R., YARMUSH, D. M. & KARGER, B. L. (1989) Protein aggregation in high-performance liquid chromatography: hydrophobic interaction chromatography of beta-lactoglobulin a. *Anal. Chem.*, 61, pp. 514–520.
GRONEMEYER, P., DITZ, R. & STRUBE, J. (2014) Trends in upstream and downstream process development for antibody manufacturing. *Bioeng.*, 1, pp. 188–212.

GUPTA, P., KATEJA, N., MISHRA, S., KAUR, H. & RATHORE, A. S. (2021) Economic assessment of continuous processing for manufacturing of biotherapeutics. *Biotechnol. Prog.*, 37, p. e3108.
HAIDACHER, D., VAILAYA, A. & HORVÁTH, C. (1996) Temperature effects in hydrophobic interaction chromatography. *Proc. Natl. Acad. Sci. U. S. A.*, 93, pp. 2290–2295.
HARDING, F. A., STICKLER, M. M., RAZO, J. & DUBRIDGE, R. (2010) The immunogenicity of humanized and fully human antibodies: residual immunogenicity resides in the CDR regions. *Mabs*, 2, pp. 256–265.
HERNANDEZ, R., PAREDES, A. & BROWN, D. T. (2008) Sindbis virus conformational changes induced by a neutralizing anti-e1 monoclonal antibody. *J. Virol.*, 82, pp. 5750–5760.
HIATT, A., WHALEY, K. J. & ZEITLIN, L. (2014) Plant-derived monoclonal antibodies for prevention and treatment of infectious disease. *Microbiol. Spectr.*, 2, [AID-0004-2012].
HILBRIG, F. & FREITAG, R. (2003) Continuous annular chromatography. *J. Chromatogr. B*, 790, pp. 1–15.
HILLSON, J., KARR, N., OPPLIGER, I. & MANNIK, M. (1993) The structural basis of germline-encoded vh3 immunoglobulin binding to staphylococcal protein a. *J. Exp. Med.*, 178, pp. 331–336.
HJERTÉN, S. (1973) Some general aspects of hydrophobic interaction chromatography. *J. Chromatogr. A*, 87, pp. 325–331.
HJERTÉN, S. (1981) Hydrophobic interaction chromatography of proteins, nucleic acids, viruses, and cells on noncharged amphiphilic gels. *Methods Biochem. Anal.*, 27, pp. 89–108.
HJERTÉN, S., ROSENGREN, J. & SVEN, P. (1974) Hydrophobic interaction chromatography: the synthesis and the use of some alkyl and aryl derivatives of agarose. *J. Chromatogr. A*, 101, pp. 281–288.
HJERTÉN, S., YAO, K., ERIKSSON, K. O. & JOHANSSON, B. (1986) Gradient and isocratic high-performance hydrophobic interaction chromatography of proteins on agarose columns. *J. Chromatogr. A*, 359, pp. 99–109.
HO, S. V., MCLAUGHLIN, J. M., CUE, B. W. & DUNN, P. J. (2010) Environmental considerations in biologics manufacturing. *Green Chem.*, 12, pp. 755–766.
HOFSTEE, B. H. (1973) Hydrophobic affinity chromatography of proteins. *Anal. Biochem.*, 52, pp. 430–448.
HOFSTEE, B. H. (1976) Hydrophobic adsorption chromatography of proteins. In: **CATSIMPOOLAS, N. (ed.)** *Methods of protein separation.* Boston: Springer, pp. 245–278.
HOFSTEE, B. H. & OTILLIO, N. F. (1978) Non-ionic adsorption chromatography of proteins. *J. Chromatogr. A*, 159, pp. 57–69.
HOLM, N. K., JESPERSEN, S. K. & THOMASSEN, L. V. et al. (2007) Aggregation and fibrillation of bovine serum albumin. *Biochim. Biophys. Acta*, 1774, pp. 1128–1138.
HONDA, C., KAMIZONO, H., SAMEJIMA, T. & ENDO, K. (2000) Studies on thermal aggregation of bovine serum albumin as a drug carrier. *Chem. Pharm. Bull.*, 48, pp. 464–466.
HORVÁTH, C., MELANDER, W. & MOLNAR, I. (1976) Solvophobic interactions in liquid chromatography with nonpolar stationary phases. *J. Chromatogr. A*, 125, pp. 129–156. (See also **MELANDER, W. & HORVÁTH, C. (1977)** below.)
HUMMEL, J., PAGKALIWANGAN, M. & GJOKA, X. et al. (2019) Modeling the downstream processing of monoclonal antibodies reveals cost advantages for continuous methods for a broad range of manufacturing scales. *Biotechnol. J.*, 14, p. e1700665.
HUTCHINSON, N., BINGHAM, N., MURRELL, N. & HOARE, M. (2006) Shear stress analysis of mammalian cell suspensions for prediction of industrial centrifugation and its verification. *Biotechnol. Bioeng.*, 95, pp. 483–491.
IMURA, Y., TAGAWA, T. & MIYAMOTO, Y. et al. (2021) Washing with alkaline solutions in protein A purification improves physicochemical properties of monoclonal antibodies. *Sci. Rep.*, 11, p. 1827.
JAGSCHIES, G., SOFER, G. K. & HAGEL, L. (2007) *Handbook of process chromatography: development, manufacturing, validation and economics.* 2nd ed. Burlington: Elsevier.
JAIN, D. & SALUNKE, D. M. (2019) Antibody specificity and promiscuity. *Biochem. J.*, 476, pp. 433–447.
JANEWAY, C. A. JR, TRAVERS, P., WALPORT, M. & SHLOMCHIK, M. J. (2001) The structure of a typical antibody molecule. In: *Immunobiology: the immune system in health and disease.* 5th ed. New York: Garland Science, pp. 115–121.

JENDEBERG, L., PERSSON, B., ANDERSSON, R. et al. (1995) Kinetic analysis of the interaction between protein A domain variants and human fc using plasmon resonance detection. *J. Mol. Recognit.*, 8, pp. 270–278.
JENDEBERG, L., NILSSON, P., LARSSON, A. et al. (1997) Engineering of fc1 and fc3 from human immunoglobulin g to analyse subclass specificity for staphylococcal protein a. *J. Immunol. Methods*, 201, pp. 25–34.
JENNISSEN, H. & HEILMEYER, L. JR (1975) General aspects of hydrophobic chromatography. Adsorption and elution characteristics of some skeletal muscle enzymes. *Biochemistry*, 14, pp. 754–760.
JESKE, D. J., JARVIS, J., MILSTEIN, C. & CAPRA, J. D. (1984) Junctional diversity is essential to antibody activity. *J. Immunol.*, 133, pp. 1090–1092.
JIN, W., XING, Z. & SONG, Y. et al. (2019) Protein aggregation and mitigation strategy in low ph viral inactivation for monoclonal antibody purification. *Mabs*, 11, pp. 1479–1491.
JOHNSON, B. (2016) Chapter 35: immunotherapy. In: *Pharmacology and therapeutics for dentistry.* 7th ed. St. Louis: Elsevier, p. 518.
JOLLES, S., SEWELL, W. A. & MISBAH, S. A. (2005) Clinical uses of intravenous immunoglobulin. *Clin. Exp. Immunol.*, 142, pp. 1–11.
JUNGBAUER, A. (2013) Continuous downstream processing of biopharmaceuticals. *Trends Biotechnol.*, 31, pp. 479–492.
JUNGBAUER, A., MACHOLD, C. & HAHN, R. (2005) Hydrophobic interaction chromatography of proteins: III. unfolding of proteins upon adsorption. *J. Chromatogr. A*, 1079, pp. 221–228.
JUNGBAUER, A., SATZER, P. & DUERAUER, A. et al. (2024) Continuous downstream processing. *Sep. Purif. Technol.*, 126439 (in press).
KANG, Y., HAMZIK, J. & FELO, M. et al. (2013) Development of a novel and efficient cell culture flocculation process using a stimulus responsive polymer to streamline antibody purification processes. *Biotechnol. Bioeng.*, 110, pp. 2928–2937.
KANJE, S., SCHEFFEL, J., NILVEBRANT, J. & HOBER, S. (2020) Engineering of protein A for improved purification of antibodies and fc-fused proteins. In: **MATTE, A. (ed.)** *Approaches to the purification, analysis and characterization of antibody-based therapeutics.* Amsterdam: Elsevier.
KAUFMANN, S. H. E. (2017) Emil von behring: translational medicine at the dawn of immunology. *Nat. Rev. Immunol.*, 17, pp. 341–343.
KELLEY, B. (2007) Very large scale monoclonal antibody purification: the case for conventional unit operations. *Biotechnol. Prog.*, 23, pp. 995–1008.
KELLEY, B. (2009) Industrialization of mAb production technology: the bioprocessing industry at a crossroads. *Mabs*, 1, pp. 443–452.
KEMPKEN, R., PREISSMANN, A. & BERTHOLD, W. (1995) Assessment of a disc stack centrifuge for use in mammalian cell separation. *Biotechnol. Bioeng.*, 46, pp. 132–138.
KETTERER, B., MOORE-KELLY, C., THOMAS, O. R. T. et al. (2019) Integrated system for temperature-controlled fast protein liquid chromatography. III. continuous downstream processing of monoclonal antibodies. *J. Chromatogr. A*, 1609, p. 460429.
KHANAL, O., SINGH, N. & TRAYLOR, S. J. et al. (2018) Contributions of depth filter components to protein adsorption in bioprocessing. *Biotechnol. Bioeng.*, 115, pp. 1938–1948.
KHANAL, O. & LENHOFF, A. M. (2021) Developments and opportunities in continuous biopharmaceutical manufacturing. *Mabs*, 13, p. 1903664.
KLASSE, P. J., SANDERS, R. W., CERUTTI, A. & MOORE, J. P. (2012) How can hiv-type-1-env immunogenicity be improved to facilitate antibody-based vaccine development? *AIDS Res. Hum. Retroviruses*, 28, pp. 1–15.
KO, K. & AHN, D. (2007) Preparation of immunoglobulin y from egg yolk using ammonium sulfate precipitation and ion exchange chromatography. *Poult. Sci.*, 86, pp. 400–407.
KOHLER, G. & MILSTEIN, C. (1975) Continuous cultures of fused cells secreting antibody of predefined specificity. *Nature*, 256, pp. 495–497.
KOHLI, N., JAIN, N., GEDDIE, M. L. et al. (2015) A novel screening method to assess developability of antibody-like molecules. *Mabs*, 7, pp. 752–758.
KOKAI-KUN, J. F. (2022a) What's the environmental impact of biopharma continuous manufacturing? Part i [online]. *Bioprocess Online.* Available from: https://www.bioprocessonline.com/doc/what-s-the-environmental-impact-of-biopharma-continuous-manufacturing-part-i-0001 [Accessed 23 December 2023].

KOKAI-KUN, J. F. (2022b) What's the environmental impact of biopharma continuous manufacturing? Part ii [online]. *Bioprocess Online.* Available from: https://www.bioprocessonline.com/doc/what-s-the-environmental-impact-of-biopharma-continuous-manufacturing-part-ii-0001 [Accessed 23 December 2023].
KORNECKI, M., MESTMÄCKER, F., ZOBEL-ROOS, S. et al. (2017) Host cell proteins in biologics manufacturing: the good, the bad, and the ugly. *Antibodies*, 6, p. 13.
KRAGH-HANSEN, U. (1990) Structure and ligand binding properties of human serum albumin. *Dan. Med. Bull.*, 37, pp. 57–84.
KRAGH-HANSEN, U., CHUANG, V. T. & OTAGIRI, M. (2002) Practical aspects of the ligand-binding and enzymatic properties of human serum albumin. *Biol. Pharm. Bull.*, 25, pp. 695–704.
KUMAR, A., UDUGAMA, I. A., GARGALO, C. L. & GERNAEY, K. V. (2020) Why is batch processing still dominating the biologics landscape? towards an integrated continuous bioprocessing alternative. *Processes*, 8, p. 1641.
LAERMANN-NGUYEN, U. & BACKFISCH, M. (2021) Innovation crisis in the pharmaceutical industry? a survey. *SN Bus. Econ.*, 1, p. 164.
LATYPOV, R. F., HOGAN, S., LAU, H. & GADGIL, H. (2012) Elucidation of acid-induced unfolding and aggregation of human immunoglobulin IgG1 and IgG2 Fc. *J. Biol. Chem.*, 287, pp. 1381–1396.
LAY, M., FEE, C. & SWAN, J. (2006) Continuous radial flow chromatography of proteins. *Food Bioprod. Process.*, 84, pp. 78–83.
LEANDRO, M. & ISENBERG, D. A. (2021) Rituximab–the first twenty years. *Lupus*, 30, pp. 371–377.
LÉGER, J.-M., DE BLEECKER, J. L. & SOMMER, C. et al. (2013) Efficacy and safety of privigen® in patients with chronic inflammatory demyelinating polyneuropathy: results of a prospective, single-arm, open-label phase III study (the prima study). *J. Peripher. Nerv. Syst.*, 18, pp. 130–140.
LEVY, R., WEISS, R., CHEN, G. & IVERSON, B. L. (2001) Production of correctly folded Fab antibody fragment in the cytoplasm of Escherichia coli trxB gor mutants via the coexpression of molecular chaperones. *Protein Expr. Purif.*, 23, pp. 338–347.
LI, F., VIJAYASANKARAN, N., SHEN, A. Y. & KISS, R. (2010) Cell culture processes for monoclonal antibody production. *Mabs*, 2, pp. 466–479.
LI, H., YANG, Y. & ZHANG, Y. et al. (2015) A hydrophobic interaction chromatography strategy for purification of inactivated foot-and-mouth disease virus. *Protein Expr. Purif.*, 113, pp. 23–29.
LIENQUEO, M. E., MAHN, A., SALGADO, J. C. & ASENJO, J. A. (2007) Current insights on protein behaviour in hydrophobic interaction chromatography. *J. Chromatogr. B*, 849, pp. 53–68.
LINDSKOG, E. K. (2018) The upstream process: principal modes of operation. In: **JAGSCHIES, G., LINDSKOG, E., LACKI, K. & GALLIHER, P. M. (eds.)** *Biopharmaceutical processing.* Amsterdam: Elsevier.
LINKE, B., HUANG, Y.-C. & DORNFELD, D. (2012) Establishing greener products and manufacturing processes. *Int. J. Precis. Eng. Manuf.*, 13, pp. 1029–1036.
LIU, H. F., MA, J., WINTER, C. & BAYER, R. (2010) Recovery and purification process development for monoclonal antibody production. *Mabs*, 2, pp. 480–499.
LOPEZ, M., CLARKSON, M. R. & ALBIN, M. et al. (2006) A novel mechanism of action for anti-thymocyte globulin: induction of **CD4+, CD25+, FOXP3+** regulatory T cells. *J. Am. Soc. Nephrol.*, 17, pp. 2844–2853.
LU, L. L., SUSCOVICH, T. J., FORTUNE, S. M. & ALTER, G. (2018) Beyond binding: antibody effector functions in infectious diseases. *Nat. Rev. Immunol.*, 18, pp. 46–61.
MADABHUSHI, S. R., GAVIN, J., XU, S. et al. (2018) Quantitative assessment of environmental impact of biologics manufacturing using process mass intensity analysis. *Biotechnol. Prog.*, 34, pp. 1566–1573.
MADADKAR, P., SADAVARTE, R., BUTLER, M., DUROCHER, Y. & GHOSH, R. (2017) Preparative separation of monoclonal antibody aggregates by cation-exchange laterally-fed membrane chromatography. *J. Chromatogr. B*, 1055, pp. 158–164.
MADEIRA, P. P., ROCHA, I. L. & ROSA, M. E. et al. (2022) On the aggregation of bovine serum albumin. *J. Mol. Liq.*, 349, p. 118183.
MAHAL, H., BRANTON, H. & FARID, S. S. (2021) End-to-end continuous bioprocessing: impact on facility design, cost of goods, and cost of development for monoclonal antibodies. *Biotechnol. Bioeng.*, 118, pp. 3468–3485.

MALONEY, D. G., LILES, T. M. & CZERWINSKI, D. K. et al. (1994) Phase I clinical trial using escalating single-dose infusion of chimeric anti-CD20 monoclonal antibody (IDEC-C2B8) in patients with recurrent b-cell lymphoma. *Blood*, 84(8), pp. 2457–2466.
MATA-GÓMEZ, M. A., YAMAN, S. & VALENCIA-GALLEGOS, J. A. et al. (2016) Synthesis of adsorbents with dendronic structures for protein hydrophobic interaction chromatography. *J. Chromatogr. A*, 1443, pp. 191–200.
MAZZER, A. R., PERRAUD, X., HALLEY, J. & O'HARA, J. (2015) Protein A chromatography increases monoclonal antibody aggregation rate during subsequent low ph virus inactivation hold. *J. Chromatogr. A*, 1415, pp. 83–90.
MCCUE, J. T. (2009) Theory and use of hydrophobic interaction chromatography in protein purification applications. In: **ABELSON, J. N. & SIMON, M. I. (eds.)** *Methods in Enzymology, 463.* Amsterdam: Elsevier, pp. 405–414.
MCCULLOUGH, K., SMALE, C. & CARPENTER, W. et al. (1987) Conformational alteration in foot-and-mouth disease virus virion capsid structure after complexing with monospecific antibody. *Immunology*, 60, pp. 75–82.
MCNERNEY, T., THOMAS, A. & SENCZUK, A. et al. (2015) PDADMAC flocculation of chinese hamster ovary cells: enabling a centrifuge-less harvest process for monoclonal antibodies. *Mabs*, 7, pp. 413–427.
MEDCHEMEXPRESS (2025) Rituximab (synonyms: anti-human CD20 type i, chimeric antibody) – batch hy-p9913 or 463076 – purity by sec-hplc of 97.77% [online]. MedChemExpress. Available from: https://file.medchemexpress.com/batch_PDF/HY-P9913/Rituximab-COA-463076-MedChemExpress.pdf [Accessed 12 January 2025].
MELANDER, W., CORRADINI, D. & HORVÁTH, C. (1984) Salt-mediated retention of proteins in hydrophobic-interaction chromatography: application of solvophobic theory. *J. Chromatogr. A*, 317, pp. 67–85.
MELANDER, W. & HORVÁTH, C. (1977) Salt effects on hydrophobic interactions in precipitation and chromatography of proteins: an interpretation of the lyotropic series. *Arch. Biochem. Biophys.*, 183, pp. 200–215.
MIAN, I. S., BRADWELL, A. R. & OLSON, A. J. (1991) Structure, function and properties of antibody binding sites. *J. Mol. Biol.*, 217, pp. 133–151.
MICHNIK, A. (2002) Thermal stability of bovine serum albumin, dsc study. *J. Therm. Anal. Calorim.*, 71, pp. 509–519.
MILITELLO, V., VETRI, V. & LEONE, M. (2003) Conformational changes involved in thermal aggregation processes of bovine serum albumin. *Biophys. Chem.*, 105, pp. 133–141.
MOHTY, M. (2007) Mechanisms of action of antithymocyte globulin: t-cell depletion and beyond. *Leukemia*, 21, pp. 1387–1394.
MOLODENSKIY, D., SHIRSHIN, E. & TIKHONOVA, T. et al. (2017) Thermally induced conformational changes and protein–protein interactions of bovine serum albumin in aqueous solution under different pH and ionic strengths as revealed by SAXS measurements. *Phys. Chem. Chem. Phys.*, 19, pp. 17143–17155.
MOMAN, R. N., GUPTA, N. & VARACALLO, M. (2022) Physiology, albumin. In: *StatPearls* [online]. Treasure Island (FL): StatPearls Publishing. Available from: https://www.ncbi.nlm.nih.gov/books/NBK459198 [Accessed 1 December 2024].
MONTAÑO, R. F. & MORRISON, S. L. (2002) Influence of the isotype of the light chain on the properties of igg. *J. Immunol.*, 168, pp. 224–231.
MOUSSA, E. M., PANCHAL, J. P. & MOORTHY, B. S. et al. (2016) Immunogenicity of therapeutic protein aggregates. *J. Pharm. Sci.*, 105, pp. 417–430.
MUCA, R., MAREK, W. & PIĄTKOWSKI, W. (2010) Influence of the sample-solvent on protein retention, mass transfer and unfolding kinetics in hydrophobic interaction chromatography. *J. Chromatogr. A*, 1217, pp. 2812–2820.
MUCA, R., PIĄTKOWSKI, W. & ANTOS, D. (2009a) Effects of thermal heterogeneity in hydrophobic interaction chromatography. *J. Chromatogr. A*, 1216, pp. 6716–6727.
MUCA, R., PIĄTKOWSKI, W. & ANTOS, D. (2009b) Altering efficiency of hydrophobic interaction chromatography by combined salt and temperature effects. *J. Chromatogr. A*, 1216, pp. 8712–8721.

MÜLLER, T. K., CAO, P. & EWERT, S. et al. (2013) Integrated system for temperature-controlled fast protein liquid chromatography comprising improved copolymer modified beaded agarose adsorbents and a travelling cooling zone reactor arrangement. *J. Chromatogr. A*, 1285, pp. 97–109.
MÜLLER, T. K. & FRANZREB, M. (2012) Suitability of commercial hydrophobic interaction sorbents for temperature-controlled protein liquid chromatography under low salt conditions. *J. Chromatogr. A*, 1260, pp. 88–96.
MÜLLER, E. & VAJDA, J. (2016) Routes to improve binding capacities of affinity resins demonstrated for protein A chromatography. *J. Chromatogr. B*, 1021, pp. 159–168.
NAGRATH, D., XIA, F. & CRAMER, S. M. (2011) Characterization and modeling of nonlinear hydrophobic interaction chromatographic systems. *J. Chromatogr. A*, 1218, pp. 1219–1226.
NAPODANO, C., MARINO, M., STEFANILE, A. et al. (2021) Immunological role of igg subclasses. *Immunol. Investig.*, 50, pp. 427–444.
NATIONAL ACADEMIES OF SCIENCES, ENGINEERING AND MEDICINE (2021) *Innovations in pharmaceutical manufacturing proceeding of a workshop—in brief. Innovations in pharmaceutical manufacturing on the horizon: technical challenges, regulatory issues, and recommendations.* Washington, D.C.: National Academies Press.
NEJATISHAHIDEIN, N. & ZYDNEY, A. L. (2021) Depth filtration in bioprocessing—new opportunities for an old technology. *Curr. Opin. Chem. Eng.*, 34, p. 100746.
NGUYEN, M. N., PRADHAN, M. R., VERMA, C. & ZHONG, P. (2017) The interfacial character of antibody paratopes: analysis of antibody–antigen structures. *Bioinformatics*, 33, pp. 2971–2976.
NORIS, M. & REMUZZI, G. (2013) Overview of complement activation and regulation. *Semin. Nephrol.*, 33, pp. 479–492.
NWEKE, M. C., RATHORE, A. S. & BRACEWELL, D. G. (2018) Lifetime and aging of chromatography resins during biopharmaceutical manufacture. *Trends Biotechnol.*, 36, pp. 992–995.
OSTREICHER, E. A., ARNOLD, T. E. & CONWAY, R. S. (2019) Charge-modified filter media. In: **JORNITZ, M. W.** *Filtration and purification in the biopharmaceutical industry.* 3rd ed. Boca Raton: CRC Press.
OTT, V., MÜLLER, J. & SCHIRMER, C. et al. (2022) Qualification of a single-use disk stack separator for cell separation in mammalian cell-based antibody production. *Chem. Ing. Tech.*, 94, pp. 1936–1943.
PABST, T. M., THAI, J. & HUNTER, A. K. (2018) Evaluation of recent protein A stationary phase innovations for capture of biotherapeutics. *J. Chromatogr. A*, 1554, pp. 45–60.
PALMBERGER, D., RENDIĆ, D. & TAUBER, P. et al. (2011) Insect cells for antibody production: evaluation of an efficient alternative. *J. Biotechnol.*, 153, pp. 160–166.
PAPPANO, A., WIER, W. G., PAPPANO, A. & WIER, W. G. (2013) The microcirculation and lymphatics. *Cardiovasc. Physiol.*, [vol./pages not fully specified], pp. 153–170.
PAVLASOVA, G. & MRAZ, M. (2020) The regulation and function of CD20: an “enigma” of b-cell biology and targeted therapy. *Haematologica*, 105, pp. 1494–1506 (approx.).
PERKINS, T. W., MAK, D. S., ROOT, T. W. & LIGHTFOOT, E. N. (1997) Protein retention in hydrophobic interaction chromatography: modeling variation with buffer ionic strength and column hydrophobicity. *J. Chromatogr. A*, 766, pp. 1–14.
PETERS JR, T. (1995) *All about albumin: biochemistry, genetics, and medical applications.* San Diego: Academic Press.
PIERPONT, T. M., LIMPER, C. B. & RICHARDS, K. L. (2018) Past, present, and future of rituximab—the world’s first oncology monoclonal antibody therapy. *Front. Oncol.*, 8, p. 163.
PIETRZYKOWSKI, M., FLANAGAN, W., PIZZI, V. et al. (2013) An environmental life cycle assessment comparison of single-use and conventional process technology for the production of monoclonal antibodies. *J. Clean. Prod.*, 41, pp. 150–162.
POGUE, G. P., VOJDANI, F. & PALMER, K. E. et al. (2010) Production of pharmaceutical-grade recombinant aprotinin and a monoclonal antibody product using plant-based transient expression systems. *Plant Biotechnol. J.*, 8, pp. 638–654.
POLLOCK, J., COFFMAN, J., HO, S. V. & FARID, S. S. (2017) Integrated continuous bioprocessing: economic, operational, and environmental feasibility for clinical and commercial antibody manufacture. *Biotechnol. Prog.*, 33, pp. 854–866.
POPESCU, B. F. G. & LUCCHINETTI, C. F. (2012) Pathology of demyelinating diseases. *Annu. Rev. Pathol.*, 7, pp. 185–217.

PORATH, J., SUNDBERG, L. & FORNSTEDT, N. et al. (1973) Salting-out in amphiphilic gels as a new approach to hydrophobia adsorption. *Nature*, 245, pp. 465–466.
QUEIROZ, J. A., TOMAZ, C. T. & CABRAL, J. M. (2001) Hydrophobic interaction chromatography of proteins. *J. Biotechnol.*, 87, pp. 143–159.
RAMOS-DE-LA-PEÑA, A. M., GONZÁLEZ-VALDEZ, J. & AGUILAR, O. (2019) Protein A chromatography: challenges and progress in the purification of monoclonal antibodies. *J. Sep. Sci.*, 42, pp. 1816–1827.
RAOUFINIA, R., MOTA, A. & KEYHANVAR, N. et al. (2016) Overview of albumin and its purification methods. *Adv. Pharm. Bull.*, 6, pp. 495–507.
RATHORE, A. S., AGARWAL, H., SHARMA, A. K. & PATHAK, M. (2015) Continuous processing for production of biopharmaceuticals. *Prep. Biochem. Biotechnol.*, 45, pp. 836–849.
RAYAT, A. C., CHATEL, A., HOARE, M. & LYE, G. J. (2016) Ultra scale-down approaches to enhance the creation of bioprocesses at scale: impacts of process shear stress and early recovery stages. *Curr. Opin. Chem. Eng.*, 14, pp. 150–157.
REFF, M. E., CARNER, K. & CHAMBERS, K. S. et al. (1994) Depletion of b cells in vivo by a chimeric mouse human monoclonal antibody to CD20. *Blood*, 83, pp. 435–445.
REVERBERI, R. & REVERBERI, L. (2007) Factors affecting the antigen-antibody reaction. *Blood Transfus.*, 5, pp. 227–240.
RICKER, R. D. & SANDOVAL, L. A. (1996) Fast, reproducible size-exclusion chromatography of biological macromolecules. *J. Chromatogr. A*, 743, pp. 43–50.
RIOS, A. G., RIBEIRO, A. M., RODRIGUES, A. E. & FERREIRA, A. F. (2023) Bovine serum albumin and myoglobin separation by ion-exchange smb. *Ind. Eng. Chem. Res.*, 62, pp. 13932–13942.
RISKE, F., SCHROEDER, J., BELLIVEAU, J. et al. (2007) The use of chitosan as a flocculant in mammalian cell culture dramatically improves clarification throughput without adversely impacting monoclonal antibody recovery. *J. Biotechnol.*, 128, pp. 813–823.
ROBERTS, J. A. & CARTA, G. (2023) Protein adsorption and separation with monomodal and multimodal anion exchange chromatography resins. part II. mechanisms of protein aggregation on the chromatographic surface. *J. Chem. Technol. Biotechnol.*, 98, pp. 357–368.
ROBERTS, J. A., KIMERER, L. & CARTA, G. (2020) Effects of molecule size and resin structure on protein adsorption on multimodal anion exchange chromatography media. *J. Chromatogr. A*, 1628, p. 461444.
ROUX, K. H., STRELETS, L. & MICHAELSEN, T. E. (1997) Flexibility of human igg subclasses. *J. Immunol.*, 159, pp. 3372–3382.
SARGENT, B. (2018) Bovine serum albumin–more complex than you might think [online]. *Cell Culture Dish.* Available from: https://cellculturedish.com/bovine-serum-albumin-more-complex-than-you-might-think/ [Accessed 6 January 2024].
SARPATWARI, A., AVORN, J. & KESSELHEIM, A. S. (2015) Progress and hurdles for follow-on biologics. *N. Engl. J. Med.*, 372, pp. 2380–2382.
SCHINDELIN, J., ARGANDA-CARRERAS, I. & FRISE, E. et al. (2012) Fiji: an open-source platform for biological-image analysis. *Nat. Methods*, 9, pp. 676–682.
SCHROEDER, H. W. & CAVACINI, L. (2010) Structure and function of immunoglobulins. *J. Allergy Clin. Immunol.*, 125, pp. S41–52.
SCHWAB, I. & NIMMERJAHN, F. (2013) Intravenous immunoglobulin therapy: how does igg modulate the immune system? *Nat. Rev. Immunol.*, 13, pp. 176–189.
SCOPES, R. K. (1993) *Protein purification: principles and practice.* 3rd ed. New York: Springer.
SEIDEL-MORGENSTERN, A., KESSLER, L. C. & KASPEREIT, M. (2008) New developments in simulated moving bed chromatography. *Chem. Eng. Technol.*, 31, pp. 826–837.
SELA-CULANG, I., KUNIK, V. & OFRAN, Y. (2013) The structural basis of antibody-antigen recognition. *Front. Immunol.*, 4, p. 302.
SERT, F., HıZ, D., GÜLMEZ, M. et al. (2022) Temperature and ph-dependent behaviors of mAb drugs: a case study for trastuzumab. *Sci. Pharm.*, 90, p. 21.
SHAIKH, S. & JAISWAL, P. (2018) Biopharmaceuticals market size, share, competitive landscape and trend analysis report, by type and application – global opportunity analysis and industry forecast, 2018–2025 [online]. *Allied Market Research.* Available from: https://www.alliedmarketresearch.com/biopharmaceutical-market [Accessed 13 May 2020].

SHALTIEL, S. & ER-EL, Z. (1973) Hydrophobic chromatography: use for purification of glycogen synthetase. *Proc. Natl. Acad. Sci. U. S. A.*, 70, pp. 778–781.
SHEPARD, C. C. & TISELIUS, A. (1949) The chromatography of proteins. the effect of salt concentration and ph on the adsorption of proteins to silica gel. *Discuss. Faraday Soc.*, 7, pp. 275–285.
SHESHUKOVA, E., KOMAROVA, T. & DOROKHOV, Y. (2016) Plant factories for the production of monoclonal antibodies. *Biochemistry (Mosc.)*, 81, pp. 1118–1135.
SHI, C., ZHANG, Q. L., JIAO, B. & CHEN, X. J. (2021) Process development and optimization of continuous capture with three-column periodic counter-current chromatography. *Biotechnol. Bioeng.*, 118, pp. 3313–3322.
SHIRE, S. J., SHAHROKH, Z. & LIU, J. (2004) Challenges in the development of high protein concentration formulations. *J. Pharm. Sci.*, 93, pp. 1390–1402.
SHUKLA, A. A., ETZEL, M. R. & GADAM, S. (2006) *Process scale bioseparations for the biopharmaceutical industry.* Boca Raton: CRC Press.
SHUKLA, A. A., GUPTA, P. & HAN, X. (2007a) Protein aggregation kinetics during protein A chromatography: case study for an fc fusion protein. *J. Chromatogr. A*, 1171, pp. 22–28.
SHUKLA, A. A., HUBBARD, B., TRESSEL, T. et al. (2007b) Downstream processing of monoclonal antibodies–application of platform approaches. *J. Chromatogr. B*, 848, pp. 28–39.
SHUKLA, A. A., WOLFE, L. S., MOSTAFA, S. S. & NORMAN, C. (2017) Evolving trends in mAb production processes. *Bioeng. Transl. Med.*, 2, pp. 58–69.
SHULKA, A. A. & GOTTSCHALK, U. (2013) Single-use disposable technologies for biopharmaceutical manufacturing. *Trends Biotechnol.*, 31, pp. 147–154.
SIDDIQUI, S., COX, J., HERZIG, R. et al. (2019) Anti-thymocyte globulin in haematology: recent developments. *Indian J. Med. Res.*, 150, pp. 221–227.
SMITH, S. L. (1996) Ten years of orthoclone okt3 (muromonab-cd3): a review. *J. Transpl. Coord.*, 6, pp. 109–119.
SOMASUNDARAM, B., PLEITT, K. & SHAVE, E. et al. (2018) Progression of continuous downstream processing of monoclonal antibodies: current trends and challenges. *Biotechnol. Bioeng.*, 115, pp. 2893–2907.
SRINIVASAN, R. & RUCKENSTEIN, E. (1980) Role of physical forces in hydrophobic interaction chromatography. *Sep. Purif. Methods*, 9, pp. 267–370.
STAVNEZER, J., GUIKEMA, J. E. J. & SCHRADER, C. E. (2008) Mechanism and regulation of class switch recombination. *Annu. Rev. Immunol.*, 26, pp. 261–292.
STEIN, M. R., NELSON, R. P. & CHURCH, J. A. et al. (2009) Safety and efficacy of Privigen®, a novel 10% liquid immunoglobulin preparation for intravenous use, in patients with primary immunodeficiencies. *J. Clin. Immunol.*, 29, pp. 137–144.
STICKEL, J. J. & FOTOPOULOS, A. (2000) Pressure-flow relationships for packed beds of compressible chromatography media at laboratory and production scale. *Biotechnol. Prog.*, 17, pp. 744–751.
STRATIS (2023) Monoclonal antibodies market size is projected to reach usd 390.58 billion by 2030, growing at a cagr of 10.2%: straits research [online]. *GlobeNewswire.* Available from: https://www.globenewswire.com/en/news-release/2023/03/15/2628105/0/en/Monoclonal-Antibodies-Market-Size-is-projected-to-reach-USD-390-58-Billion-by-2030-growing-at-a-CAGR-of-10-2-Straits-Research.html [Accessed 28 June 2023].
STÜBGEN, J.-P. (2008) B-cell-targeted therapy with rituximab and autoimmune neuromuscular disorders. *J. Neuroimmunol.*, 204, pp. 1–12.
SUDLOW, G., BIRKETT, D. & WADE, D. (1975) The characterization of two specific drug binding sites on human serum albumin. *Mol. Pharmacol.*, 11, pp. 824–832.
SUGIO, S., KASHIMA, A., MOCHIZUKI, S. & NODA, M. (1999) Crystal structure of human serum albumin at 2.5 å resolution. *Protein Eng.*, 12, pp. 439–446.
SUSANTO, A., HERRMANN, T., VON LIERES, E. & HUBBUCH, J. (2007) Investigation of pore diffusion hindrance of monoclonal antibody in hydrophobic interaction chromatography using confocal laser scanning microscopy. *J. Chromatogr. A*, 1149, pp. 178–188.
SUSHANT, T. & ONKAR, S. (2021) Monoclonal Antibodies Market Size, Share, Competitive Landscape and Trend Analysis Report, by Source, Indication and End User : Global Opportunity Analysis and Industry Forecast, 2021-2030 [online]. *Allied Market Research.* Available from:

https://www.alliedmarketresearch.com/monoclonal-antibodies-market-A11789 [Accessed 21 September 2021].
TAN, S., CAMPI, E. M., BOYSEN, R. I. et al. (2020) Batch binding studies with thermo-responsive polymer grafted sepharose 6 fast flow sorbents under different temperature and protein loading conditions. *J. Chromatogr. A*, 1625, p. 461298.
TAN, S., SAITO, K. & HEARN, M. T. (2018) Stimuli-responsive polymeric materials for separation of biomolecules. *Curr. Opin. Biotechnol.*, 53, pp. 209–223.
TISELIUS, A. (1948) Adsorption separation by salting out. *Arkiv Kemi. Mineral. Geol.*, B(26), p. 5 (Historical formatting).
TO, B. C. & LENHOFF, A. M. (2007) Hydrophobic interaction chromatography of proteins: I. the effects of protein and adsorbent properties on retention and recovery. *J. Chromatogr. A*, 1141, pp. 191–205.
TODD, P. A. & BROGDEN, R. N. (1989) Muromonab CD3. a review of its pharmacology and therapeutic potential. *Drugs*, 37, pp. 871–899.
TONEGAWA, S. (1983) Somatic generation of antibody diversity. *Nature*, 302, pp. 575–581.
TOPALĂ, T., BODOKI, A., OPREAN, L. & OPREAN, R. (2014) Bovine serum albumin interactions with metal complexes. *Clujul Med.*, 87, pp. 215–219.
TOSOH (2018) Hydrophobic interaction chromatography [online]. Available from: https://www.separations.eu.tosohbioscience.com/OpenPDF.aspx?path=~/File%20Library/TBG/Products%20Download/Brochure/b15p70a.pdf [Accessed 28 July 2024].
TRAPP, A., FAUDE, A., HOROLD, N. et al. (2018) Multiple functions of caprylic acid-induced impurity precipitation for process intensification in monoclonal antibody purification. *J. Biotechnol.*, 279, pp. 13–21.
TSURUSHITA, N., HINTON, P. R. & KUMAR, S. (2005) Design of humanized antibodies: from anti-tac to zenapax. *Methods*, 36, pp. 69–83.
UEBERBACHER, R., RODLER, A., HAHN, R. & JUNGBAUER, A. (2010) Hydrophobic interaction chromatography of proteins: thermodynamic analysis of conformational changes. *J. Chromatogr. A*, 1217, pp. 184–190.
VAILAYA, A. & HORVÁTH, C. (1996) Retention thermodynamics in hydrophobic interaction chromatography. *Proc. Natl. Acad. Sci. U. S. A.*, 93, pp. 2290–2295.
VAN ERP, E. A., LUYTJES, W., FERWERDA, G. & VAN KASTEREN, P. B. (2019) Fc-mediated antibody effector functions during respiratory syncytial virus infection and disease. *Front. Immunol.*, 10, p. 548.
VAN OSS, C. J., GOOD, R. J. & CHAUDHURY, M. K. (1986) Nature of the antigen-antibody interaction. *J. Chromatogr. A*, 376, pp. 111–119.
VAN REIS, R. & ZYDNEY, A. (2007) Bioprocess membrane technology. *J. Membr. Sci.*, 297, pp. 16–50.
VÁZQUEZ-REY, M. & LANG, D. A. (2011) Aggregates in monoclonal antibody manufacturing processes. *Biotechnol. Bioeng.*, 108, pp. 1494–1508.
VIDARSSON, G., DEKKERS, G. & RISPENS, T. (2014) IgG subclasses and allotypes: from structure to effector functions. *Front. Immunol.*, 5, p. 520.
WALCHLI, R., RESSURREICAO, M., VOGG, S., FEIDL, F., ANGELO, J., XU, X., GHOSE, S., LI, Z. J., LE SAOUT, X., SOUQUET, J., BROLY, H. & MORBIDELLI, M. (2020) Understanding mab aggregation during low pH viral inactivation and subsequent neutralization. *Biotechnol. Bioeng.*, 117, pp. 687–700.
WALTHER, J., GODAWAT, R., HWANG, C., ABE, Y., SINCLAIR, A. & KONSTANTINOV, K. (2015) The business impact of an integrated continuous biomanufacturing platform for recombinant protein production. *J. Biotechnol.*, 213, pp. 3–12.
WANG, Y., LIU, J., BURROWS, P. D. & WANG, J. Y. (2021) B cell development and maturation. In: **WANG, J. Y. (ed.)** B cells in immunity and tolerance. 1st ed. Berlin: Springer, pp. 1–22.
WARNER, T. N. & NOCHUMSON, S. (2003) Rethinking the economics of chromatography. *BioPharm Int.*, 16, pp. 58–60.
WEIGEL, T., SOLIMAN, R., WOLFF, M. W. & REICHL, U. (2019) Hydrophobic-interaction chromatography for purification of influenza a and b virus. *J. Chromatogr. B*, 1117, pp. 103–117.
WHITE, R. C., RUFF, C. J. & NELSON, T. E. (1981) Purification of glycogen debranching enzyme from rabbit muscle using omega-aminoalkyl agarose chromatography. *Anal. Biochem.*, 115, pp. 388–390.
WINAU, F. & WINAU, R. (2002) Emil von behring and serum therapy. *Microbes Infect.*, 4, pp. 185–188.

WRIGHT, J. A., BAZILE, C., CLARK, E. S., CARLESSO, G., BOUCHER, J., KLEIMAN, E., MAHMOUD, T., CHENG, L. I., LÓPEZ-RODRÍGUEZ, D. M. & SATTERTHWAITE, A. B. (2021) Impaired b cell apoptosis results in autoimmunity that is alleviated by ablation of Btk. *Front. Immunol.*, 12, p. 705307.
XENOPOULOS, A. (2013) A new, integrated, continuous purification process template for monoclonal antibodies. *Paper presented at the Integrated Continuous Biomanufacturing Conference, Castelldefels, Spain, 20–24 October 2013.*
XENOPOULOS, A. (2015) A new, integrated, continuous purification process template for monoclonal antibodies: process modeling and cost of goods studies. *J. Biotechnol.*, 213, pp. 42–53.
ZHANG, Y. & CREMER, P. S. (2006) Interactions between macromolecules and ions: the hofmeister series. *Curr. Opin. Chem. Biol.*, 10, pp. 658–663.
ZHENG, J., WANG, L. & TWAROWSKA, B. et al. (2015) Caprylic acid-induced impurity precipitation from protein A capture column elution pool to enable a two-chromatography-step process for monoclonal antibody purification. *Biotechnol. Prog.*, 31, pp. 1515–1525.
ZYDNEY, A. L. (2016) Continuous downstream processing for high value biological products: a review. *Biotechnol. Bioeng.*, 113, pp. 465–475.